

# *The Influence of Grout Installation Parameters on Shaft Bearing Capacity of Screw-Injection Piles*

*Santiago Alejandro Aguilar*



**TU Delft**



**VAN'THEK**

# The Influence of Grout Installation Parameters on Shaft Bearing Capacity of Screw-Injection Piles

Santiago Alejandro Aguilar

in fulfilment of the requirements for the degree of  
**Master of Science**  
at the Delft University of Technology,  
to be defended publicly on Thursday December 9, 2021 at 9:00 AM.

Student number:	4430387	
Thesis committee:	Prof. Dr. Ir. J. Ken Gavin,	TU Delft, supervisor
	Ir. D.A. Dirk de Lange,	Deltares/TU Delft
	Dr. Ir. Steffen Grünewald,	TU Delft
	Dr. Ir. Federico Pisanò,	TU Delft
	Ir. Simon van Dijk,	Voorbij Funderingstechniek B.V.
	Ir. Bartho Admiraal,	Volker Staal en Funderingen B.V.
	Ing. Patrick IJnsen,	Gebr. van 't Hek B.V.

An electronic version of this thesis is available at <http://repository.tudelft.nl/>.



# Preface

This thesis is written as the final requirement of the Master Science in Geo-Engineering at the Technische Universiteit Delft. This research was conducted in collaboration between the research programme of the TU Delft, Deltares, and the NVAF . The supervision research project was led two groups. One led by Professor Dr. Ir. J. Ken Gavin, Ir. D.A. Dirk de Lange and Dr. Ir. S. Grünewald from the The TU Delft. Second led by Ir. Simon van Dijk, Ir. Bartho Admiraal, and Ing. Patrick IJnsen from Voorbij Funderingstechniek B.V., Volker Staal en Funderingen B.V., Gebr. van 't Hek B.V. respectively which form part of the NVAF group.

The main focus of this thesis is the assessment of the effects that different grout properties have on the shaft capacity of screw-injection piles (SI-piles). The research carried out in this thesis serves to have a better understanding about the behaviour of different grout mixtures have during the installation process of the SI-piles. Additionally, this research focuses on the indirect relationships between multiple properties that are related to the shaft capacity and how the different grout mixtures affect those properties as well. This thesis is directed to readers who are interested in gaining more insight in foundation works and the studying of shaft capacity of piles.

This thesis report is the product of multiple months of research and analysis and would not have been possible without the help received and support received from my committee, my peers and family. I would like to express my appreciation to Dirk de Lange for his involvement and assistance when I needed help. I would also like to express my gratitude towards my parents and brother that provided me with full support for the entirety of this journey.

Santiago Alejandro Aguilar  
Delft, December 2021



# Abstract

In modern piling technology screw piles are used as a type of deep foundation for engineering structures, with the principal benefit of using said piles is that they offer an installation method that is virtually noise and vibration free. This makes these piles ideal for construction works in urban areas where surrounding structures can be affected by vibrations that would be produced from the installation of a driven pile. Since their initial production in the 1980s in Europe, multiple variations of screw piles are on the market today. This Msc thesis focuses on the Screw-Injection piles (SI-piles) commonly known as Fundex piles. SI-piles are a type of partial ground displacement piles where only a portion of the soil surrounding the pile is being pushed radially outwards during the rotational motion of screwing in the installation process. The other portion is transported back with grout flowing to the surface.

The current Dutch practice already have NEN guidelines on how to predict bearing capacity for SI-piles. These guidelines consist of CPT-based methods with an empirical correlation factor, the  $\alpha$  pile class factor, which helps to relate the bearing capacity to the soil surrounding the pile. Nevertheless, one aspect that is not well understood is the effect that different properties of the injected grout have at the soil-pile interface and for bearing capacity. In this thesis two grout properties are being manipulated which are the Water/Binder and W/C ratios of the grout mixture, and the injection flow rate of the grout with the purpose to see whether and/or to what extent a difference exists in the shaft bearing capacity for SI-piles.

A full-scale experiment was conducted on 15 piles in order to evaluate the effect of these varying parameters. This research is composed of four targeted variations of W/B ratio and two injection flow rates, 5 groups of 3 piles each to be more precise. The piles were subjected to a static pile load test in tension, which means that the bearing capacity is composed of mainly the shaft resistance of the pile. The analysis breaks down in four main parts to analyse the indirect relationships between the properties that are accounted for in the empirical parameter  $\alpha$ . These four parts include the assessment of the load-displacement behaviour of the SI-piles, assessment of radial soil stress (CPT data), assessment of the records during the installation process (torque, RPM), the grout properties during installation and after 28 and 56 days of curing, and lastly, the pile shape (volume) after extraction of pile.

The assessment of the load-displacement behaviour showed that the predictions using the NEN guidelines for bearing capacity were extremely accurate for most pile groups (above 0.970 measured/predicted ratio). But for the pile groups with higher W/B ratio and with the highest flow rate (Groups C and D respectively) the measured shaft capacity would be much lower. A direct relationship between the W/C and W/B ratio is difficult to conclude since for pile B2 and C1 that had the same W/C ratio, the difference in the measured/predicted ratio was about 21%. In the case of flow rate it is entirely seen that a higher flow rate leads to a

significant decrease in measured shaft capacity. The NEN suggests a value of  $\alpha_t$  for SI-piles of 0.009, yet the shaft capacity for groups with a higher W/C ratio and flow rate could be better predicted with an  $\alpha_t \approx 0.00793$ . Additionally, another important research objective is to try to optimise the  $\alpha_t$  parameter by comparing the  $q_c$  values for the pre-installation, the average post-installation and minimum value of the post-installation CPTs. This resulted in the  $\alpha_t$  derived from the pre-installation CPT to have a much lower Coefficient of Variation, CoV, of approximately 0.08 whereas the average and minimum post-CPT  $\alpha_t$  had a CoV of 0.12 and 0.11 respectively.

The assessment of the soil stresses is comprised of an analysis of the changes in cone resistance,  $q_c$ , throughout the field. The analysed data collected shows that for varying W/B ratios there is no solid relationship that relates the change in  $q_c$  after the grout installation. However, a higher flow rate seems to have a significant impact on the cone resistance, leading to a general decrease of  $q_c$  after installation, having a decrease as low as -16.53% for pile D1, whereas for all other pile groups there was an increase in  $q_c$  after installation, increases as high as 30% (pile A3).

The assessment of the records during installation include the analysis of the torque during the installation process. It is seen that in both cases, high W/B ratio and high flow rate, there is a decrease in torque, but the flow rate of 115 [l/min] had a more significant impact than the increase in W/B ratio.

The assessment of backflow grout resulted in higher W/C ratios having higher increases in density of the backflow fluid, and that high flow rate leads to a lower backflow density, this was supplemented with the sand transport data which suggests that higher W/B ratios lead to more sand transport out of the soil body. Furthermore, an inversely proportional relationship was found between W/B and W/C ratios and both the axial and bending stresses; the same inverse relationship is found with the flow rate. Additionally, the shear stress of the grout and of the soil were compared in order to determine if the failure is purely geotechnical or also structural.

The pile shape assessment resulted in a higher W/B ratio leading to a higher pile diameter, regardless of the flow rate during injection. There is also a very clear, almost perfectly linear, relationship between the mean diameter of the extracted pile and the measured shaft capacity. However not all piles were extracted and this includes piles installed with the highest W/C ratios (group C) and thus the aforementioned relationship has only been shown for a limited set of piles.

# List of Figures

2.1	Different types of drilled displacement piles (Basu and Prezzi,2009) . . . . .	5
2.2	Illustration of the Fundex pile's tip (Larisch, 2014) . . . . .	6
2.3	Step-by-step of a screw-injection pile . . . . .	7
2.4	Influence of the shape of the pile tip in soil displacement (Larisch, 2014) . . . . .	8
2.5	Example of how a tie-rod looks like in a rebar cage . . . . .	9
3.1	Pile response and Load-settlement response (Mark Randolph and Susan Gourvenec, 2017) . . . . .	12
3.2	Shape of the failure mechanism around a pile tip defined by Van Mierlo Koppejan, 1952. Photo from (Van Baars et al.) . . . . .	15
3.3	Pile grout delivery system for a SI pile . . . . .	16
3.4	Pile crown diameter. The shaded regions are the steel strips that determine the actual concrete pile diameter. . . . .	17
3.5	Grout injection in the course of pile rotation (Li et al, 2020) . . . . .	19
3.6	Load-settlement behaviour with grouting with different W/C ratios - for 7 days curing in loose sand (Dayakar et al, 2012) . . . . .	20
3.7	Load-settlement behaviour with grouting with different W/C ratios - for 7 days curing in medium dense sand (Dayakar et al, 2012) . . . . .	20
3.8	Relation between the penetration depth and the torque for different relative density states (Jeffrey et al, 2016) . . . . .	22
3.9	The observed consistency curve for a Bingham plastic, where $P_0$ is the actual yield point and $4/3$ is the apparent yield point. Creep is neglected in this depiction. (Ryen et al, 2017) . . . . .	24
3.10	(A) Plug flow of a Bingham plastic in round pipe, where $RP/2L < \tau_0$ . (B) Mixed flow of a Bingham plastic in round pipe. $RP/2L < \tau_0$ , $rP/2L = \tau_0T$ . (Ryen et al, 2017) . . . . .	24
4.1	Aerial satellite image of the test site. . . . .	28
4.2	CPT locations at the test site. The numbered locations next to the black triangles are the CPT locations and the black circles denoted by the letters A & B are locations where core samples are taken . . . . .	29
4.3	Location of the post-installation and pre-installation CPTs with relation to the Rijksdriehoekscoördinaten, RDX and RDY coordinates. . . . .	32
4.4	Typical set up of the Static Pile Load Test . . . . .	33
4.5	Loading scheme for the Test piles of Lemmer . . . . .	34
4.6	General outline of the research methodology . . . . .	34
5.1	Load-Displacement plot showing the load in [kN] the pile head rise in [mm] and the time duration of the static pile load test for pile A1. . . . .	38
5.2	W/B ratio at injection vs the M/P ratio for all 15 piles. . . . .	40
5.3	Flow rate of the grout vs the M/P ratio for Group B and D. . . . .	40

5.4	Contour plot of the average cone resistance of the pre-installation situation, where the red crosses indicate the location where the CPTs were taken. . . . .	42
5.5	CPT profiles with Pre- and Post- installation $q_c$ data for the full depth (from ground level to -9.5m NAP) for pile E1. . . . .	43
5.6	CPT profiles with Pre- and Post-installation $q_c$ data for the sand section (-4.5 to -9.5m NAP) for pile E1). . . . .	43
5.7	Contour map of the average cone resistance in the post-installation situation where the red crosses represent the location of the post-CPTs. . . . .	44
5.8	Ratio of change in $q_c$ along the depth of the sand section for pile E1. . . . .	45
5.9	Cone resistance vs the W/B ratio of the injection grout mixture. . . . .	46
5.10	Cone resistance vs the injection flow rate of the grout mixture. . . . .	47
5.11	$q_c$ vs shaft capacity for the three piles of each group, with error bars indicating the variation in each pile group. . . . .	48
5.12	The average $q_c$ values for each category vs shaft capacity. . . . .	48
5.13	Order of installation of the piles over the 3 day period of installation. . . . .	49
5.14	Torque vs. W/B ratio of the injection grout fluid of all piles in Group A, B, C and E. . . . .	50
5.15	Torque vs. Group average W/B ratio of the injection grout fluid. . . . .	50
5.16	Torque vs. flow rate of injected grout. . . . .	51
5.17	Torque vs. change in cone resistance for all piles. . . . .	52
5.18	Torque vs. the average change in cone resistance per pile group. . . . .	52
5.19	Torque vs. M/P ratio for all piles. . . . .	53
5.20	Percentage of sand in the backflow grout in relation to the W/B ratio. . . . .	55
5.21	The relationship between the W/B ratio and the amount of sand transported out of the soil. . . . .	56
5.22	Average density increase between the injected grout and the collected back-flow vs. W/C ratio of the injection grout fluid. . . . .	58
5.23	Average density increase between the injected grout and the collected back-flow vs. flow rate of injection grout. . . . .	59
5.24	Average density increase between the injected grout and the collected back-flow vs. M/P ratio. . . . .	59
5.25	UCS vs W/B ratio at injection at both depths -6m and -9m NAP for all piles in Groups A,B, C, and E after pile installation. . . . .	61
5.26	Bending stress vs average W/B ratio at injection at both depths -6m and -9m NAP for all piles in Groups A, B, C, and E after pile installation. . . . .	62
5.27	Average density increase between the injected grout and the collected back-flow vs. flow rate of injection of grout. . . . .	63
5.28	Average density increase between the injected grout and the collected back-flow vs. flow rate of injection of grout. . . . .	63
5.29	Photograph of the extracted piles from the test site in Lemmer, Friesland. . .	65
5.30	Size of diameters along the pile length. . . . .	66
5.31	Discretization of the pile after extraction into nodes in the diameter positions. . . . .	66
5.32	Pile volume increase vs W/B ratio at injection. . . . .	67
5.33	Average diameter size vs M/P ratio. . . . .	67
5.34	Summary of research findings. <b>Note:</b> for $V_{gsl}$ we do not know the transport data for piles of Group C. . . . .	68

7.1	Load-Displacement plot for pile B1, for which one can see the negative pile head rise. . . . .	76
7.2	Inclination of Pile B1 . . . . .	76
7.3	Inclination of Post CPT 14 (East) . . . . .	77
7.4	Inclination of Pile B1 . . . . .	80
A.1	Pile D1: Pre-installation vs (average) Post-installation Cone Resistance . . . .	85
A.2	Pile E1: Pre-installation vs (average) Post-installation Cone Resistance . . . .	86
A.3	Pile C1: Pre-installation vs (average) Post-installation Cone Resistance . . . .	86
A.4	Pile E2: Pre-installation vs (average) Post-installation Cone Resistance . . . .	87
A.5	Pile C2: Pre-installation vs (average) Post-installation Cone Resistance . . . .	87
A.6	Pile C3: Pre-installation vs (average) Post-installation Cone Resistance . . . .	88
A.7	Pile D2: Pre-installation vs (average) Post-installation Cone Resistance . . . .	88
A.8	Pile A1: Pre-installation vs (average) Post-installation Cone Resistance . . . .	89
A.9	Pile E3: Pre-installation vs (average) Post-installation Cone Resistance . . . .	89
A.10	Pile B1: Pre-installation vs (average) Post-installation Cone Resistance . . . .	90
A.11	Pile B2: Pre-installation vs (average) Post-installation Cone Resistance . . . .	90
A.12	Pile D3: Pre-installation vs (average) Post-installation Cone Resistance . . . .	91
A.13	Pile B3: Pre-installation vs (average) Post-installation Cone Resistance . . . .	91
A.14	Pile A2: Pre-installation vs (average) Post-installation Cone Resistance . . . .	92
A.15	Pile A3: Pre-installation vs (average) Post-installation Cone Resistance . . . .	92
A.16	Pile D1: Pre-installation vs (average) Post-installation Cone Resistance . . . .	93
A.17	Pile E1: Pre-installation vs (average) Post-installation Cone Resistance . . . .	94
A.18	Pile C1: Pre-installation vs (average) Post-installation Cone Resistance . . . .	94
A.19	Pile E2: Pre-installation vs (average) Post-installation Cone Resistance . . . .	95
A.20	Pile C2: Pre-installation vs (average) Post-installation Cone Resistance . . . .	95
A.21	Pile C3: Pre-installation vs (average) Post-installation Cone Resistance . . . .	96
A.22	Pile D2: Pre-installation vs (average) Post-installation Cone Resistance . . . .	96
A.23	Pile A1: Pre-installation vs (average) Post-installation Cone Resistance . . . .	97
A.24	Pile E3: Pre-installation vs (average) Post-installation Cone Resistance . . . .	97
A.25	Pile B1: Pre-installation vs (average) Post-installation Cone Resistance . . . .	98
A.26	Pile B2: Pre-installation vs (average) Post-installation Cone Resistance . . . .	98
A.27	Pile D3: Pre-installation vs (average) Post-installation Cone Resistance . . . .	99
A.28	Pile B3: Pre-installation vs (average) Post-installation Cone Resistance . . . .	99
A.29	Pile A2: Pre-installation vs (average) Post-installation Cone Resistance . . . .	100
A.30	Pile A3: Pre-installation vs (average) Post-installation Cone Resistance . . . .	100
B.1	2D Contour Plot of depth -4m to -5m NAP . . . . .	101
B.2	2D Contour Plot of depth -4m to -5m NAP . . . . .	102
B.3	2D Contour Plot of depth -4m to -5m NAP . . . . .	102
B.4	2D Contour Plot of depth -4m to -5m NAP . . . . .	103
B.5	2D Contour Plot of depth -7m to -8m NAP . . . . .	103
B.6	2D Contour Plot of depth -9m to -9.5m NAP . . . . .	104
B.7	2D Contour Plot of depth -4m to -5m NAP . . . . .	105
B.8	2D Contour Plot of depth -7m to -8m NAP . . . . .	105
B.9	2D Contour Plot of depth -9m to -9.5m NAP . . . . .	106
B.10	2D Difference Contour Plot post- vs pre-installation of depth -4m to -5m NAP	106

---

B.11 2D Difference Contour Plot post- vs pre-installation of depth -7m to -8m NAP	106
B.12 2D Difference Contour Plot post- vs pre-installation of depth -9m to -9.5m NAP	107
C.1 Torque for pile category A	110
C.2 Torque for pile category B	111
C.3 Torque for pile category C	112
C.4 Torque for pile category D	113
C.5 Torque for pile category E	114
D.1 Load vs pile head settlement for pile A1	115
D.2 Load vs pile head settlement for pile A2	116
D.3 Load vs pile head settlement for pile A3	116
D.4 Load vs pile head settlement for pile B1	117
D.5 Load vs pile head settlement for pile B2	117
D.6 Load vs pile head settlement for pile B3	118
D.7 Load vs pile head settlement for pile C1	118
D.8 Load vs pile head settlement for pile C2	119
D.9 Load vs pile head settlement for pile C3	119
D.10 Load vs pile head settlement for pile D1	120
D.11 Load vs pile head settlement for pile D2	120
D.12 Load vs pile head settlement for pile D3	121
D.13 Load vs pile head settlement for pile E1	121
D.14 Load vs pile head settlement for pile E2	122
D.15 Load vs pile head settlement for pile E3	122

# List of Tables

2.1	Pile Class factors, dimensionless parameters . . . . .	10
3.1	Different W/C ratios and their notations . . . . .	19
4.1	Volumetric Weight of Soils . . . . .	29
4.2	Table of the pile group subdivision with their respective W/B ratio and grout flow parameters. <b>Note:</b> W/B ratio is the same as W/C ratio for all pile groups except for E. . . . .	30
4.3	Preliminary Pull-out force calculations based on the Pre-installation CPTs . . . . .	31
5.1	W/B ratios during the pile installation. . . . .	38
5.2	Comparison of the measured and predicted shaft capacity . . . . .	39
5.3	The different measured $\alpha_t$ parameters of the different pile categories and their respective Coefficient of Variation, COV. . . . .	41
5.4	This table shows the percentage of change of cone resistance (improvement being positive, decrease being negative). . . . .	45
5.5	This table shows properties obtained from the extraction of the piles and in the last column it shows the amount of sand transported out of the soil as a unit of volume (liters). . . . .	55
5.6	Shows multiple properties of the backflow grout, the water content and bleeding are expressed in percentage (weight of water over the weight of the dry sample, and bleeding is the percentage of the volume of the sample immediately after extraction and after 1 hour). The density of grout during injection and backflow is shown along with the percentage of increase in density. . . . .	57
5.7	Stress tests for Unconfined Compressive Tests. . . . .	60
5.8	Stress tests for Bending Tests. *One of the samples for category C had the largest $\sigma_{bt}$ recorded at 2.6 kN, thus drastically increasing the percentage of change of $\sigma_{bt}$ *. . . . .	61
5.9	Shear stress of the grout and shear stress of the soil. . . . .	64
7.1	Assessment of $\alpha_t$ parameters, *CoV = Coefficient of variation . . . . .	79
7.2	Comparison of the measured and predicted shaft capacity with and without the limit of $q_c \leq 15$ MPa . . . . .	82



# List of Symbols

$\alpha$	Pile class factor
$\alpha_p$	Pile class factor for the pile tip
$\alpha_s$	Pile class factor for pile in compression
$\alpha_t$	Pile class factor for pile in tension
$\tau_s$	Shear strength [kN]
$q_c$	Cone resistance [MPa]
$q_b$	Base resistance [MPa]
$V$	Axial capacity of the pile [kN]
$Q_s$	Ultimate shaft resistance [kN]
$Q_b$	Ultimate base resistance [kN]
$W'_p$	Self weight of the pile [kN]
$D$	Diameter of the pile [m]
$r$	Radius of the shaft [m]
$L$	Length of the pile [m]
$\sigma'_f$	Horizontal effective stress at failure [kPa]
$\delta$	Mobilized coefficient of friction
$s_u$	In situ undrained strength [MPa]
$f_s$	Shaft friction [kPa]
$T$	Torque [kNm]
$J$	Polar moment of inertia [m <sup>4</sup> ]
$c$	Creep coefficient
$\delta_1$ and $\delta_2$	Pile head displacement at times $t_1$ and $t_2$ [mm]
$F_t$	Pull-out force [kN]
$\sigma_{uc}$	Failure load of the UCS test [MPa]
$\sigma_{bt}$	Failure load of the bending test [MPa]
$\rho_{inj}$	Density of injected grout [kg/m <sup>3</sup> ]
$\rho_{backflow}$	Density of backflow grout [kg/m <sup>3</sup> ]
$\rho_{28d}$	Density of grout 28 days after installation
$\rho_w$	Density of water
$\rho_s$	Density of sand
$v_l$	Volume fraction of the water loss
$V_{total}$	Total volume of injected grout during installation
$V_s$	Volume of sand transported out of the soil
$V_{pile,annulus}$	Volume of the annulus of the pile
$V_{gsl}$	Volume of injected grout that reaches the surface level, or volume of backflow
$\%sand$	Mass fraction of the sand



# Contents

List of Figures	vii
List of Tables	xi
List of Symbols and Nomenclature	xiii
1 Introduction	1
1.1 General Introduction . . . . .	1
1.2 Project Background . . . . .	2
1.3 Motivation . . . . .	2
1.4 Research Question and Objectives Statement . . . . .	2
1.5 Research Approach and Strategy . . . . .	3
2 State-of-the-Art of Screw-Injection Piles	5
2.1 Introduction . . . . .	5
2.2 Screw Piles Description of Installation Process . . . . .	6
2.2.1 Installation Monitoring . . . . .	7
2.3 Current Use of Cast-in-Place Screw Piles in The Netherlands . . . . .	8
2.3.1 Detailed Installation Parameters . . . . .	8
2.3.2 Standards and Load-Bearing Capacity . . . . .	10
3 Literature Study	11
3.1 Theoretical Framework. . . . .	11
3.1.1 The Basis for Design of Pile Foundations . . . . .	11
3.1.2 Axial Loaded Piles. . . . .	13
3.1.3 Settlement Behaviour . . . . .	13
3.1.4 Piles in Tension vs Compression . . . . .	13
3.1.5 Determining Bearing Capacity: Dutch NEN1997-1 and CUR166. . . . .	13
3.2 Influence of Grout. . . . .	15
3.2.1 Influence of Grout at the Pile Shaft . . . . .	16
3.2.2 Installation Process of Grout in Pile Shaft. . . . .	17
3.2.3 Water/Cement Ratio (W/C) . . . . .	18
3.2.4 Chemical Composition of the Grout Mixture . . . . .	20
3.3 Additional Aspects of Installation . . . . .	21
3.3.1 Penetration Depth and Torque . . . . .	21
3.4 Grouting Flow Properties . . . . .	22
4 Testing and Data Collection	27
4.1 Experimental Framework . . . . .	27
4.1.1 Site Investigation . . . . .	27
4.1.2 Pile Configuration. . . . .	29
4.1.3 Preliminary Force Calculations. . . . .	29
4.1.4 Pile Installation . . . . .	31

4.1.5	Test Set up: Static Pile Load Test . . . . .	32
4.2	Data Collection and Methodology . . . . .	33
4.2.1	Collection of Grout Samples . . . . .	33
4.2.2	Assessment of Radial Soil Stresses . . . . .	34
4.2.3	Assessment of Grout Properties and Shear Strength . . . . .	35
4.2.4	Assessment of Pile Shape . . . . .	35
4.2.5	Assessment of Load-Displacement Data . . . . .	35
5	Analysis . . . . .	37
5.1	Load-Displacement Analysis . . . . .	37
5.1.1	Comparison Predicted vs Measured Data . . . . .	38
5.1.2	Alpha-Factor Analysis . . . . .	41
5.2	Analysis of CPT Data . . . . .	42
5.2.1	Description of Soil Properties and Variability . . . . .	42
5.2.2	Effects of Installation on Cone Resistance . . . . .	43
5.2.3	Relationship Between Grout Installation Parameters and Average Cone Resistance (Sand Section) . . . . .	46
5.2.4	Relationship Between Cone Resistance and Shaft Capacity . . . . .	48
5.3	Analysis of Records of Installation . . . . .	49
5.3.1	Order of Installation . . . . .	49
5.3.2	Torque vs Grout Installation Parameters . . . . .	50
5.3.3	Torque vs Cone Resistance . . . . .	52
5.3.4	Torque vs Shaft Capacity. . . . .	53
5.3.5	Estimation of Total Amount of Sand Removed by Grout Flow. . . . .	54
5.4	Grout Properties Analysis . . . . .	57
5.4.1	Change in Grout Material Properties . . . . .	57
5.4.2	Density Change vs Grout Installation Parameters. . . . .	57
5.4.3	Density Change vs Shaft Capacity . . . . .	58
5.4.4	W/B ratio vs UCS Bending Test . . . . .	60
5.4.5	Flow Rate vs UCS Bending Test . . . . .	63
5.4.6	Shear Stress of Grout vs Shaft Capacity . . . . .	64
5.5	Pile Shape Analysis . . . . .	65
5.5.1	Pile Volume Increase . . . . .	65
5.6	Final Analysis. . . . .	68
6	Conclusion and Recommendations . . . . .	71
6.1	Conclusion . . . . .	71
7	Discussion . . . . .	75
7.1	Evaluation on Data Processing and Collection. . . . .	75
7.1.1	Static Pile Load Test. . . . .	75
7.1.2	Installation Process and Sample Collection . . . . .	75
7.1.3	Pre- and Post-Installation Data. . . . .	76
7.2	Deviation from the NEN 9997-1. . . . .	80
7.3	Observations on the Validity of Obtained Results . . . . .	81

---

Bibliography	83
A Appendix A: Pre- Post-Installation Changes	85
A.1 CPT Profiles. . . . .	85
A.2 Ratio of Increment . . . . .	93
B Appendix B: Contour Plots	101
B.1 Contour Plots of the Mean Post-Installation CPT . . . . .	101
C Appendix C: Installation Parameters	109
D Appendix D: Load-Settlement Data	115
E Appendix E: Laboratory Data on Grout Samples	123



# 1

## Introduction

### 1.1. General Introduction

Screw-injection piles are a type of partial ground displacement piles widely used for its relatively large dimensions. Partial ground displacement refers to piles where only a portion of the soil surrounding the pile is being pushed radially outwards during screwing motion and another portion being removed from the soil body, in the case of screw-injection piles this soil material is removed via grout flowing back into the surface carrying some soil particles. Further, the pile system is installed free from vibrations and without excessive noise. Two main systems can be distinguished: in which the driving casing is retrieved and in which the driving casing is part of the final pile.

During installation, grout flows via the pile tip along the casing towards the surface level. Due to screw movement, the grout will be mixed up with sand adjacent to the screw tip. The pile driver can vary with grout flow, the composition of the grout, rotation speed and direction and pull down force in order to reach the target depth and to create the pile. Different piling companies tend to have their own methodology also depending on where in the world these piles are being applied. Compared to a driven precast pile, the pile driver has more degrees of freedom. Of course, the soil conditions will limit these to a certain extend.

At the moment, knowledge on how these variables will affect the end product and its behavior is scarce. Therefore, the NVAF (industry association of all Dutch piling companies) in contribution with the research programme of the TUD/Deltares is preparing full-scale field experiments to investigate the effect of numerous execution parameters. Within these parameters comes the focus of this paper, which will be on grout installation parameters and more specifically grout flow and grout composition and their effect on the load-settlement behaviour of screw-injection (SI) piles. Multiple piles will be installed and each pile will be installed with a specific grout flow and grout composition. By static testing and retrieving the piles after testing, the influence on these parameters can be assessed. A full-scale set of tensile load test (uplift capacity) to determine bearing capacities on ground displacement screwed piles whether and, if so, to what extent does the bearing capacity of the ground displacement screwed piles differ with grout lubrication, whereby the grout lubrication is manipulated with regard to composition and flow rate, while the other execution parame-

ters are kept constant as much as possible.

## 1.2. Project Background

The NVAF (Nederlandse Vereniging Aannemers Funderingswerken) is the industry association of foundation works that unites multiple companies from The Netherlands. The objective of this industry association is to gather knowledge, optimize and/or enhance foundation work processes and developing a better understanding of the nature of how certain processes occur regarding geotechnical works. A previous experiment has been conducted to determine if the shape of the pile tip influences the bearing capacity of the pile. The follow-up of this study is now to investigate the effects of grout lubrication in the construction of screw-injection ground displacement piles. In order to assess the variations on Water/cement (W/C) ratio or Water/Binder (W/B) ratio and grout flow during installation, in liters/minute, 15 piles are going to be tested.

## 1.3. Motivation

The NVAF has carried out scale tests before in 2017 on ground displacement screw piles without grout lubrication. This research intended to evaluate different shapes of pile tips and how they influenced the bearing capacity of said piles. In order to continue research and develop more information on SI piles, the NVAF proposed a follow-up of this research was developed with the intention to investigate the significance of the nature of grout lubrication on improving the bearing capacity of the SI piles, notably on the characteristics of grout injection flow rate and W/C ratio. Grouting is a ground improvement technique and also when applied to piles can increase the bearing capacity, thus manipulation of grouting parameters is worth analyzing for future piled constructions in The Netherlands. This Msc thesis focuses on observing the effect on shaft bearing capacity of said SI piles with variations in the W/C ratio and injection flow rate.

## 1.4. Research Question and Objectives Statement

The main research question is: Is it possible to determine whether, and if so, to what extent a difference exists in the shaft bearing capacity in tension for screw-injection cast-in-place piles (otherwise also known as Fundex piles) made with grout lubrication where the two main variables are grout flow, calculated in litres per minute (l/m) and Water/cement ratio (and/or Water/Binder ratio)?

The direct and indirect effects of the varying installation parameters are assessed in this thesis. Some objectives of this research are listed below:

- Observe the influence on load-settlement behaviour changes in the W/C ratio, can the amount of cement poured in the grout mixture be optimised?
- Observe the effect on load-settlement behaviour of high grout injection rate, does this represent any significant change during the process of installation?

- Compare measurements on piles to the predictions of bearing capacity and the load-settlement curves obtained from the static pile load test with multiple pile installation properties.
  - Does the effect of change in cone resistance due to the installation of the SI-piles have any significant influence on the shaft capacity?
  - Can variations in the grout installation parameters optimize the torque seen during the installation process?
  - To what extent does the grout material in the soil have a significant impact on the shaft capacity? This includes the shear strength and density of the backflow grout.
  - Can we find a direct relationship between the increase in pile volume and the shaft capacity?
- Optimisation of the alpha factor, can different  $\alpha$  factors be assigned depending on the input grout parameters?

## 1.5. Research Approach and Strategy

The following strategy is undertaken in order to answer the research question:

- **State-of-the-art description of screw injection piles and their installation process.**
- **Literature Study: Study of the effects of grout installation parameters:** W/C ratio and grout injection flow rate
- **Research Methodology:** Description of the pile installation process, data collection, tests performed on the installed piles and general outline of the research.
- **Analysis of Available Data:** Processing of the data collected. Answering the research objectives. Development of direct and indirect relationships between the four main pillars of this research: CPT data, recorded data during the installation process, grout backflow properties data, and the pile shape data after pile extraction.



# 2

## State-of-the-Art of Screw-Injection Piles

### 2.1. Introduction

This chapter covers in detail what a screw pile is and the process of installation used in current Dutch practice. There are various types of said piles which can be seen in Figure 2.1:

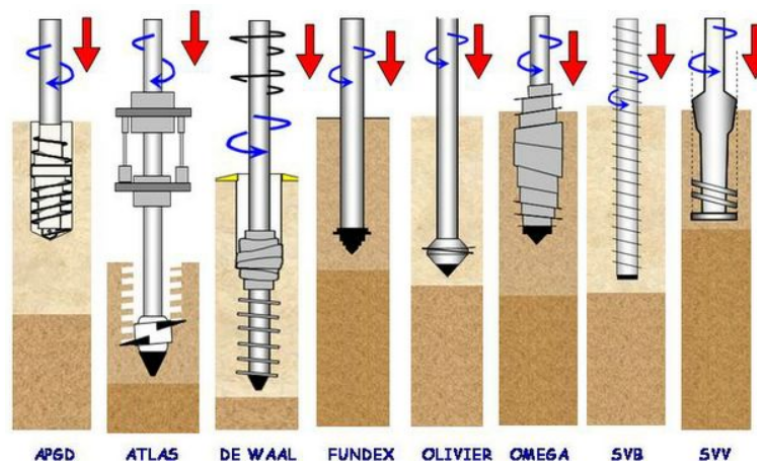


Figure 2.1: Different types of drilled displacement piles (Basu and Prezzi,2009)

Full-displacement screw piles were developed in the 1980s in Europe (Bustamante and Gianeselli 1998). The Atlas pile was first introduced in the 1980s by the Belgian company Franki. As the development in technology improved, the increasing rotational torque and vertical pull-down force capacities of piling rigs, screw auger displacement piles became more economical and thus more utilized. Several different auger shapes and geometries have been developed by different manufacturers, some of these variations are shown in Figure 2.1. However these piles can be broken down further into two main categories, short displacement piles (Olivier, Atlas and Fundex) and long displacement piles (de Waal, SVV, Omega and APGD). This distinction arises from the length of the drilling screw. In this thesis the focus will be on the Fundex type pile, this also can have a grout delivery system for which in this paper it is referred to as the screw-injection pile (SI), for which this type of pile relies on a full-helical flange to cut through, which acts as a displacement body for which there is little or no soil transport occurring during installation.

## 2.2. Screw Piles Description of Installation Process

There are a variety of pile foundation types used in geotechnical engineering practice today. Within the spectrum of pile foundation choices, on one hand, the non-displacement piles, which include bored piles or drilled shafts, and on the other hand, there are the full-displacement piles (ground-displacement piles), which include closed-ended pipe piles or precast reinforced concrete piles (Basu et al. 2010). Ground-displacement screw piles are designed to move the soil around them completely during penetration. This generates a specific influence radius in the soil, which generates stresses and displacement around the pile during installation and extraction processes. This displacement serves to increase the shaft capacity of the pile. There are a set of advantages from using said piles. Notably, these systems are noise and vibration-free, which is an advantage for works in urban areas.

The screw injection piles that are going to be the primary focus of this paper are a type of drilled displacement piles that consist of cast-in-situ concrete piles, installed by torque and downward pressure, which has received a lot of attention because of its vibration-free nature which produces a low-noise operation. These are often called Fundex piles because of the company that first developed such types of piles. These are a type of short-displacement piles that has especially gained attention for constructions in urban areas where the noise produced by pile driving is an important factor to consider. These piles consist of a rotary pile tip of a rather conical shape that has a steel casing attached to it. When drilling begins, the SI-piles are inserted into the soil by exerting rotation force using the hydraulic machine. A constant downward force is also required for advancing the downward movement of the piles. Normally for Fundex piles, high torque capacities are needed due to the large amount of soil being displaced. Additionally, the drill tip will not retract back to the surface, this drill tip therefore will stay at the bottom of the pile, this is otherwise known as a sacrificial drill tip (Larisch, 2014). The tip of a Fundex pile is shown in Figure 2.2.

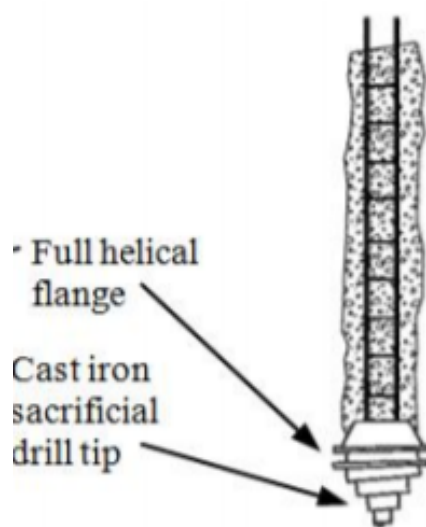


Figure 2.2: Illustration of the Fundex pile's tip (Larisch, 2014)

As the pile is being drilled the grout mixture is being added. After the drilling depth is reached, the reinforcing steel cage is then added and the casing is removed from the pile. Figure 2.3 shows an illustration of the screw injection pile installation process.

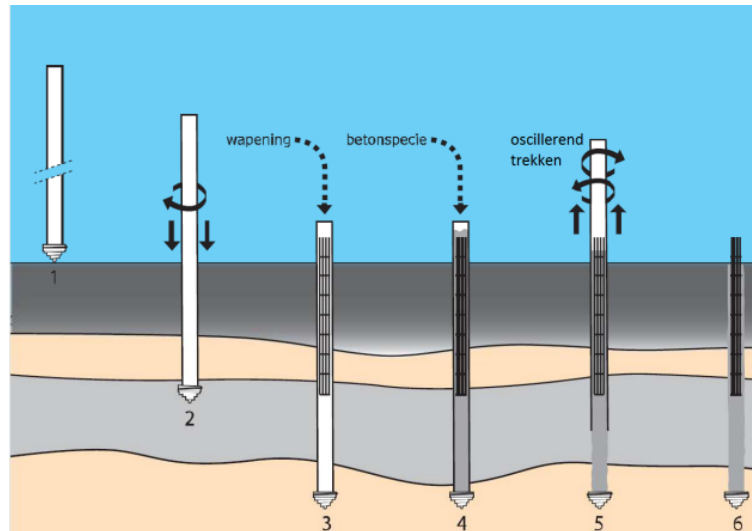


Figure 2.3: Step-by-step of a screw-injection pile

One of the major advantages of using SI-piles is that they are not sensitive to soil decompression and over-excavation due to the fact that there is limited soil transport taking place, the soil is dispersed sideways. This results in densification in the soil surrounding the pile shaft, typically leading to improved load-settlement curves, in other words, improved bearing capacity. The soil is displaced and densified when the installation force, derived from the torque and the downward pressure, exceeds the resistance of the soil resistance. The shape of the pile tip is an important factor, as it plays a key factor in knowing if soil transport occurs or not, Figure 2.4 shows different pile tips and their effects. This method of pile foundation is based on principles found in helical screw piles. Where the central shaft, typically of a cylindrical shape, is used for torque transmission during installation, which transfers axial loads to the helical plates and providing structural stability against overturning and lateral forces [4].

### 2.2.1. Installation Monitoring

Typically various parameters that are monitored during the installation process of a screw cast-in-place injection pile. These are the following:

1. Depth of installation
2. Penetration rate
3. Rotational torque

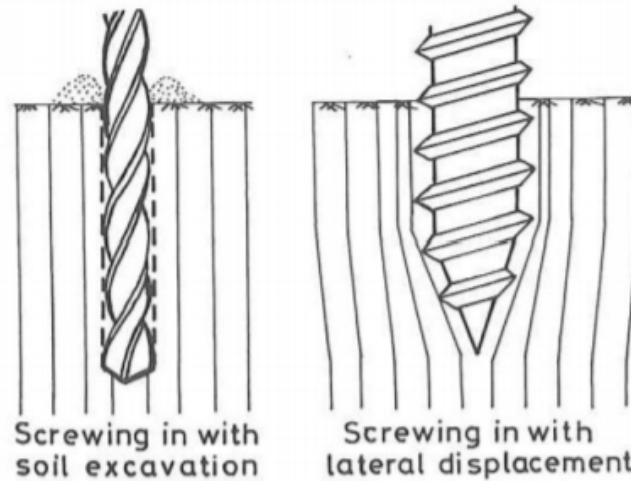


Figure 2.4: Influence of the shape of the pile tip in soil displacement (Larisch, 2014)

4. Pull-down force
5. Concrete and grout pressures
6. Grout flow lubrication
7. Extraction rate

## 2.3. Current Use of Cast-in-Place Screw Piles in The Netherlands

### 2.3.1. Detailed Installation Parameters

Currently in The Netherlands, there are multiple names used for cast-in place ground-displacement concrete piles that are manufactured using a screw-inserted steel casing (steel auxiliary tube). Some of these names are the following and vary depending on the supplying company. These companies are the following:

- Fundex pile (Verstraeten)
- BVS pile (BAM Displacement Screw pile) (BAM Grondtechniek)
- Terr-econ pile (Terracon)
- Hekpaal (Van 't Hek)
- VSP (Voorbij Funderingstechniek)
- TVSi (VSF)
- HGSI pile (Heijmans)
- VGS pile (Vroom Earth-displacing screw pile) (Vroom)

- TVSi-pile (Volker Staal en Funderingen)

With a screw pile, it is possible that a grout injection takes place at the tip when the pile is inserted. This pile type is therefore called an SI-pile. This promotes the insertion of the piles in the presence of solid soil layers by reducing the skin friction during installation. For all SI-piles. Water and/or grout injection takes place at the bottom of the pile when the pile is inserted.

As previously stated in this chapter, torque and axial downwards forces are crucial parameters during the installation process. In The Netherlands typical ranges of torque tend to range between 400 to 500 [kNm] and the downward forces tend to range between 500 to 800 kN. Table 2.1 provides some numbers showing the limits of torque and axial force for different suppliers in The Netherlands (Smienk et al., 2010).

Another characteristic that is important to consider for the installation process is the amount of sound that is emitted when installing cast-in place screw piles. The average decibel at 10m distance from the pile being installed is within the range of 80 to 85 dB.

The screw tip also has a varied range of possible diameters, these can range from 340mm to 950mm. The diameter of the pile tip will always be larger than that of the pile shaft partly because of the casing that is removed after the concrete has been poured in. Now that transverse dimensions have been covered, for the longitudinal dimensions of the Fundex type pile, the maximum pile lengths that are currently used in The Netherlands are approximately 65m long, bored in two segments.



Figure 2.5: Example of how a tie-rod looks like in a rebar cage

An example of drilling rigs used in current practice is the IHC FUNDEX TBX or TTD type which has a high torque capacity and can be used with grout injection. This machine can

have up to 17 RPM (revolutions per minute).

### 2.3.2. Standards and Load-Bearing Capacity

The standards used nowadays are the NEN9997-1 with the CUR guideline 2001-4. Due to the shape of the pile tip, a pile class factor that accounts for the friction generated during installation is the following for cast-in-place screw piles. This pile class factor is denoted by the symbol,  $\alpha$ , and has different values for the pile tip, for a pile in compression, and for a pile in tension. Table 2.2 denotes the different types of friction factors, their values for SI piles and their symbols.

Type	Pile tip	Compression	Tension
Notation	$\alpha_p$	$\alpha_s$	$\alpha_t$
Value for SI-Piles	0.63	0.009	0.009

Table 2.1: Pile Class factors, dimensionless parameters

The pile factors in Table 2.2 are from the NEN9997-1 standard. These factors work in the relationship between the shear strength at the pile interface and the base resistance through equations 2.1 and 2.2:

$$\tau_s = \alpha_s q_c \quad (2.1)$$

$$q_b = \alpha_p q_c \quad (2.2)$$

Where  $\tau_f$  is the shear strength,  $q_b$  is the base resistance and  $q_c$  is the cone resistance.

However, an important aspect to keep in mind is that for anchor piles of the Fundex type, a value of  $\alpha_t = 0.9\%$  is considered the minimum value that can be taken. In modern practice, this factor is often taken to the upper limit of  $\alpha_t = 1.2\%$  which signifies that larger forces are needed to uplift the pile.

# 3

## Literature Study

### 3.1. Theoretical Framework

#### 3.1.1. The Basis for Design of Pile Foundations

Pile foundations belong to the category of deep foundations for which the basic principle is to have a long columnar tube that goes down in a soil medium. The primary purpose of such a structure is to transfer construction loads into stronger soil layers below the surface. In the western Netherlands, soil layers are typically composed of Holocene (soft, clayey) and Pleistocene (sandy) soils. For construction works with large loads in locations where soft soils are found, pile foundations are needed to transfer the construction loads into a stiffer medium deeper in the subsoil to provide the necessary bearing capacity to hold the structure stable.

The design methods for piled foundations must account for the complex processes that occur during installation and loading of said pile, and it has to be carried out using the information from a site investigation. The geotechnical design of piled foundations involves assessment of site investigation and addresses certain design aspects such as:

- Bearing Capacity
- Lateral capacity
- Installation: hole stability, grouting and drivability
- Group effect, relevant for the overall foundation stiffness
- Other considerations (seismic response for instance)

Pile foundation strength is usually linked to the friction angle for soils in drained conditions and to the undrained strength for soils in undrained conditions. The bearing capacity of a pile is composed of two terms that define the load transfer which are the shaft resistance, which is the friction along the pile's length, and the base resistance, which is the resistance at the pile tip, and another term that is the self-weight of the pile. A schematisation of a

single pile is shown in Figure 3.1:

$$V = Q_s + Q_b - W'_p \quad (3.1)$$

Where  $Q_s$  is the ultimate shaft resistance,  $Q_b$  is the ultimate base resistance,  $W'_p$  is the self-weight of the pile and  $V$  is the ultimate bearing capacity of the pile. Note that these three terms have force units [kN] and that  $Q_s$  and  $Q_b$  are not the same as shaft resistance,  $\tau_s$ , and base resistance,  $q_b$ . The terms in this equation can be broken down further be-

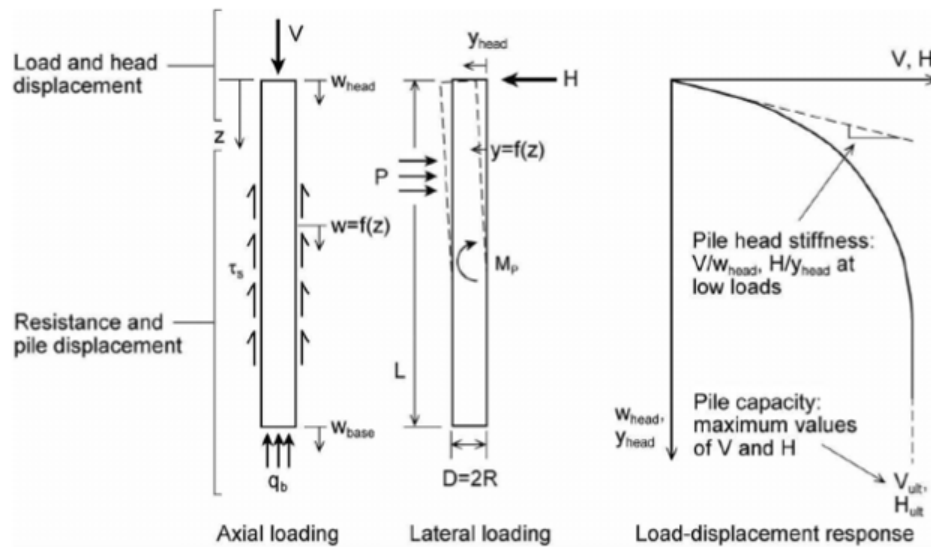


Figure 3.1: Pile response and Load-settlement response (Mark Randolph and Susan Gourvenec, 2017)

cause they differ depending on the type of soil that the pile is installed onto. For uncemented soils, the shaft resistance is a function of the horizontal effective stress at failure that acts on the shaft,  $\sigma'_f$  and the mobilized coefficient of friction  $\delta$  (Mark Randolph and Susan Gourvenec, 2017).

$$Q_s = \pi D \int_0^L \tau_{sf} dz = \pi D \int_0^L \sigma'_f \tan \delta dz \quad (3.2)$$

A parameter that is dictated by the roughness of the pile-soil interface and the effect of loading on strength, stiffness and consolidation of the soil material,  $\alpha$  (Mark Randolph and Susan Gourvenec, 2017). There is quite a lot of uncertainty regarding this parameter because it accounts for the many mechanisms previously mentioned but it is the most utilized method to determine the shaft resistance. For the ultimate shaft resistance equation 3.2 is still used.

$$\tau_s = \alpha q_c \quad (3.3)$$

The ultimate base resistance,  $Q_b$ , is the product of the pile base area and the maximum stress that can be mobilised on that base,  $q_b$ . Equation 3.4 shows the equation for ultimate

base resistance for a circular pile.

$$Q_b = \frac{\pi D^2}{4} q_b \quad (3.4)$$

### 3.1.2. Axial Loaded Piles

There are three general methods to investigate pile behaviour which are the following:

- Empirical methods, experimentally based and not fully based on soil mechanics principles
- Methods based on simplified theory and/or analytical correlations
- Methods of site-specific analysis based on advanced analytical and/or numerical analysis. Such analyses may include finite element methods, material point methods, boundary element methods, etc.

The bearing capacity of single piles consists out of the bearing capacity at the base of the pile and the positive skin friction around the pile shaft. In Dutch practice, the maximum base bearing capacity is determined by the method of Koppejan. This empirical method is based on the results of a Cone Penetration Test (CPT). The maximum shaft resistance is also based on CPT results (Van Gorp, 2014).

An important key point to keep in mind when working in Dutch conditions is the effect of the negative skin friction that occurs due to clayey soil consolidation. This negative skin friction applies an extra load onto the pile (Rajapakse, 2016). Eurocode 7 determines this effect via the Slip-method.

### 3.1.3. Settlement Behaviour

For settlement calculations of a single pile, there are two major aspects to consider. These are the settlement at the pile base, and the elastic deformation of the pile. In Dutch practice, the load-transfer method, first proposed by Coyle and Reese (1966) is used to determine said settlements.

### 3.1.4. Piles in Tension vs Compression

Piles that experience tension loads are those piles that are being pulled-out. This happens for instance for constructions below the water table. There are two primary effects that need to be considered when dealing with piles in tension, which are the pull out resistance, and the rise of the tension pile with the accompanying soil mass (this is related to the group effect, soil heave and weight of the soil plug around the pile). The most critical aspect for this research is that when piles are in tension then there is no base resistance, which means the resistance is mainly supported by the shaft resistance. This also means that they have different friction factor  $\alpha$ .

### 3.1.5. Determining Bearing Capacity: Dutch NEN1997-1 and CUR166

The NEN is The Royal Netherlands Standardization Institute and it sets the standards for all geotechnical projects done in The Netherlands. In Eurocode 7 on the serviceability limit

state (SLS) design of compression and tension piles is provided in section §7.6.4. This section states that the vertical displacement under SLS conditions shall be assessed against the requirements given. This is a method that defines the SLS by calculating the pile displacement, in other words it consists of looking at the load-settlement behaviour of the pile and after a certain amount of displacement is achieved (the SLS) than the load corresponding to that displacement is the maximum load that the pile can carry before failure, or the bearing capacity. The failure load or bearing capacity is defined as the load for which the displacement is 10% the diameter of the base of the pile.

In order to determine the shaft resistance a pile class factor is used. This factor is a friction coefficient that describes the roughness of the pile-soil interface, and is dependent on the installation method used for the pile. There are three variations of this factor according to the Eurocode 7, these are the coefficient for the pile tip, for a pile in compression, and a pile in tension, with their respective symbols  $\alpha_p$ ,  $\alpha_s$ ,  $\alpha_t$ . In this thesis the interest lies in tension piles and thus  $\alpha_t$  is going to be used. For Screw-injection piles this factor is equal to 0.009 but this value can be considered as a minimum and can have an upper limit up to 0.012. The Dutch method is also a direct CPT method, for which the cone resistance obtained from conducted CPT tests are used to determine the shaft resistance, this leads to the following equation:

$$\tau_s = \alpha_t q_c \quad (3.5)$$

Where:  $\tau_s$  is the shaft resistance,  $\alpha_t$  is the friction coefficient for a pile in tension, and  $q_c$  is the cone resistance from the CPT.

The second important component for bearing capacity is the base resistance of the pile. For this Van Mierlo Koppejan (1952) determined that the shear band failure at the pile tip follows a logarithmic spiral that spirals along the pile shaft. The proposed influence zone according to this logarithmic spirals is up to 0.7D to 4D underneath the pile tip and in between 5D to 8D above the pile tip level. The following figure shows a representation of the Van Mierlo Koppejan shear band model.

From Figure 3.20 one can see that there exists 3 different regions (I, II, and III) for which there are different cone resistance values. Having this in mind, the following equation shows the determination of the pile base resistance:

$$q_b = \frac{1}{2} \alpha_p \beta s \left( \frac{q_{c;I;avg} + q_{c;II;avg}}{2} + q_{c;III;avg} \right) \quad (3.6)$$

Where:  $q_b$  is the base resistance,  $\alpha_p$  is the pile tip friction coefficient,  $\beta$  is a factor that takes into account the pile foot shape,  $s$  is a factor that takes into account the cross-sectional shape of the pile base, and lastly the  $q_{c;N;avg}$  are the average cone resistances for the 3 different sections of the shear band defined by Van Mierlo Koppejan. However for our research on SI-piles, only the shaft resistance is considered as the piles are being subjected to tension, thus there is no influence from the pile base.

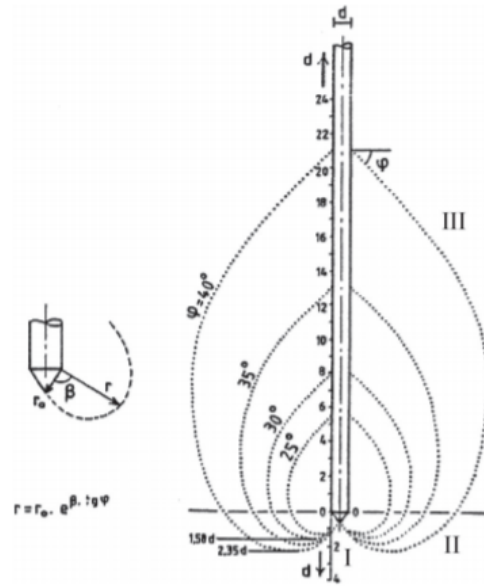


Figure 3.2: Shape of the failure mechanism around a pile tip defined by Van Mierlo Koppejan, 1952. Photo from (Van Baars et al.)

For tension pile tests the CUR166 standard is used. In The Netherlands this practice is used, and it consists of measuring the axial displacement of the pile over time, and set to a limit threshold of failure dictated by a creep criterion. The threshold is set by a creep coefficient, denoted as  $c$ , and can be determined via equation 3.19.

$$c = \frac{\delta_1 - \delta_2}{\log(t_1) - \log(t_2)} \quad (3.7)$$

For which:

$c$  = creep coefficient;

$\delta_1$  = pile head displacement at time  $t_1$ ;

$\delta_2$  = pile head displacement at time  $t_2$ .

Moreover, the ultimate shaft resistance according to the NEN9997-1 is given by equation 3.8.

$$F_t = \sum_{i=1}^n z_i (q_{c,i} * 10^3) * 2\pi r * \alpha_t [kN] \quad (3.8)$$

## 3.2. Influence of Grout

Grouting is widely used as a ground improvement technique used to improve foundations where there is a loose state of the soil. Grout can be injected into the soil, or also applied into foundations such as the pile structure. When it comes to the composition of the grout, certain elements that are of most importance, those are notably the Water/cement (W/C)

ratio and the chemical composition of the mixture itself (including additives). Grouting reduces pile settlement and improves the bearing capacity of a pile (Krasinski, 2018). However when dealing with SI-piles the main objectives are to enhance soil displacement near the pile tip and reduce the friction during the extraction of the casing which in turn improves the skin/shaft friction of the pile.

### 3.2.1. Influence of Grout at the Pile Shaft

For cast-in-place SI piles the grout delivery system is situated only at the base and as the pile is being drilled the grout flows outwards to the soil but also around the pile that is being screwed downwards.



Figure 3.3: Pile grout delivery system for a SI pile

Grout can affect the soil in multiple ways. Having a grout pressure that is too high may cause unexpected fractures on the soil body; the pore-water pressure also increases which decreases the effective stress of the soil (Fattahpour, 2015). Therefore, it is clear that certain grout installation parameters, notably the W/C ratio, which affects the water content in the grout mixture, and the grout injection flow, which affects the pressure at which the grout leaves the delivery system and it affects the amount of flow going into the soil.

### 3.2.2. Installation Process of Grout in Pile Shaft

For a typical set of screw piles, the pile is equipped with an internal pipe through which the grout flows. Said pipe extends downwards through the bore of the tubular pile shaft. Fluid grout is then injected with high pressure into the soil surrounding the pile. Said pressures can be even greater than 200 psi. The two main characteristics of a screw pile are its load-bearing capacity and its lateral deflection capacity. Excluding the influence of the soil conditions, the load-bearing capacity is largely influenced by the diameter and length of the pile, as well as the pile tip shape or helices (in the case of helical piles) that it may have (Nasr, 2008). These pile parameters in turn also affect the torque applied. Short full-displacement piles will require greater torque than long full-displacement, this was discussed in section 2.2. In the course of installation, the grout is being injected as the pile is being rotated downwards, which therefore also spreads the grout vertically along the pile as it is moving. The focus of this research is primarily on the Fundex type screw-injection pile where grout does not eject from the sides of the pile as shown in Figure 3.7 for the case of the helical pile.

It is essential that a combination of medium grouting pressure occurs simultaneously during the rotation of the pile. This allows for higher load-bearing capacities compared to grouting in a stationary position (Nasr, 2008).

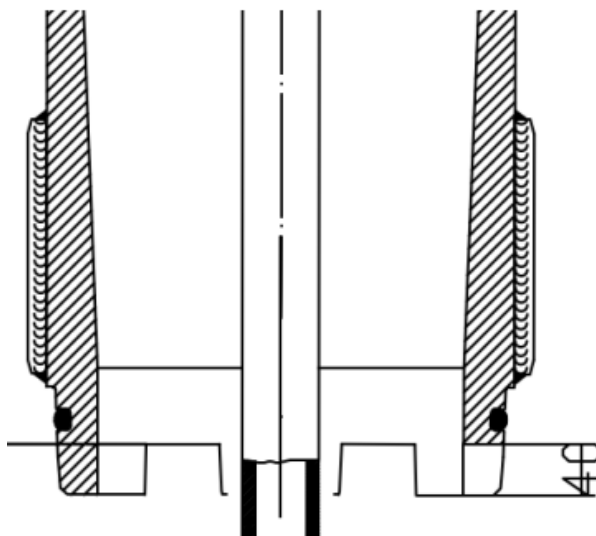


Figure 3.4: Pile crown diameter. The shaded regions are the steel strips that determine the actual concrete pile diameter.

For SI-piles as the delivery of the grout happens at the base but from there it is spread through the shaft in moments. The first moment is when the pile is being pushed vertically down during screwing and the rotation happens clockwise (under standard pile tip shape, but this drilling direction is dictated by the screwing direction of the pile tip), the second moment occurs when the casing is being extracted for which the rotation changes direc-

tions (from clockwise to counter-clockwise and back to clockwise) over a time interval of a few seconds. The oscillation of the casing during extraction has to do with the construction of the casing bottom; Figure 3.4 shows two steel strips sitting around the pipe collar; these determine the actual concrete pile diameter.

### 3.2.3. Water/Cement Ratio (W/C)

The water-cement ratio (W/C) is a ratio based on the weight of the water and the cement used in a mixture. This ratio is of importance for cement-based materials such as concrete, grout and mortars. The W/C ratio directly influences the strength, durability and flowability of the mixture material. Additionally, other elements are often added into the mix such as superplasticizers and sand. For concrete typical ranges of the W/C ratio are between 0.4 or 0.6. However, for grout, the amount of water exceeds the amount of cement.

The water-cement ratio affects the following aspects of the grout material: deformation modulus, compressive strength, permeability. The compressive strength of the material as well as the Young's modulus decrease with a higher W/C ratio. However, the permeability increases quite drastically with higher W/C ratios. For grout, the amount of water that has a chemical reaction with the cement is rather limited. This leaves a surplus of water in the grouted body when using high W/C ratios. This fact in relation to the relationship found between the W/C ratio with the compressive strength and the Young's modulus leads to a reduction of mechanical performance of the grout. For projects done in cohesive soils, in order to acquire higher performance the grout with a lower W/C ratio is usually preferred as the filling degree of the grout in the void space of the soil medium plays an important role in determining the grout reinforcement effect. However, a high W/C ratio reduces the viscosity when grout permeates into the void spaces of the soil medium, not to mention that lower viscosity also makes the grouting process easier as it offers less resistance to make it flow through the injection system, which in turn is beneficial for improving grouting reinforcement effect (Li et al, 2020).

Two important properties that play a role regarding the grouting reinforcement effect, those are the filling rate of the grout and the effective filling rate, respectively defined as the percentage of volume of grout to the volume of the soil medium, and the effective filling rate is the percentage of the volume of the cement component to the void volume of the soil. From Figure 3.5 it can be seen that as the W/C ratio increases, the filling rate increases and tends towards reaching 100% for W/C ratios of approximately 1.5, whilst the effective ratio will logically decrease as W/C increases. Figure 3.5 shows the filling rate for a fine sand with particle size ranging from 0.063-2.5mm. However, one aspect to note is that the particle size and the closest packing of the sand particles are of importance, often the sand particle pores are not large enough for the cement particles to infiltrate.

It is of interest to know typical values for W/C used in the field (Dayakar et al, 2012) conducted an experiment on permeation grouting on sandy soil with variations of the W/C ratio as the body of sand was subjected to compression. Table 3.1 shows the 7 different W/C ratios used in the study. From this, the relationship between the load-settlement be-

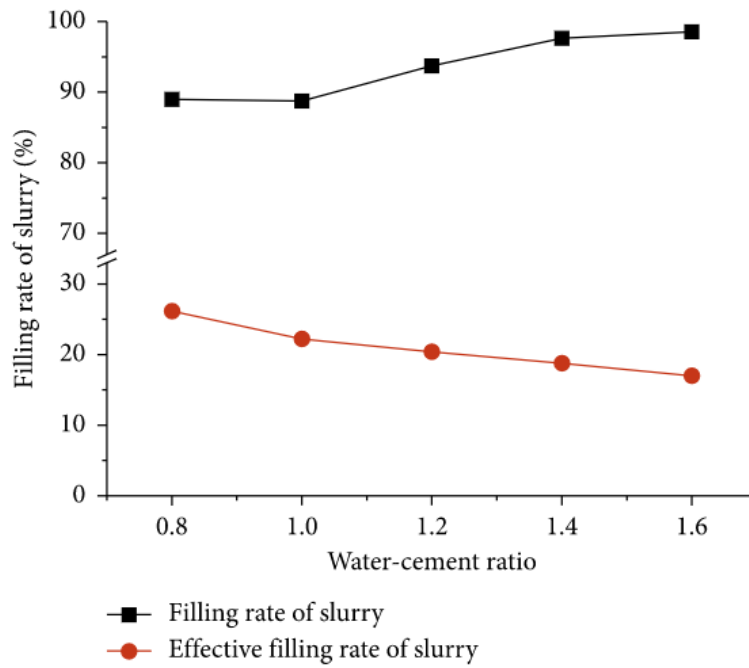


Figure 3.5: Grout injection in the course of pile rotation (Li et al, 2020)

haviour and the W/C ratio was determined.

Notation	Water	Cement
G1	10	1
G2	9	1
G3	8	1
G4	7	1
G5	6	1
G6	5	1
G7	4	1

Table 3.1: Different W/C ratios and their notations

The effects on the load-settlement behaviour have been evaluated for different W/C ratios is shown in the following set of Figures 3.6 3.7 (whilst keeping the notation stated in Table 1):

From Figures 3.10 and 3.11 it can be seen that the lower W/C ratios in both dense and loose sands tend to have less settlements. For loose sands the load-settlement relationship is more clearer whilst for the denser sands the relationship is not as direct as for the loose sands yet the tendency is still the same. This leads to the conclusion that the higher the W/C ratio, the more tendency for higher settlement will there be for a particular load. The capacity of the pile in current practice is judged by its load-settlement behaviour, after a certain percentage of settlement occurs failure is considered. So linking that back to the W/C ratio, the lower it is the less settlements occur and thus leading to a higher pile capac-

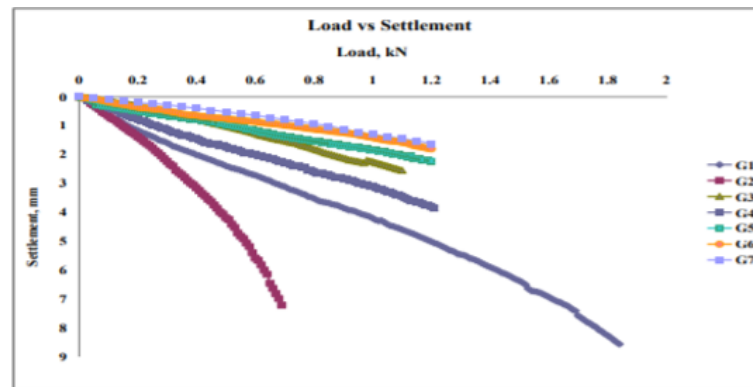


Figure 3.6: Load-settlement behaviour with grouting with different W/C ratios - for 7 days curing in loose sand (Dayakar et al, 2012)

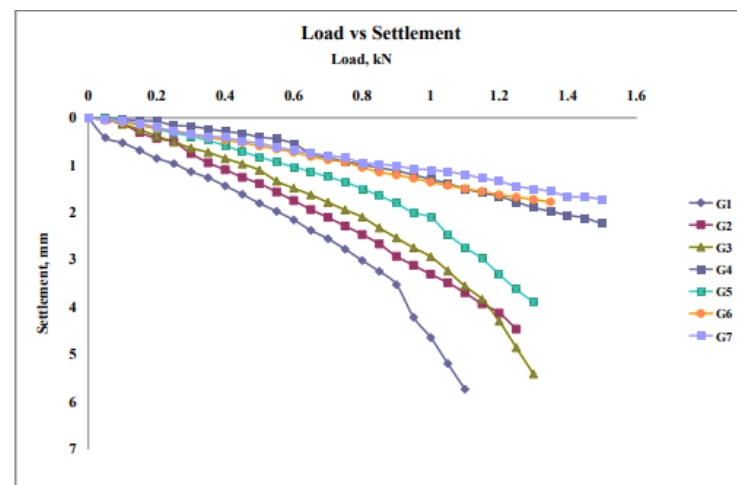


Figure 3.7: Load-settlement behaviour with grouting with different W/C ratios - for 7 days curing in medium dense sand (Dayakar et al, 2012)

ity. While this experiment was not conducted for SI-piles, the effect of higher W/C ratios towards the grout is observed in this experiment which suggests that it is possible for SI-piles installed with grout with higher W/C ratios the shaft capacity should tend to decrease. For screw-injection piles a W/C ratio in the range of 1.25-2.0 is what is normally used in practice in The Netherlands.

### 3.2.4. Chemical Composition of the Grout Mixture

There are four main phenomena involved when dealing with grout composition which are the bleeding (which is the effect of segregation between the water and sand particles where the coarser grains sink and the fine grains are pushed upwards) the setting time, the strength and the viscosity (Azadi, 2017). Bentonite is a known clay from the montmorillonite group which has always been used for reducing the bleeding, yet it causes a reduction in the strength of the grout. Another main ingredient of chemical grouting is Sodium silicate, which is typically used to increase the strength of the cement-based grout, as well as to reduce the bleeding as well. Appropriate percentages of this additive were obtained in the range of 2%-5% (Azadi, 2017).

The most important phenomenon to consider for the grout is the excessive bleeding, which

is the free water in the grout mix that rises upwards to the cement particles settling by gravitational action. Although something called internal bleeding can also occur which affects the bonds of the cement paste, this makes the cement mixture to be prone to micro-cracking once it hardens (Azadi, 2017). The main factors that lead to excessive bleeding are the composition, and the higher the W/C ratio is, the more likely there is for excessive bleeding to occur.

### 3.3. Additional Aspects of Installation

#### 3.3.1. Penetration Depth and Torque

For a cast-in-place screw pile, the penetration depth is greatly influenced by the relative density of the soil surrounding the pile. As mentioned in previous sections, screw cast-in-place piles are a type of ground displacement piles and thus are pushing the surrounding soil in the horizontal direction, which causes soil densification at the soil-pile interface. The diameter of the pile is an important factor that affects the relative density changes as penetration depth increases. However, on average the apparent density changes that occur during the screwing motion in dense sands are minimal compared to their initial relative densities (Jeffrey, 2016).

Depending on this compaction experienced during the screwing, higher torque is required. Screw piles can be used for a variety of scenarios due to how deep these piles can reach and also due to the soil conditions that these are being drilled onto. Although considerable depths can be reached via screw piles, harder soil bodies such as dense sand can cause problems for penetration. In such cases, it is required to have some grout flow in order to lubricate the pile casing as it is being screwed downwards since it reduces the friction at the pile-soil interface. For screw piles, the installation torque increases linearly with penetration depth. This can be seen in Figure 3.8. Grout injection helps to enhance penetration speed, reducing the torque and increasing the rotation speed.

It is important to understand that there is an important relationship between torque and shear stress. Torque causes a body to rotate about an axis, and shear stress depends on the applied torque, the distance of the radius of the shaft and the polar moment of inertia, which is a quantity that describes torsional deformations and it is a function of geometry which is independent of the shaft material.

$$\tau = \frac{Tr}{J} \quad (3.9)$$

$$J = \frac{\pi}{2}r^4 \quad (3.10)$$

Where  $\tau$  is the shear stress,  $T$  is the torque [ $kNm$ ],  $r$  is the radius of the shaft, and  $J$  is the polar moment of inertia [ $m^4$ ]. Moving onto the shear strain,  $\gamma$ , this is determined by the angle of the rotation,  $\theta$  as well as the distance of the radius and the length of the shaft,  $L$ . Equation 3.6 is applicable for both elastic and plastic ranges of a material (Collins, 2019).

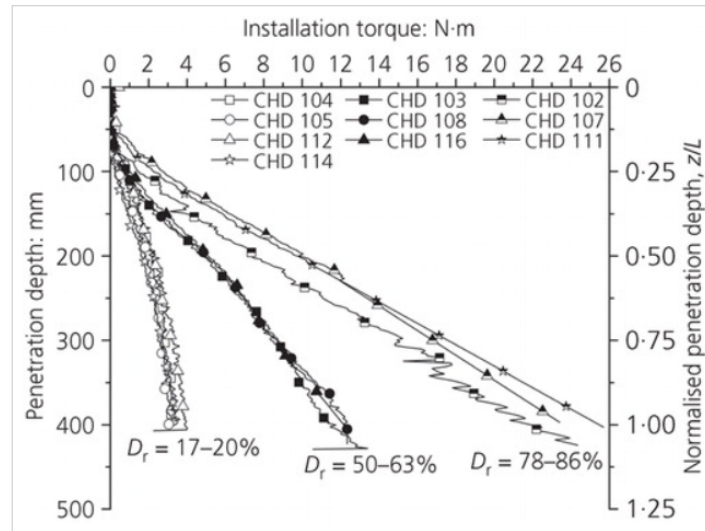


Figure 3.8: Relation between the penetration depth and the torque for different relative density states (Jeffrey et al, 2016)

$$\gamma = \frac{r\theta}{L} \quad (3.11)$$

Now that the basics of torque and its relationship with shear stress and strain have been covered it is important to notice that this has a direct relation to the shaft resistance experienced during the drilling of a screw cast-in place pile, this can be seen in equations 3.2 and 3.3. The  $\alpha$  parameter in equation 3.3 is described as a roughness parameter and it is a coefficient of friction ranging from 0-1 (or 0% to 100%). There is a link between this friction at the pile-soil interface and its relation to the torque induced by the screwing motion of the screw pile, and as previously stated in this section, with higher penetration depth there will be higher torque needed, meaning higher forces required to maintain the screwing motion. Grout lubrication serves to reduce the torque of the shaft as it is being installed. Lubrication minimizes the heat generated at the pile-soil interface when the pile is in motion. This is why for harder materials such as sands and especially dense sands in order to penetrate deeper into the soil it is common to utilize grout not only for its lubrication benefits but also because as discussed in section 3.5 it supplements the base and shaft resistances and thus improves the pile capacity overall.

### 3.4. Grouting Flow Properties

For this research, it is important to look into the flow properties of the grout. It must be recognized that grout is not a Newtonian fluid, but rather it approaches the properties of a Bingham plastic, but in some cases, it can also be a pseudoplastic material for which its dynamic viscosity can either increase or decrease with increasing shear stress. This difference exist due to the composition of said grout, but in this thesis, the primary focus is on Bingham plastic grout mixtures. These types of fluids act as solids until subjected to yield stress and then act as a liquid. For grout mixtures, water is added and in a barrel, the mixture is stirred at a certain speed to keep said mixture in liquid. The penetration rate is also

affected by the grout mixture's composition (which includes the aggregates and the ratio of water/cement) because the viscosity of said grout is a parameter relating to the internal friction in the fluid which limits the movement of the screw motion of the screw injection pile as it is drilling. The grout is mainly used as lubrication in order to enhance the penetration depth, so there is an important link between these two. Now another parameter that comes into play since we are dealing with fluid dynamics is the flow rate at which the fluid is travelling through the delivery pipe, this is in units of volume over time. Given a set of assumptions such as laminar flow, incompressible fluid and that the Bingham plastic will act as a perfectly Newtonian fluid after reaching the yield stress, then the Hagen-Poiseuille law can be used to relate the pressure drop to the dynamic viscosity and the flow rate of a fluid flowing through a pipe, this is defined in equation 3.8 ((Ryen et al. 2017):

$$Q = \pi \frac{(\Delta P)r^4}{8\eta L} \quad (3.12)$$

For which  $Q$  is the flow rate in litres per second [ $l/s$ ],  $\Delta P$  accounts for the pressure difference between the two ends of a section of the pipe, measured in [ $Pa$ ],  $\eta$  is the dynamic viscosity measured in Pascal seconds, [ $Pa \cdot s$ ], and  $L$  is the length of the section in [ $m$ ].

What is observed during plastic flow for Bingham plastics is that at pressures below the yield point some slow creep can be observed. The suspension flows as a solid plug which is lubricated by a film of liquid at the capillary walls of the pipe. What the presence of this creep tells us is that no matter how low the pressure is, there will always be some flow, even if this might be diminutive. Green (1949) redefined the standard model of the Bingham plastic and concluded that there was no absolute yield point but an approximation to this yield point can be derived which corresponds to the yield point required to initiate laminar flow (Ryen et al, 2017). This can be seen in Figure 3.9:

For the flow of a Bingham plastic in a round pipe, the following applies according to Green (1949); as the pressure gradually increases from zero, the suspension begins flowing as a plug and the velocity profile will then be a straight line normal to the pipe's axis. This schematic is shown in Figure 3.10. The relationship between the shear stress and the pressure and the velocity of the flow can be seen in equation 3.9 (Ryen et al, 2017):

$$\frac{RP_0}{2L} = \tau_0 \quad (3.13)$$

$P_0$  represents the pressure required to initiate plastic flow. When pressures exceed  $P_0$ , the laminar flow progresses towards the axis of the pipe, which reduces the area of the plug in the centre of the pipe and surrounding it with a larger zone where laminar flow occurs. This can be seen in Figure 3.14 (B). Having said this, an important property of these types of fluid behaviour is that the plug can never be fully reduced to 0, no matter how large the pressure becomes, this is also depicted in Figure 3.13 in the flow pressure vs flow rate relationship for which one can see that the asymptotic value of perfect laminar flow can never be reached, just approached. As 'r' approaches zero, P approaches infinity to satisfy the equation for the shear stress. This leads to the conclusion that the consistency curve for

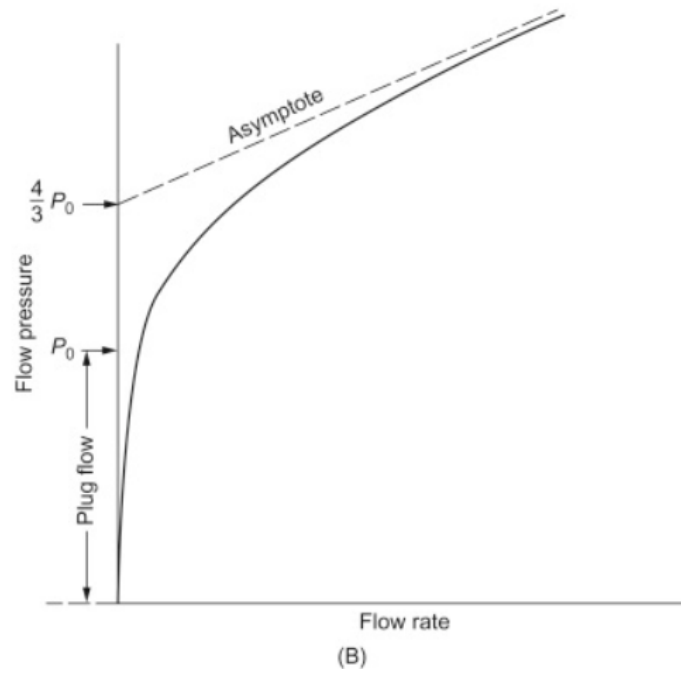


Figure 3.9: The observed consistency curve for a Bingham plastic, where  $P_0$  is the actual yield point and  $4/3$  is the apparent yield point. Creep is neglected in this depiction. (Ryen et al, 2017)

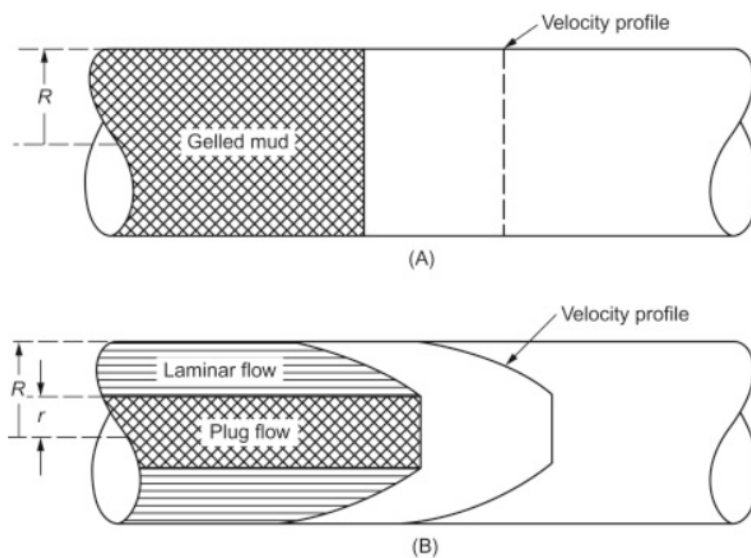


Figure 3.10: (A) Plug flow of a Bingham plastic in round pipe, where  $R\rho/2L < \tau_{y0}$ . (B) Mixed flow of a Bingham plastic in round pipe.  $R\rho/2L < \tau_{y0}$ ,  $r\rho/2L = \tau_{y0}$ . (Ryen et al, 2017)

a Bingham plastic in a round pipe is therefore always nonlinear regardless of how large or small the shear rate is (Ryen et al, 2017).

Understanding these concepts relating to the fluid flow for a Bingham plastics are important in understanding how grout flows through the delivery tube in the screw-injection pile. The relationship between the velocity profile and the pressure in a tube has been discussed and from this, it is important to understand that the more the flow is laminar the better

flowability of the fluid there will be as can be seen via the change in velocity profile in Figure 3.14 (B). In current Dutch practice, the injection flow of the grout for SI-piles is determined with a function of the injection flow rate in [ $m^3/min$ ] and the surface area of displacement,  $A_{disp}$ . This ratio is estimated to be between 0.5 and 0.75. For the SI-piles that are going to be analysed in this paper, an injection flow rate of approximately 75 [ $l/min$ ] is going to be considered. From this information it would appear that increasing the flow rate of the grout delivery system higher than 75 litres per minute gives a diminutive increase in the performance of the grout acting as a lubricating agent for the screw pile, this may signify that the velocity profile and/or that the viscosity remains unchanged past this point.



# 4

## Testing and Data Collection

### 4.1. Experimental Framework

As described in the introduction of this thesis paper, the NVAF in conjunction with the TUD and Deltares research programme conducted a full-scale experiment to study the behaviour of screw-injection (SI) piles when varying grouting parameters during the installation phase. The two main parameters of interest were the W/C ratio and the flow rate of the grout fluid. There is also an interest in observing the effect two different cement compositions have, these two are the CEM III/B (pure portland blast furnace cement, no limestone present), the Webertech GM42 (which is a blend of 75% CEM III/B and 25% limestone). Because of the implementation of the mixture of GM42 the majority of this research will be conducted in terms of W/B ratio. Note that W/C ratio will be the same as W/B ratio for pile groups A, B, C and D. It is difficult to accurately determine the W/C ratio for group E since the specific gravity of the limestone in the mixture can vary widely, therefore the W/B is preferable to use. The purpose of the tests is to determine the tensile bearing capacity of screw piles and to what extent does the shaft bearing capacity of ground displacement screwed piles differ from grout lubrication. A full-scale static pile load test (in tension) was conducted, for which 8 loading steps were applied and the load-settlement behaviour was analysed. A total of 15 piles were tested, and within these 15 piles there are 5 categories of three piles each for which the installation conditions are different, this is further explained in section 4.2.1.

The test location is in the vicinity of Lemsterhoek in the industrial district in the town of Lemmer, Friesland which is in the northeastern part of The Netherlands. Soil conditions are composed of a layer of crushed type 1 sand fill (also known as Repak), peat and a denser sand layer at the bottom of the strata. The test site is in a depot site that belongs to Gebr. van 't Hek B.V. Figure 4.1 shows a satellite image of the site.

#### 4.1.1. Site Investigation

The location of the test is in the northeastern part of The Netherlands in the industrial area of Lemmer, Friesland. The 18 CPTs were split into two rows of 9 were taken; a schematization of this set-up can be seen in Figure 4.2. The intention is to model each pile as if they were single piles and not as a pile group, thus a certain centre-to-centre distance from each

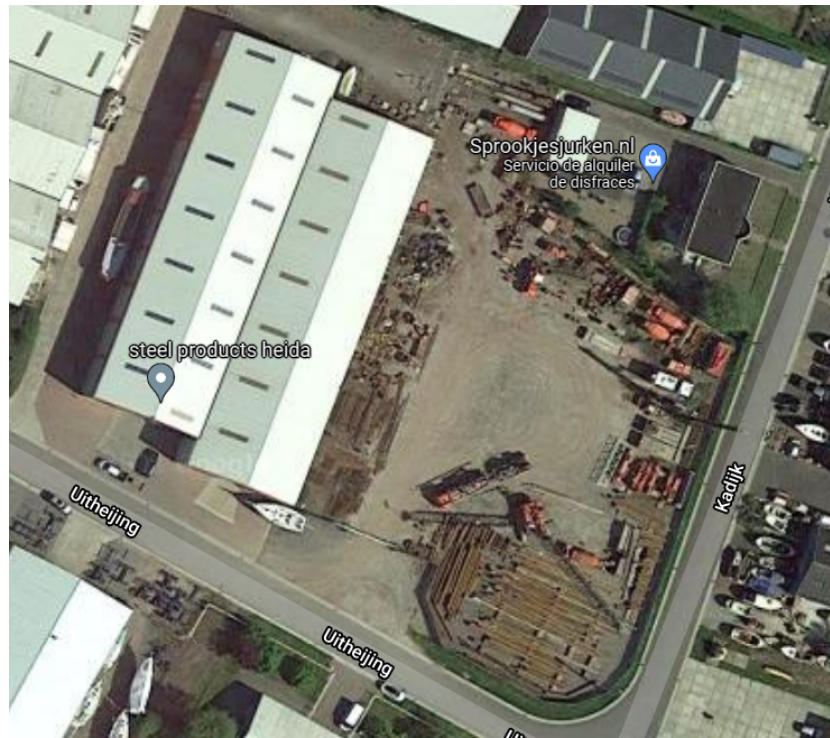


Figure 4.1: Aerial satellite image of the test site.

pile must be respected. According to the Dutch Code and Handboek Funderingen, this distance is to be in the range of 2.25 to 2.5m; however, a distance of 2.7 between each pile in a row was chosen instead to make sure that the pile group effect is avoided. Two rows were made and they are separated by a distance of 9m.

After obtaining the CPT results, the next step was to create 5 groups of 3 piles for which the cone resistances were similar. The pre-installation CPT results can be found in Appendix A. Even though the cone resistance of all the 18 piles was similar, it is important to have the pile groups that are being tested in the most homogeneous arrangement. For this, the mean squared error (MSE) allowed us to compare the data sets of the cone resistance and pair up the most similar soil conditions to form the groups. Equation 4.1 shows how the MSE is obtained:

$$\text{MSE} = \frac{1}{n} \sum_{i=1}^n (q_{c;i} - \hat{q}_{c;i})^2 \quad (4.1)$$

Where  $q_c$  is cone resistance for one CPT and the  $\hat{q}_c$  represents the second CPT that is being compared to the first.

It is important to note that soil investigations have been done on the site for previous projects, thus data on the volumetric weight of the soil has been obtained and can be seen in Table 4.1.

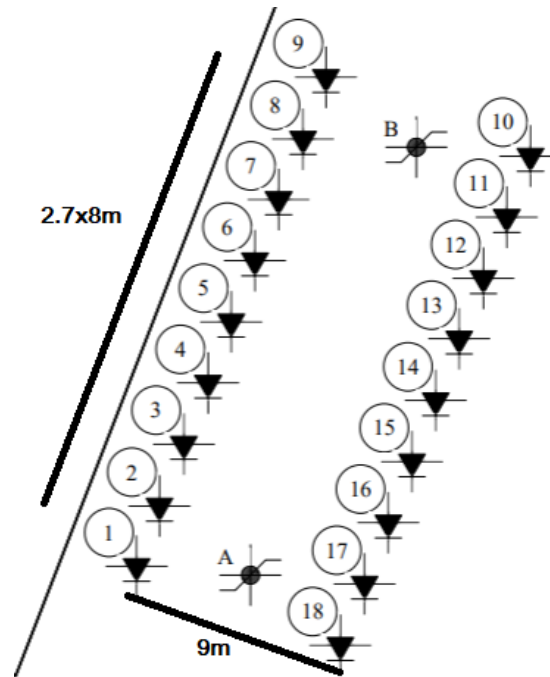


Figure 4.2: CPT locations at the test site. The numbered locations next to the black triangles are the CPT locations and the black circles denoted by the letters A & B are locations where core samples are taken

Soil type	Volumetric Weight [ $kN/m^3$ ]
Repak	19
Peat	1
Sand	10

Table 4.1: Volumetric Weight of Soils

#### 4.1.2. Pile Configuration

Table 4.2 shows the final subdivision of groups along with the varying parameters attributed to each category.

As can be seen in the table above, for each variation 3 data points being collected, the notable differences between these pile groups are the following set of W/B ratios: 1.25, 2, 2.5, 3.75; the different grout injection flow rates were 75 and 115 [ $l/min$ ] and lastly, the Group E piles are made with a different cement mixture, Webertech GM42, whereas the remainder of the piles is made with the CEMIII B cement.

#### 4.1.3. Preliminary Force Calculations

Before installation of the piles, it is important to make certain predictions on what the expected bearing capacity of the pile will be. For this, the NEN9997-1 Dutch code is used as a guideline to perform such calculations. First and foremost it is important to know that the tests are being done in tension, meaning that the bearing capacity will depend entirely on shaft capacity since the resistance of the pile being pulled upwards will solely come from the pile-soil interface. From this we know that the relevant area for this problem is found

CPT	Pile	Ground Level	W/B* ratio	Flow Rate	$F_{t;\alpha=0.9\%}$	$F_{t;\alpha=1.2\%}$
[-]	[-]	[-]	[-]	[l/min]	[kN]	[kN]
Group A						
9	A1	-0.28	1.25	75	972	1296
17	A2	-0.35	1.25	75	999	1332
18	A3	-0.33	1.25	75	1132	1509
Group B						
12	B1	-0.28	2.5	75	1159	1545
13	B2	-0.25	2.5	75	1132	1509
15	B3	-0.29	2.5	75	1219	1625
Group C						
4	C1	-0.42	3.75	75	1531	2042
6	C2	-0.43	3.75	75	1438	1918
7	C3	-0.45	3.75	75	1485	1980
Group D						
1	D1	-0.43	2.5	115	1432	1909
8	D2	-0.49	2.5	115	1372	1829
14	D3	-0.30	2.5	115	1432	1909
Group E						
2	E1	-0.45	2.0	75	1125	1500
5	E2	-0.48	2.0	75	1432	1909
11	E3	-0.27	2.0	75	1225	1634

Table 4.2: Table of the pile group subdivision with their respective W/B ratio and grout flow parameters.  
**Note:** W/B ratio is the same as W/C ratio for all pile groups except for E.

at the area of the pile interface; in other words, the circumference of the pile multiplied by its height. Equation 4.2 has been used to solve for the pull-out force of the piles.

$$F_t = \sum_{i=1}^n z_i (q_{c;i} * 10^3) * 2\pi r * \alpha_t [kN] \quad (4.2)$$

Where  $z_i$  is the depth interval corresponding to the cone resistance value from the CPTs,  $q_c$ , the multiplication by  $10^3$  is due to the fact that the cone resistance is expressed as MPa and thus it is necessary in order to keep units consistent with  $kN$ . Then the coefficient of friction is a crucial parameter that has been discussed in section 3.8.4, and this is dependent on the method of installation of the pile. As stated by the NEN9997-1, for screw piles this factor is of the order of 0.9% however since a grout solution is being added into the soil, an upper limit must be considered, this upper bound is of the order of 1.2%. Because of these two limits of the coefficient of friction, two results for pull-out force are calculated for each pile, this can also be seen in the last two columns of Table 4.3. These calculations were essential for two main reasons, the first being that the results of the field are going to be compared to these values, and the second reason is that this also allows us to know what force the anchor rod passing through the concrete piles is supposed to be capable of withstanding. An important point to add is only the sand layer will be considered in the

preliminary calculations. Looking at the friction angle, medium sand can range from (30-36) whereas peat is in-homogeneous by nature and of very low friction angle, could be very close to 0 (Ritonga, A. S., 2020). This means that most of the resistance will come from the sand layer. However, an important deviation from the NEN9997-1 is done here. The code states a limit of 15 MPa must be applied to the cone resistance when making the preliminary design of piles in tension, however here in this research no limit is considered for  $q_c$ .

CPT Position	Pile Name	Preliminary Failure Load
[-]	[-]	[kN]
1	D1	1432
2	E1	1125
4	C1	1532
5	E2	1432
6	C2	1438
7	C3	1485
8	D2	1372
9	A1	972
11	E3	1225
12	B1	1159
13	B2	1132
14	D3	1432
15	B3	1219
17	A2	999
18	A3	1132

Table 4.3: Preliminary Pull-out force calculations based on the Pre-installation CPTs

#### 4.1.4. Pile Installation

Two sets of CPT readings were applied to the site, one which is the pre-installation CPTs which were taken at the central axis of where the piles were to be installed, and the second set are the post-installation CPTs, this set includes two CPTs per pile location which are located at approximately 0.75m from the pre-installation CPT location. The pre-installation CPTs are put in place in order to develop the preliminary design for the pull-out force required to lift the piles and the soil cone failure to know if the soil would not collapse during the pile pulling operation. Normally post-installation techniques are only executed to see the ground improvement after the installation of the piles. Figure 5.1 shows the distribution of the pre- and the post-installation according to the Rijksdriehoekscoördinaten Dutch coordinate system.

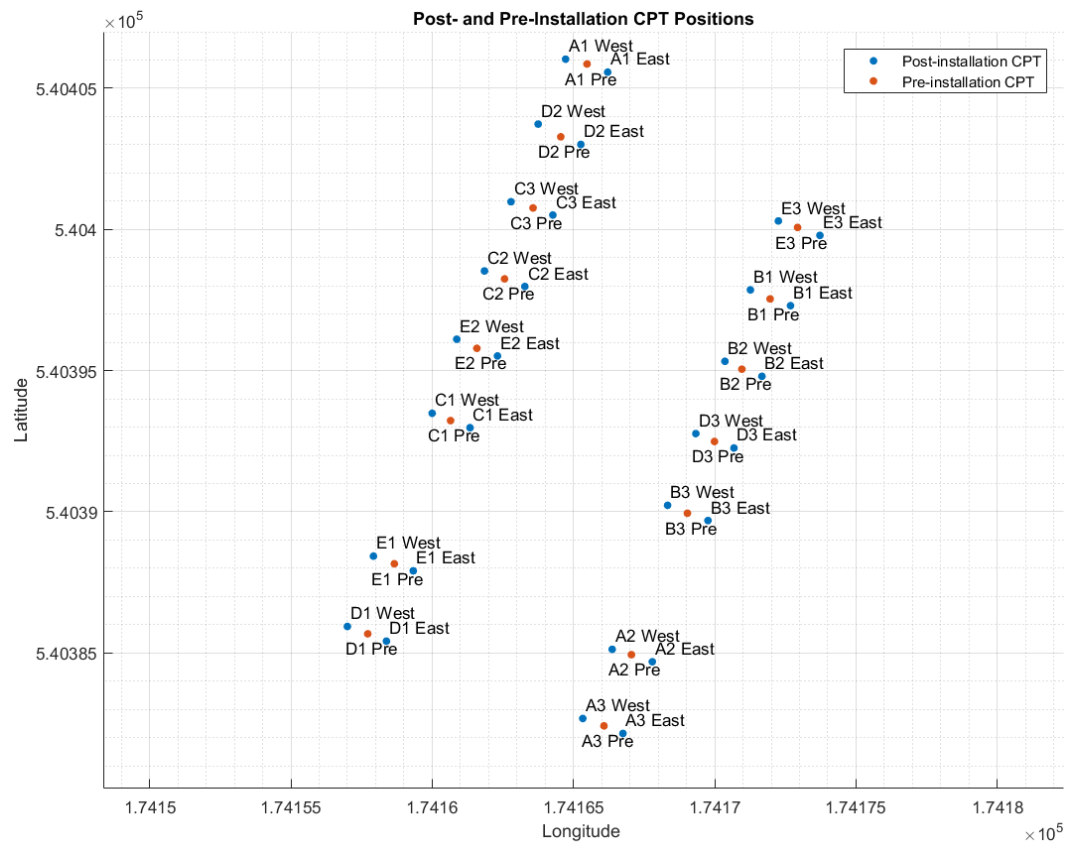


Figure 4.3: Location of the post-installation and pre-installation CPTs with relation to the Rijksdriehoekskoördinaten, RDX and RDY coordinates.

#### 4.1.5. Test Set up: Static Pile Load Test

The failure load of the tension piles is determined on the peak tensile load measured in the NPR 7201\_2017+A1\_20 Geotechnical as stated in the NPR 7201\_2017+A1\_2020 Geotechnical Engineering in which it describes the determination of the axial bearing capacity of foundation piles by means of test loads for a axial bearing capacity of foundation piles utilizing test loads for a class B test. The test set-up consists of a double H beam with pulling screw-on child beams. The main beams are supported on bulkhead stacks with a clearance from the centre pile of at least 2.5m. A maximum of 5 % increase in the horizontal grain tension on pile occurs due to bulkhead stacks.

**The procedure of the test:** Pull-out force,  $F_t$  can initially be assumed to be equal to the prediction with  $\alpha_t = 0.9\%$ .

Load steps for tensile test  $\Delta F = F_t/8$ . The failure criterion is met when the head displacement reaches  $> 0.1 \cdot \text{Diameter of the pile} = 47 \text{ mm}$ .

For the first 5 steps, use a time of 20 minutes per step instead of 1 hour to determine the creep limit. After load step 4, return to the initial Force,  $F_i$  and maintain this for 15 minutes. Continue with step 5 to establish elastic pile deformation.

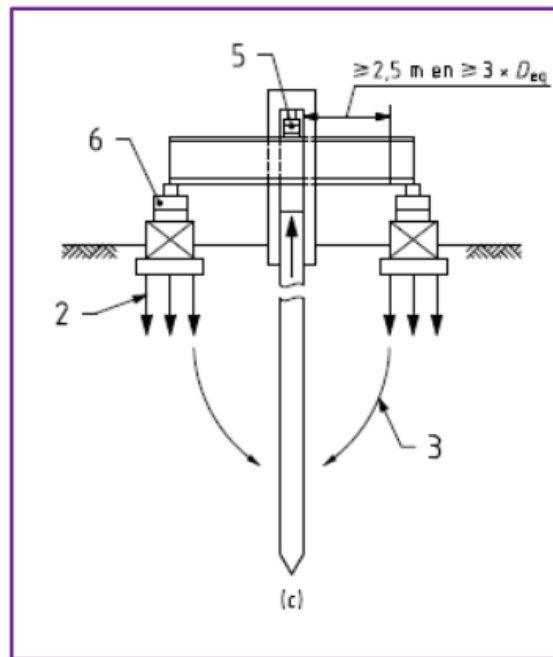


Figure 4.4: Typical set up of the Static Pile Load Test

- Apply tension to the assembly with  $F_i$  (no load)  $< 0.05 * F_{pullout}$
- Apply load step  $\Delta F$  in  $> 5$  minutes
- Maintain force for at least 1 hour (20 minutes)
  - If head displacement last 20 minutes  $< 0,1$  mm = ready
  - Otherwise, check every 20 minutes for 0.1 mm up to a maximum of 4 hours
- Apply next load step in  $> 5$  minutes

## 4.2. Data Collection and Methodology

The general outline of the research methodology can be seen in Figure 4.4. Five main areas are looked into, the arrows represent the link between these areas and the grout parameters and the shaft capacity (or frictional capacity).

### 4.2.1. Collection of Grout Samples

During the installation of the piles, there are multiple times where grout samples are collected. The injection grout is measured first, and during installation, the backflow grout is collected at two instances, when the pile reaches depth -6m NAP and -9m NAP. The intention is to collect sufficient grout at these three instances mentioned to be subjected to three tests. These tests are comprised of two UCS tests and one Bending test. A bleeding test is also applied for which grout is placed on a graduated cylinder and after one hour the

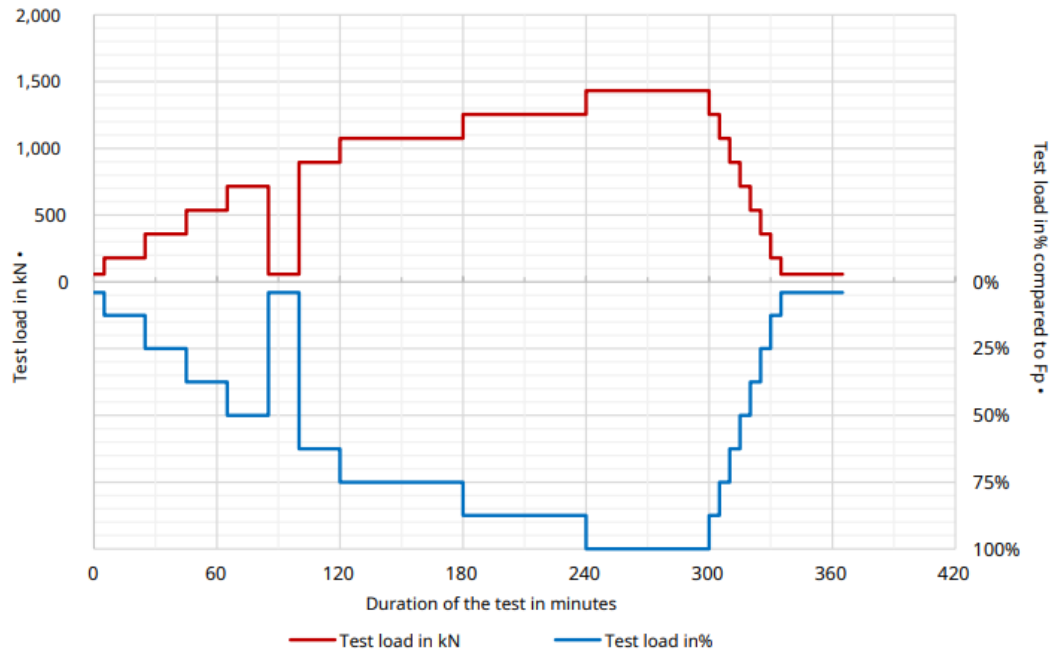


Figure 4.5: Loading scheme for the Test piles of Lemmer

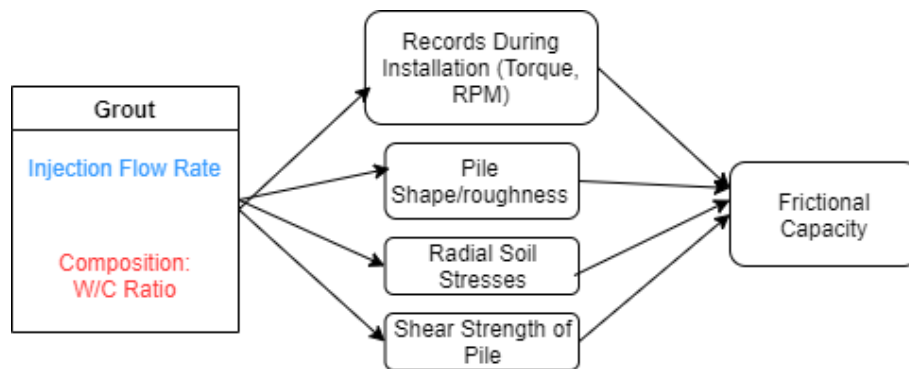


Figure 4.6: General outline of the research methodology

bleeding would be observed. This process is applied for all 15 piles. The reason for collecting backflow data is because, as stated in Chapter 2, SI-piles are partial displacement piles for which the grout transport and mixing with the surrounding soil is a portion of that displacement. Additionally, grout being mixed with the surrounding soil will also envelop the piles and thus become a part of the pile-soil interface. Multiple relationships can be drawn from the tests: (A) the relationship between the initial grout flow and the backflow material properties (densities, bleeding), (B) the relationship between the backflow properties and the final (measured) bearing capacity.

#### 4.2.2. Assessment of Radial Soil Stresses

**The effects of the installation method on soil properties/soil stresses will be studied by analysing CPT data (before and after pile installation).** Two sets of CPTs are taken, one before the installation of the piles, and the other after the installation. Normally only pre-installation CPTs are taken in order to develop the preliminary design for the pull-out force,

but the post-installation CPTs are taken to observe and to measure the difference in soil conditions. This means looking at the improvement or reduction in the cone resistance, one of the most crucial parameters that are currently utilised in the Dutch standards in order to determine the shaft resistance of a tension pile. The purpose of this assessment is to find (A) the relationship between the grout parameters (W/B and flow rate) and  $q_c$ , (B) the relationship between the  $\Delta q_c$  and the shaft bearing capacity  $F_t$ .

#### **4.2.3. Assessment of Grout Properties and Shear Strength**

**Effects of installation method on pile strength by testing grout samples (unconfined compression and bending).** After the collection of the samples, an assessment of the collected return flow of the grout was conducted. The relevant properties are the density, [ $kg/m^3$ ]; the bleeding after one hour of collection, in percentage %; the dry and wet weight of the samples, as well as the weight of the water present in the sample; the cement content of the samples, one per pile category; and finally the tests performed on hardened samples after 28 and 56 days of curing, these tests include a compression strength test and the bending stress test. These properties are taken for depths of -6 and -9m NAP. The collected data can be seen in Appendix E.

#### **4.2.4. Assessment of Pile Shape**

**Effects of installation method on pile geometry and roughness will be researched by extracting the piles.** Several piles of the site were removed and the diameters of these piles are taken. It was not possible to extract all the piles (from CPT position 1 to 9) due to the fact that this row was next to an existing building and could compromise the stability of the structure. This means that only piles from CPT positions 11, 12, 13, 14, 15, 17 and 18 were extracted. The diameter of these piles was taken for every meter along its length. The purpose of taking these measurements is to observe the spread of the grout along the pile and to see if there is any relationship between the thickness of the grout bulb or grout volume around the pile and the shaft bearing capacity.

#### **4.2.5. Assessment of Load-Displacement Data**

**Effects of installation method on ultimate interface shear strength will be studied by performing pile load tests.** A static pile load test is conducted for which the criteria of failure according to the Dutch codes states that failure occurs at 10% of the diameter of the pile, or more precisely 47mm. Since the piles are in tension, the load at failure is equivalent to the shaft bearing capacity. This assessment covers a comparison of the measured capacities to the predictions, a mobilised shear stress analysis, and an analysis of the  $\alpha_t$  factor. The purpose of this assessment is to find a relationship between the development of stresses during loading and the grout installation parameters and also to try to optimise the empirical  $\alpha_t$  parameter.



# 5

## Analysis

In this chapter the data collected from the full-scale pile tests are analysed and the direct and indirect relationships between the grout installation parameters and the shaft capacity are drawn. The method used for prediction is the NEN-99971 which as discussed in Chapter 3 of this report, includes two key parameters which are the cone resistance,  $q_c$ , and the  $\alpha_t$  parameter which encompasses multiple aspects of the installation method and design of the pile. Grout is being mainly used in SI-piles for lubrication purposes and to fill some of the gap created from the difference in diameter between the pile tip and the casing. The aspects that are being analysed here are the change between pre-installation and post-installation  $q_c$ , the torque during the installation, the amount of sand removed due to grout backflow, the density of the backflow material (the material that partially fills the pile-soil interface), the shear stress properties, and the pile volume after complete hardening of the grout. The relationship between the grout installation parameters (W/C ratio and flow rate) and the aforementioned properties are drawn, as well as the relationship between them and the shaft capacity. For the majority of this chapter the term W/B (Water/Binder) ratio will be used since group E piles are made with a grout mixture that is not entirely based on cement as described in Chapter 4. It is important to mention that while the targeted W/B ratios were 1.25, 2.5, 3.75, 2.5, and 2.0 for Groups A, B, C, D and E respectively, the composition of the mixture injected differed slightly. Table 5.1 shows the W/B ratios used during the test.

### 5.1. Load-Displacement Analysis

This section discusses the results of the static pile load test in tension described in Chapter 4 of this thesis. Test data of test piles A2, A3, B1 and B3 contain negative values of pile head rise. The pile head rise in the initial steps with negative values cannot be trusted. Figure 5.1 shows the load-displacement curve of pile A1. The other load-displacement curves can be found in Appendix D.

Pile Name	W/B Ratio at Pile Installation	Group Average
[-]	[-]	[-]
A1	1.26	1.29
A2	1.31	
A3	1.3	
B1	2.2	2.93
B2	3.57	
B3	3.03	
C1	3.57	3.827
C2	3.9	
C3	4.01	
D1	2.19	2.15
D2	2.34	
D3	1.92	
E1	2.45	2.527
E2	2.32	
E3	2.81	

Table 5.1: W/B ratios during the pile installation.

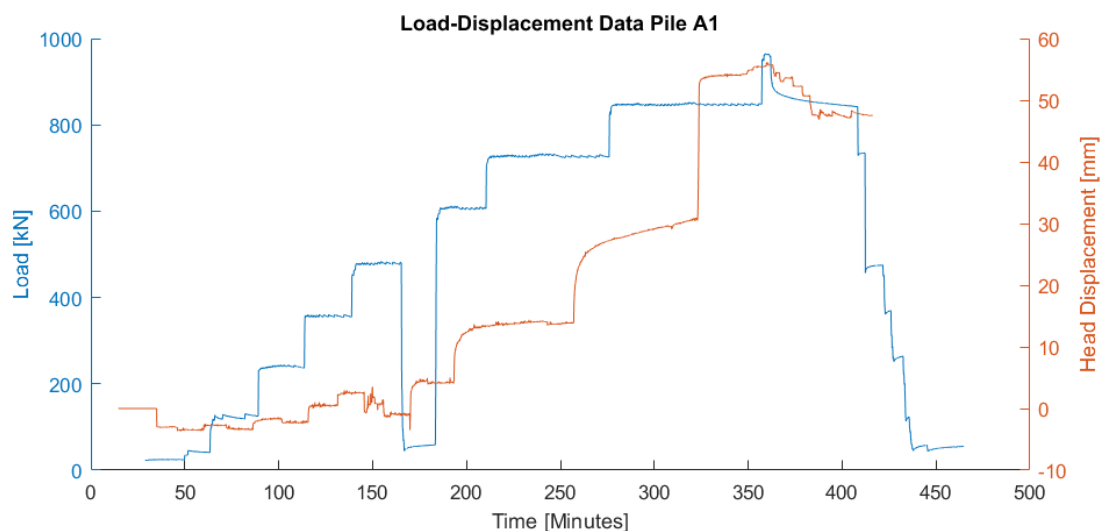


Figure 5.1: Load-Displacement plot showing the load in [kN] the pile head rise in [mm] and the time duration of the static pile load test for pile A1.

### 5.1.1. Comparison Predicted vs Measured Data

In order to examine how comparable the predicted values of shaft capacity are to the measured values from the static pile load test, the ratio of Measured/Predicted values is taken, denoted as M/P ratio. It can be seen that the predictions were very close to what was measured during the static pile load test in tension. For pile category A, B and E the M/P ratio is very close to 1 with roughly an uncertainty of  $\pm 0.079$ , but for pile categories C and D the measured results had a larger uncertainty. This potentially means that the currently used method of failure load prediction in The Netherlands is less accurate for situations where W/C ratios greater than 3.57 and where flow rates are 115 [l/min].

Pile Name	Measured Failure Load	Predicted Failure Load	Ratio [M/P]
[-]	[kN]	[kN]	[-]
A1	965	972	0.993
A2	972	999	0.973
A3	1117	1132	0.987
B1	1182	1159	1.020
B2	1210	1132	1.069
B3	1302	1219	1.068
C1	1319	1532	0.86
C2	1321	1438	0.919
C3	1272	1485	0.857
D1	1247	1432	0.870
D2	1244	1372	0.907
D3	1077	1432	0.752
E1	1102	1125	0.980
E2	1319	1432	0.921
E3	1250	1225	1.020

Table 5.2: Comparison of the measured and predicted shaft capacity

Moreover, the direct relationship between the shaft capacity (measured/predicted ratio) is compared to the W/C (or W/B) ratio, shown in Figure 5.2. One of the research objectives of this research was to **observe the influence on load-settlement behaviour changes in the W/B ratio and high injection flow rate**. It can be seen from the figure that a forced trend can be seen, thus it is not sufficient to draw a direct relationship with W/B ratio and shaft capacity. This is especially noticeable when looking at  $W/B = 3.57$  where B2 and C1 have the same W/B but very different M/P ratios, this means that it cannot be concluded that W/B ratio directly affects the shaft capacity. Figure 5.3 shows the direct effect of grout injection flow rate on the shaft capacity. With only two groups we can only say that the M/P ratio is drastically affected by the increased flow rate.

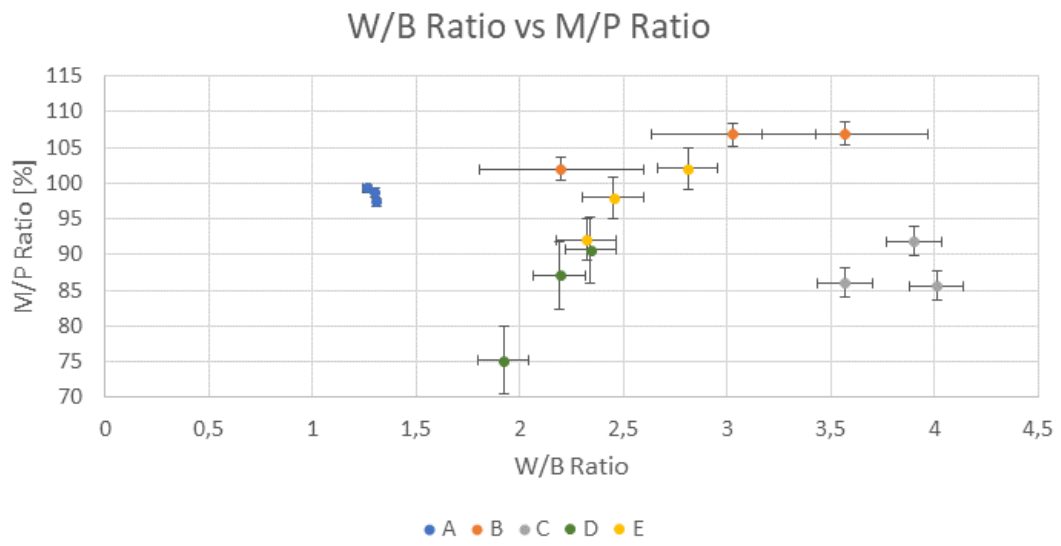


Figure 5.2: W/B ratio at injection vs the M/P ratio for all 15 piles.

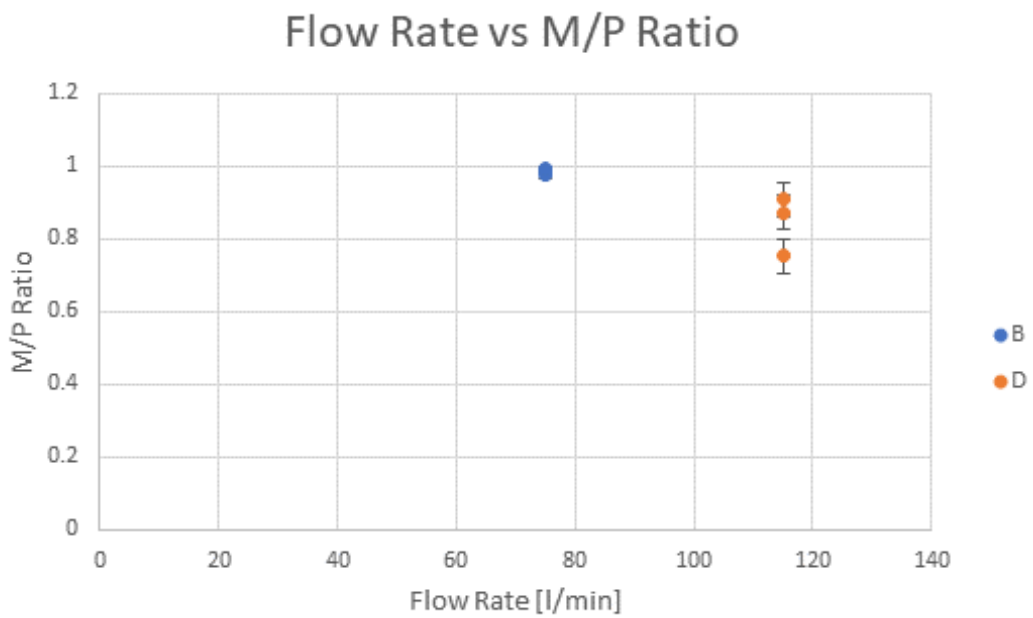


Figure 5.3: Flow rate of the grout vs the M/P ratio for Group B and D.

### 5.1.2. Alpha-Factor Analysis

Along with the cone resistance,  $q_c$ , the other parameter in the governing equation for the prediction is the  $\alpha_t$ , thus an analysis is conducted. Modified  $\alpha_t$  parameters can be derived by using the M/P ratio. This leads to the results of Table 5.3. The group mean gives us the most adequate correction factor of  $\alpha_t$  for each pile category and the Coefficient of Variation, COV, is the statistical measure of the dispersion of the data set (standard deviation) relative to the mean of said data set. A lower COV means that the factor is more adequate for the scenario in question. Due to the small sample size, it is hard to conclude that there exists a real trend regarding the high W/B ratio and high flow rate makes the  $\alpha_t$  factor closer to 0.00775. It could be interesting for further research to determine whether or not the  $\alpha_t$  factor should be around 0.00775 for higher W/B ratios (greater or equal to 3.75) and high grout injection flow rate.

Pile Name	M/P ratio	$\alpha_t$ Modified	$\alpha_t$ Mod ( $q_{c,max} = 15$ )	Group Mean (No Lim)	COV (No Lim)
[-]	[-]	[-]	[-]	[-]	[-]
A1	0.993	0.00895	0.00908		
A2	0.973	0.00878	0.00914	0.00888	0.0083
A3	0.987	0.00890	0.00946		
B1	1.020	0.00920	0.0100		
B2	1.069	0.00964	0.0101	0.00949	0.0217
B3	1.068	0.00964	0.0106		
C1	0.861	0.00777	0.0108		
C2	0.919	0.00828	0.0107	0.00793	0.0320
C3	0.857	0.00773	0.0106		
D1	0.871	0.00786	0.00982		
D2	0.907	0.00818	0.0102	0.00780	0.0426
D3	0.752	0.00737	0.00938		
E1	0.980	0.00883	0.00982		
E2	0.921	0.00831	0.0106	0.00878	0.0417
E3	1.020	0.00920	0.0106		

Table 5.3: The different measured  $\alpha_t$  parameters of the different pile categories and their respective Coefficient of Variation, COV.

## 5.2. Analysis of CPT Data

### 5.2.1. Description of Soil Properties and Variability

The soil conditions at the testing site in Lemmer, Friesland, is composed of three soil layers. From the ground surface to the bottom the following soils are found: backfill sand, peat, and sand. The layer thicknesses for the first two layers are approximately 1.2m and 2.3m. The ground level varies from -0.5m to -0.26m NAP. These conditions are seen throughout the test field where the 15 piles were installed. For this analysis only the bottom sand layer is considered for the prediction of the shaft capacity; this is because that peat has an inhomogeneous nature which could make it very difficult to take it into account for the prediction and the small top sand layer is a backfill sand so it has been manipulated thus not in its natural state.

The variability of the cone resistance,  $q_c$ , throughout the field is computed. Contour plots are used to look at an interpolated 2D field. The interpolation method used is the 'cubic' method and the models were created using MATLAB. The average  $q_c$  for the pre-installation situation for the entire sand layer (-4m to -9.5m NAP) is shown in Figure 5.2. All the  $q_c$  plots can be found in Appendix A.

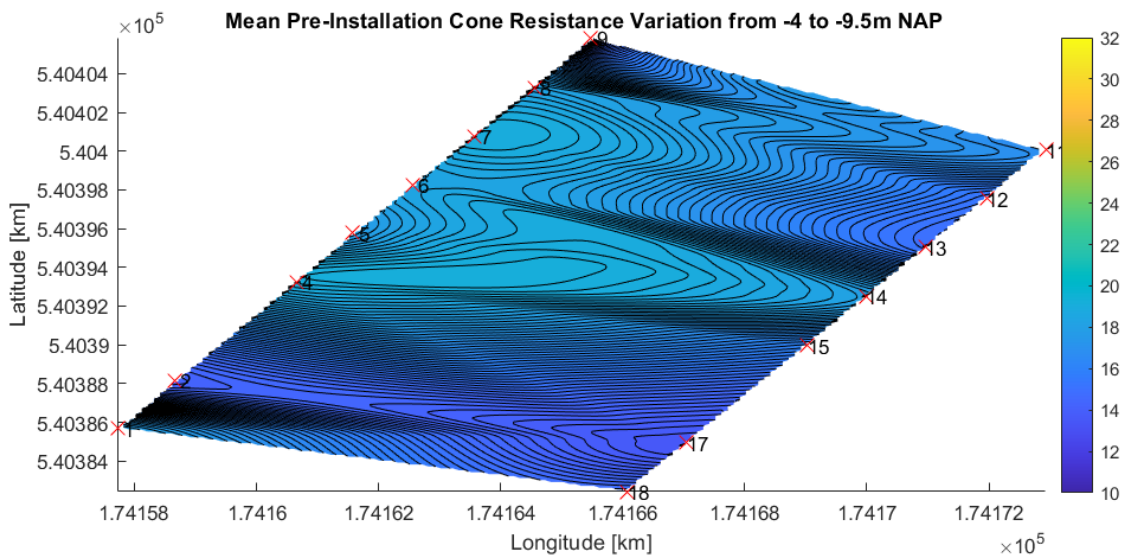


Figure 5.4: Contour plot of the average cone resistance of the pre-installation situation, where the red crosses indicate the location where the CPTs were taken.

### 5.2.2. Effects of Installation on Cone Resistance

After the installation of the 15 piles involved in this project, the post-installation CPTs were placed and the change in cone resistance was recorded. Figures 5.4 and 5.5 show the difference between the cone resistance before and after installation for the sand section until pile tip (-4m to -9.5m NAP) and the full section (from surface to pile tip) respectively. When looking at the coefficient of variation, CoV, of the pre- and post-CPTs, the CoV is roughly constant at around 0.73 when looking at the average CoV for all 15 piles. Thus there are no significant differences in standard deviations on either of the 3 scenarios of Post West/East and Pre.

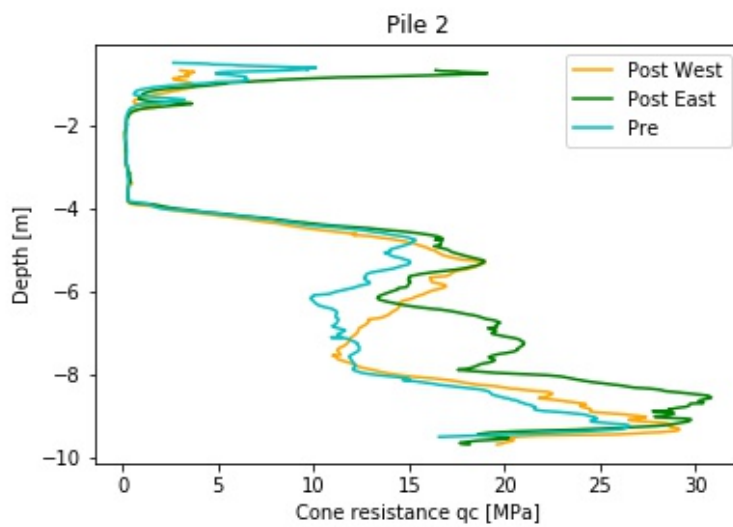


Figure 5.5: CPT profiles with Pre- and Post- installation  $q_c$  data for the full depth (from ground level to -9.5m NAP) for pile E1.

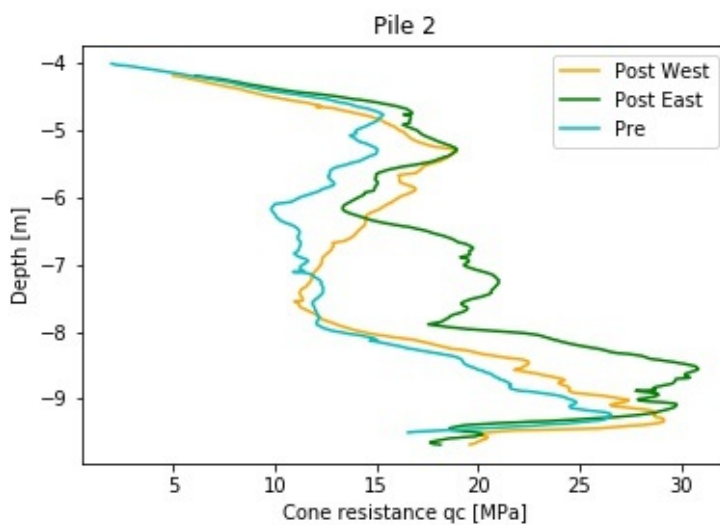


Figure 5.6: CPT profiles with Pre- and Post-installation  $q_c$  data for the sand section (-4.5 to -9.5m NAP) for pile E1).

In order to visualize the effect of the installation of the piles on  $q_c$ , a contour plot for the post-installation situation is shown in Figure 5.6.

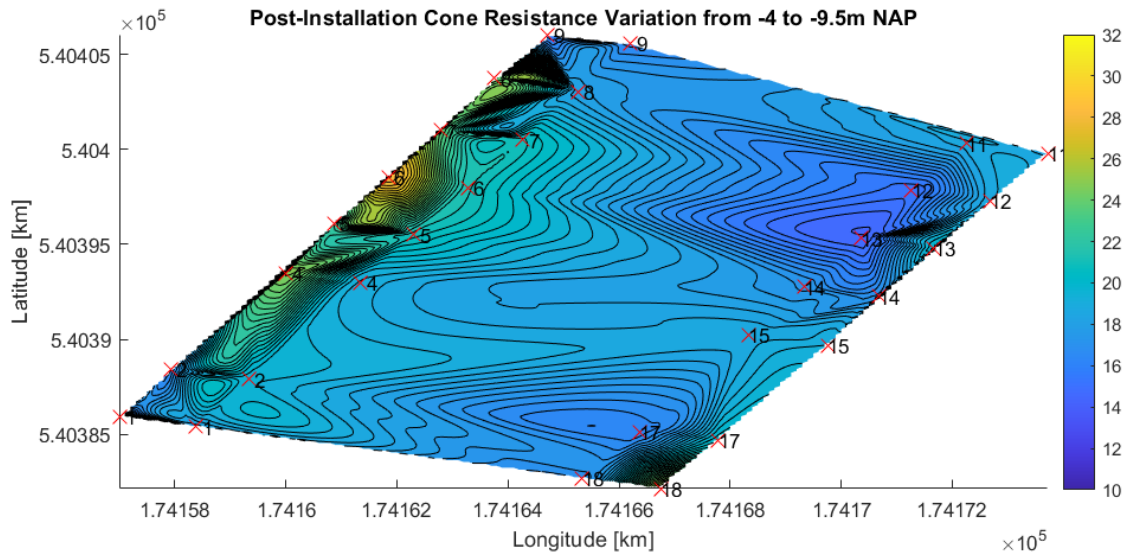


Figure 5.7: Contour map of the average cone resistance in the post-installation situation where the red crosses represent the location of the post-CPTs.

In order to compare the  $q_c$  before and after installation of the piles, the average of the post-CPT data is taken. The ratio of between the average post-CPT and the pre-CPT data is taken for the sand section, Figure 5.7 shows the change in  $q_c$  per every 0.01m in depth, where the green shaded areas represent an increase in  $q_c$  after installation, and the red shaded areas represent a decrease in  $q_c$  after installation. Two aspects are studied in this analysis. First, a comparison of the average  $q_c$  of the sand section per pile, which its purpose is to draw a relationship between the total increase in  $q_c$  and the shaft capacity. Second, a comparison of the vertical variability (measured at every 0.01m of the pile), which its purpose is to draw a relationship between the uniformity of the soil and the shaft capacity.

The average of the  $q_c$  change is captured for the entire sand section. The results of this comparison are found in Table 5.4. Table 5.5 shows the comparison between the SoF of the pre-installation and the post-installation situation. It can be seen from Table 5.4 that that Group D piles suffered from an overall decrease in cone resistance, and if a comparison is made with the M/P ratio, one can see that there is a relationship this decrease in  $q_c$  leading to a decrease in the M/P ratio. It can be concluded that a higher grout injection flow rate decreases the cone resistance in the sand layer which negatively affects the M/P ratio.

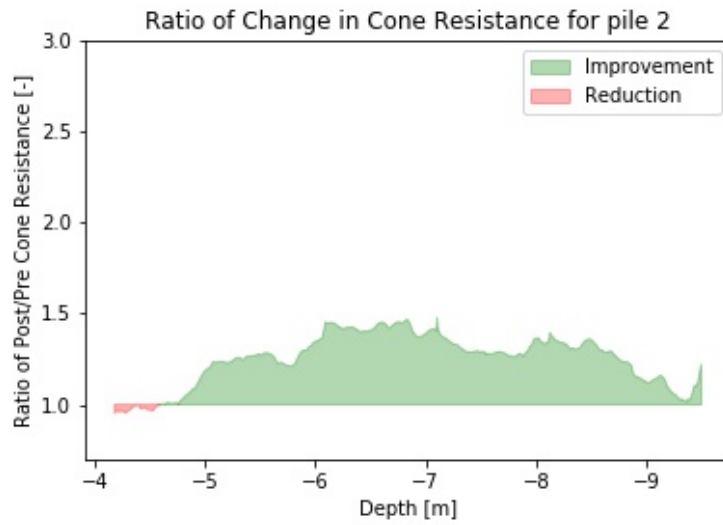


Figure 5.8: Ratio of change in  $q_c$  along the depth of the sand section for pile E1.

Pile	Mean $q_c$ of Pre CPT	Mean $q_c$ of Average Post CPT	% of Change	Group Average
[-]	[MPa]	[MPa]	[%]	[%]
A1	13.81	16.54	16.52	
A2	13.93	18.84	26.07	24.22
A3	15.37	21.99	30.08	
B1	15.72	17.54	10.35	
B2	15.57	17.91	13.09	12.87
B3	16.60	19.57	15.178	
C1	19.61	22.52	12.92	
C2	18.87	25.48	25.96	17.93
C3	19.58	23.02	14.91	
D1	18.54	15.89	-16.62	
D2	18.81	21.53	12.66	-2.83
D3	18.68	17.87	-4.54	
E1	14.57	18.47	21.09	
E2	18.27	22.09	17.30	16.08
E3	17.29	19.19	9.88	

Table 5.4: This table shows the percentage of change of cone resistance (improvement being positive, decrease being negative).

### 5.2.3. Relationship Between Grout Installation Parameters and Average Cone Resistance (Sand Section)

With the information from these tables, comparisons with the installation grout parameters have been made. First, Figure 5.9 shows the relationship between  $q_c$  and W/B ratio. The error bars tell us about the variation found in each category. It can be noticed that there is no relationship can be observed relating the increase in W/B ratio to the change in cone resistance. A possible explanation for this behaviour is that the inherent variability found in soils causes these differences in  $\Delta q_c$  rather than the changing grout installation parameters. Second, Figure 5.10 shows the relationship between cone resistance and the injection flow rate of the grout mixture. It can be seen that for pile group D (flow rate 115 l/min) the variation in  $q_c$  is extreme compared to group B, so it can only be concluded that variations in the increase in cone resistance are more predictable for flow rates of 75 l/min compared to higher flow rates like 115 l/min.

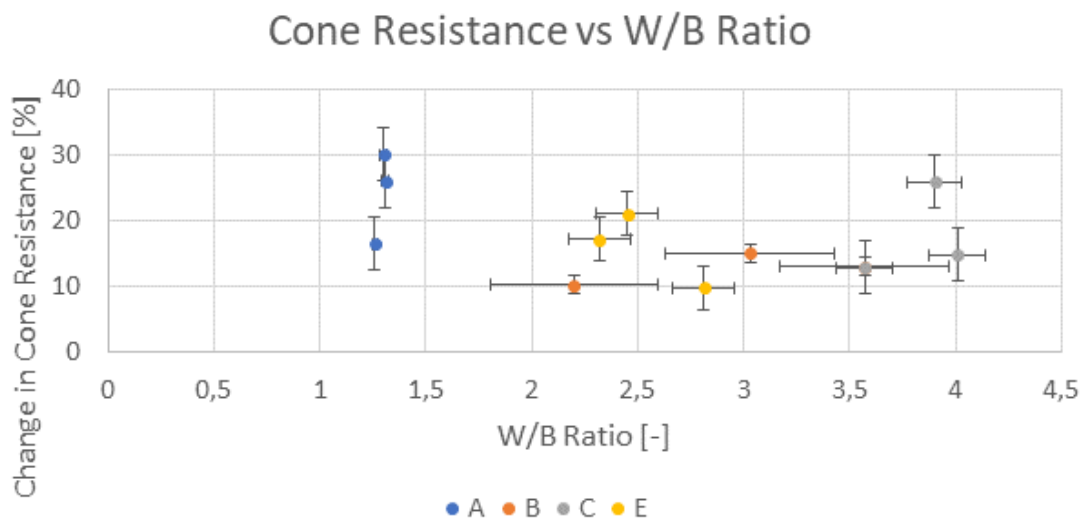


Figure 5.9: Cone resistance vs the W/B ratio of the injection grout mixture.

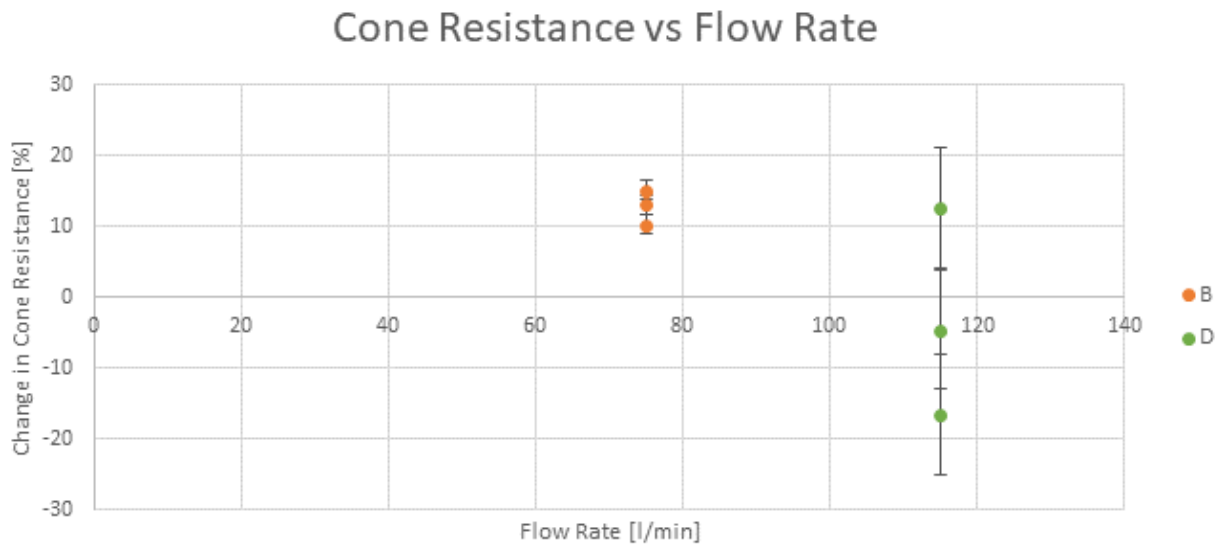


Figure 5.10: Cone resistance vs the injection flow rate of the grout mixture.

### 5.2.4. Relationship Between Cone Resistance and Shaft Capacity

In order to compare the relationship between the investigated properties and the shaft capacity, the ratio of Measured/Predicted values is used. The closer this ratio is to 1, the more accurate the prediction method used is at determining shaft capacity. It can be seen that Group D suffers from the largest variation in both M/P ratio and  $q_c$ , Group A has the lowest variation in M/P ratio and Group B has the lowest combined variation. There is a tendency that can be observed where the higher the increase cone resistance [%], the higher the M/P ratio, although the data is scattered. This is seen in Figure 5.11.

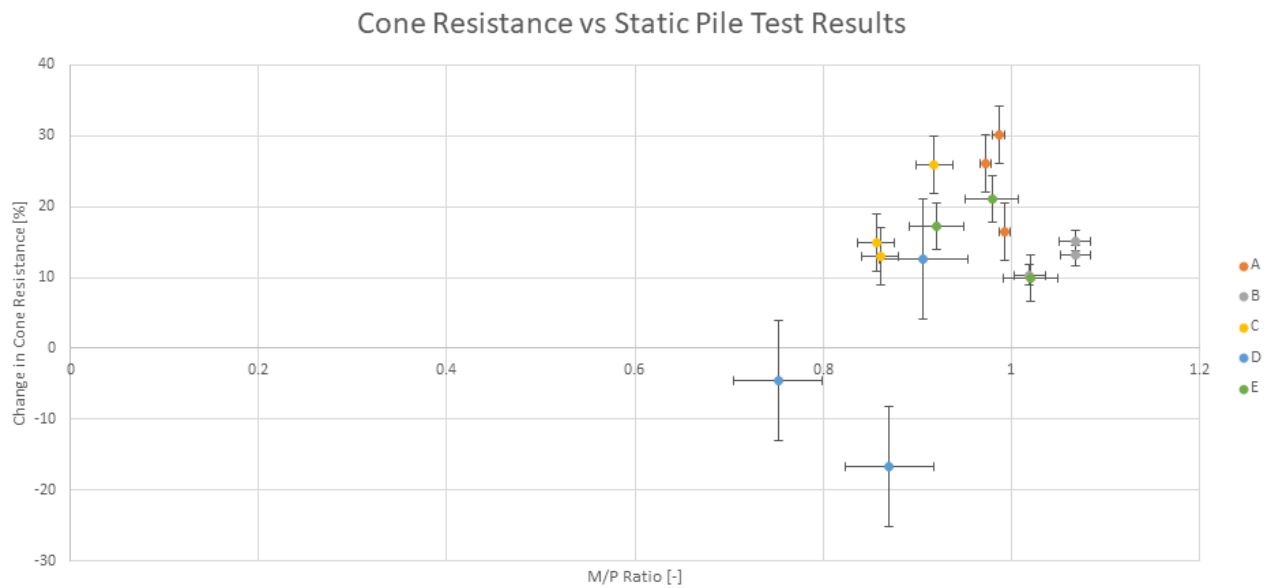


Figure 5.11:  $q_c$  vs shaft capacity for the three piles of each group, with error bars indicating the variation in each pile group.

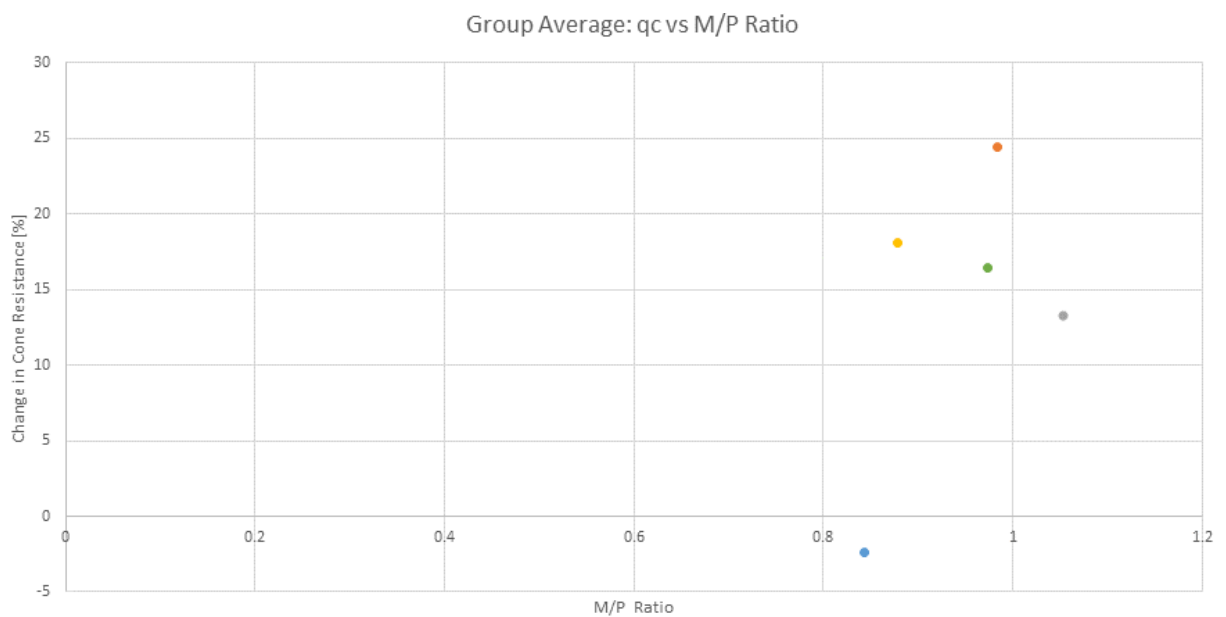


Figure 5.12: The average  $q_c$  values for each category vs shaft capacity.

### 5.3. Analysis of Records of Installation

In this section, some of the installation parameters will be analysed. The cone resistance is a measure of the shear stress of the soil (eq. 2.1), and thus it is important to know if there are any noticeable patterns that can be seen during the installation process of the SI-piles that affects the cone resistance. The grout fluid serves two main functions, as a lubrication agent during installation and to fill in the gap from the difference in diameters from the casing and the pile tip. This inherently means that there is a link between the torque, cone resistance, and  $\alpha_t$ . The applied torque was analysed per pile category in order to find a relationship between the torque and the grout installation parameters, the cone resistance, the amount of sand transported out of the soil and its consequent relationship with the shaft capacity.

#### 5.3.1. Order of Installation

It is important to mention that the piles were not installed one next to another in successive order, rather the order was scattered in order to prevent the pile group effect. Figure 5.27 shows the order for which the 15 piles were installed.

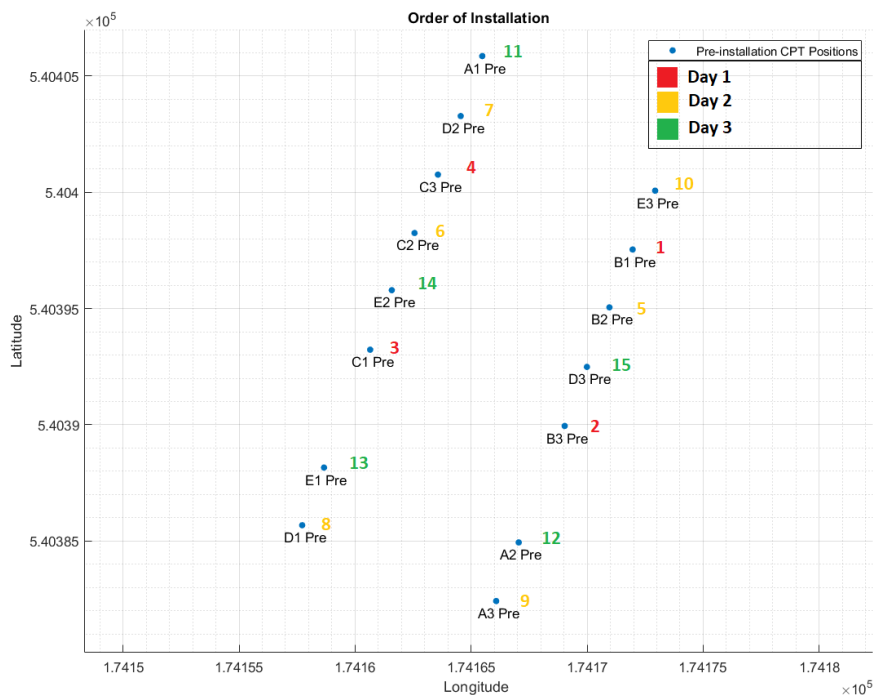


Figure 5.13: Order of installation of the piles over the 3 day period of installation.

### 5.3.2. Torque vs Grout Installation Parameters

In this section, the grout installation parameters are compared to the torque of the screwing motion during the installation of the piles. Figures 5.14 and 5.15 show that there is a clear tendency that shows that the higher the W/B ratio, the lower the torque. This is due to the higher water content which allows the grout to flow with more ease as opposed to a mixture with a higher cement content which will be more solid. Figure 5.16 shows that the higher the injection rate, the lower the torque. One reason is that with a higher injection rate there is more lubricant flow per minute (lubricant being the grout mixture).

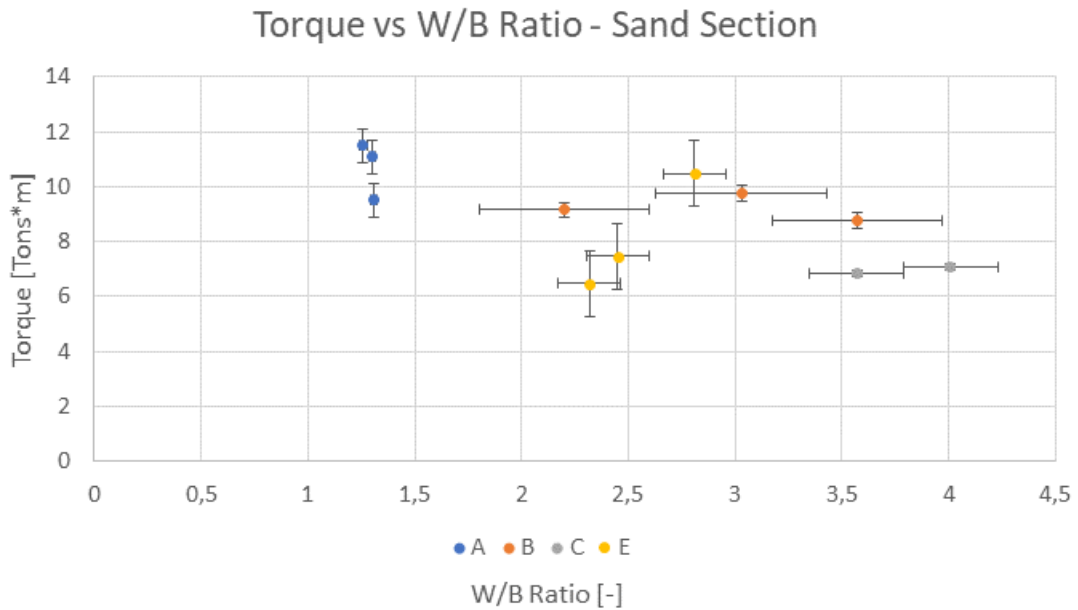


Figure 5.14: Torque vs. W/B ratio of the injection grout fluid of all piles in Group A, B, C and E.

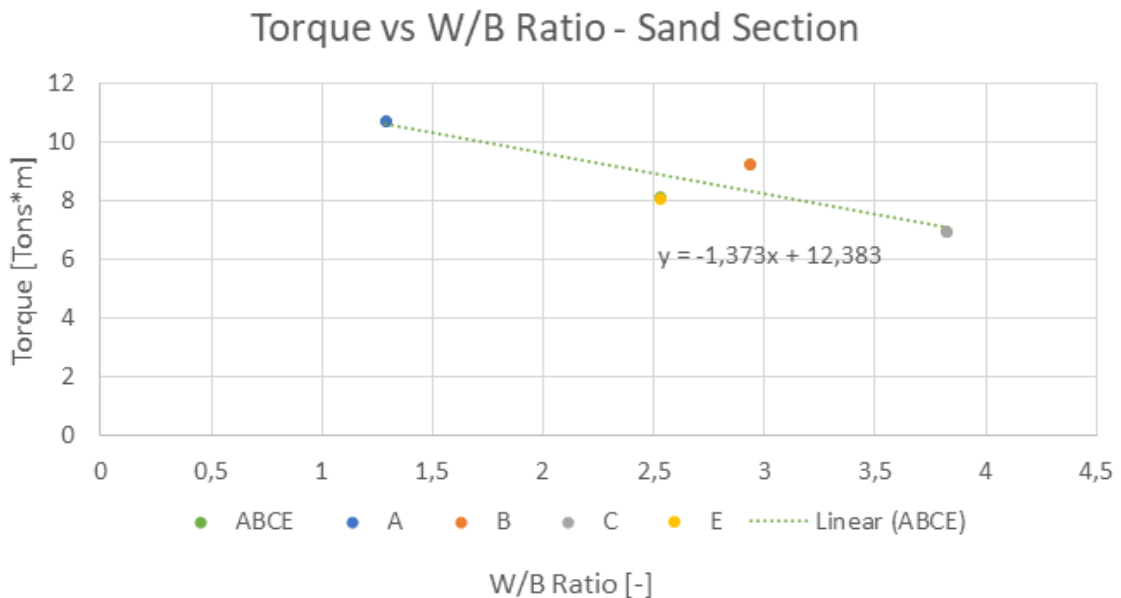


Figure 5.15: Torque vs. Group average W/B ratio of the injection grout fluid.

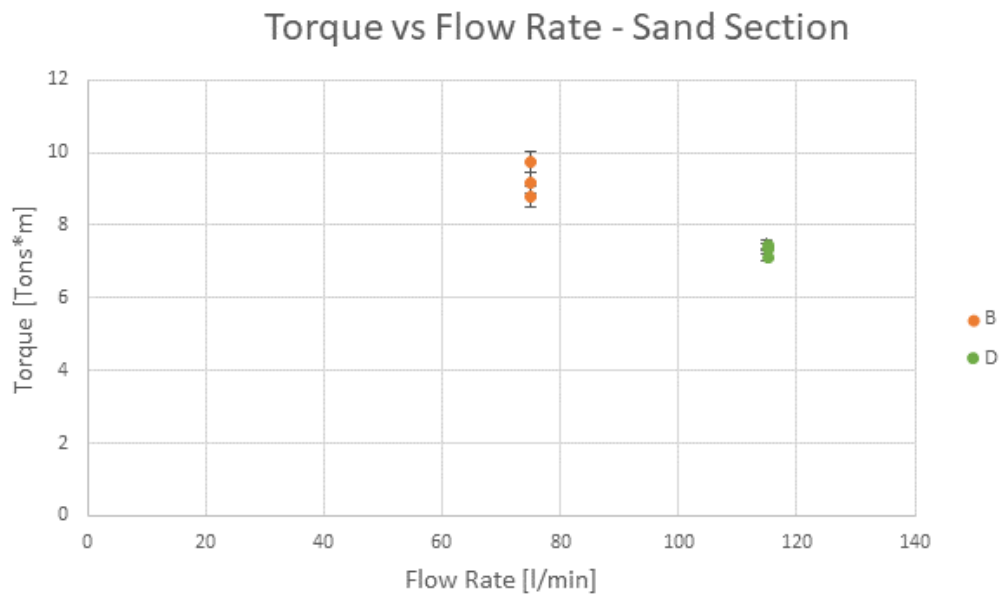


Figure 5.16: Torque vs. flow rate of injected grout.

### 5.3.3. Torque vs Cone Resistance

There exists a relationship between the torque and the change in cone resistance. Something to point out is that the variation in torque is small for pile groups D and C, despite group D having a very wide variation for change in  $q_c$ . Yet the relationship is clear, the higher the increase in cone resistance, the higher the torque. This can be seen in Figures 5.17 and 5.18; the variations of each pile group is represented by the error bars around each data point.

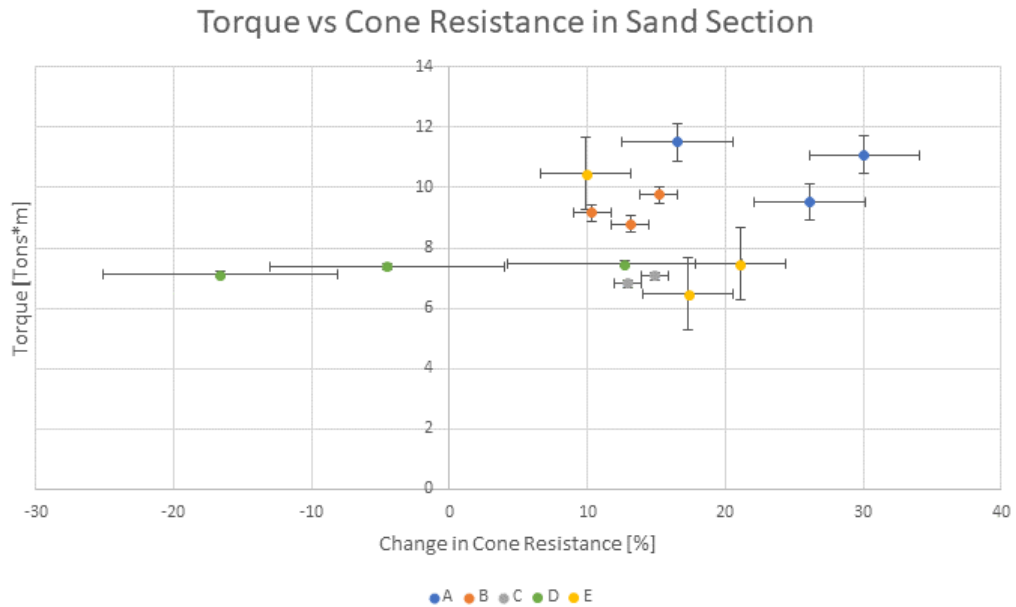


Figure 5.17: Torque vs. change in cone resistance for all piles.

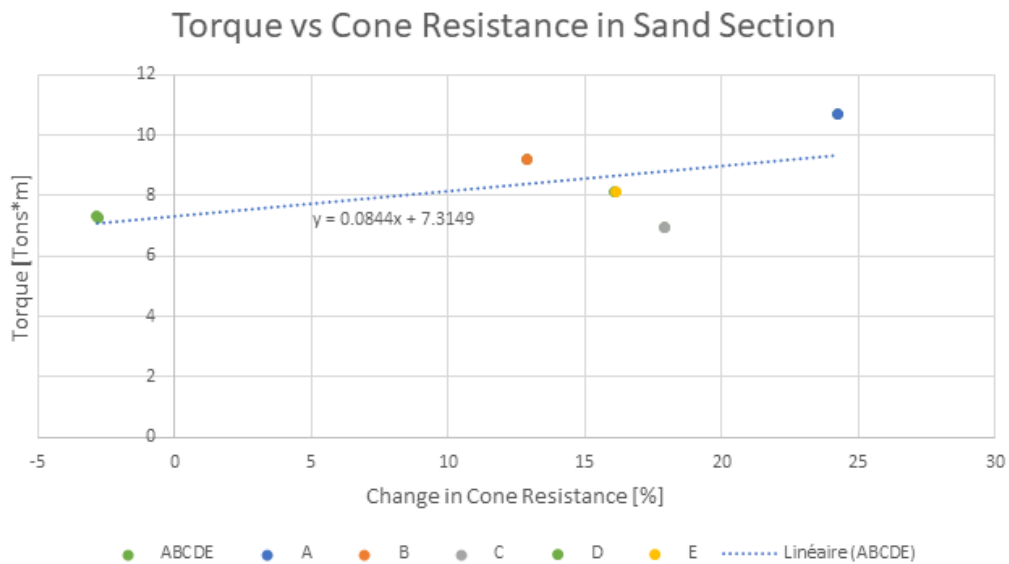


Figure 5.18: Torque vs. the average change in cone resistance per pile group.

### 5.3.4. Torque vs Shaft Capacity

Furthermore, it is important to look at the effect that torque has on the reliability of the predictions for shaft capacity. For this also a comparison with the M/P ratio is used. In Figure 5.19 one can see that for pile groups D and C have the lowest variation in torque as mentioned in the previous subsection 5.3.3; along with one data point in E they hold the lowest values of torque and one can see that they are the furthest from an M/P ratio of 1 compared to the other groups. However, it is important to note that while there is a positive tendency of a high W/B ratio leading to lower torque that is not always the case as it can be seen here with pile E3 which has a W/B ratio of 2.81 and the torque is comparable to that of the low W/B ratios of group A. Yet for high grout injection flow rate leads to consistently leads to low torque values.

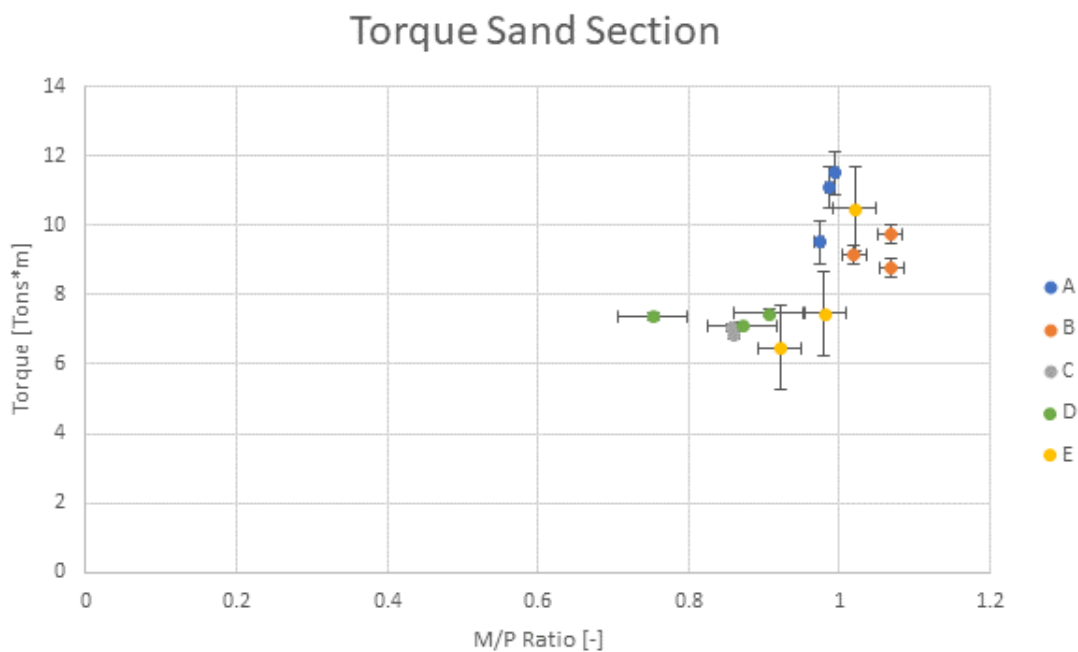


Figure 5.19: Torque vs. M/P ratio for all piles.

### 5.3.5. Estimation of Total Amount of Sand Removed by Grout Flow

Another important aspect of the installation process is to look at how much sand is transported out of the soil. As mentioned in Chapter 2 of this report, SI-piles are a partial displacement type of pile, for which some soil particles are transported back with the backflow of the grout. It is important to see how much sand is transported out and the relationship between that and the installation parameters. The sand content in the backflow grout is determined by looking at the sand content after 28 days and correcting for the water loss after that period of time; this is performed for both depth -6m and -9m NAP. This correction is described in equation 5.1 and 5.2. Figure 5.20 shows the percentage of sand present in the backflow grout (volume fraction) per group vs the W/B ratio during pile installation. It is important to note two aspects of this analysis. One is that it proved difficult to determine with great accuracy the content of cement and sand from the mixtures. Second, is that only 1 sample per pile group was tested 28 days after installation, thus limiting the accuracy of the mass fraction for piles A3, B2, B3 and D3. Additionally, the cement mixtures are different for category E, there is also the presence of limestone aggregate in the mixture which complicates obtainment of accurate percentage of sand.

$$\rho_{backflow} - v_l * \rho_w = \rho_{28d}(1 - v_l) \quad (5.1)$$

This leads to:

$$v_l = \frac{\rho_{28d} - \rho_{backflow}}{\rho_{28d} - \rho_w} \quad (5.2)$$

Where:

$v_l$  is the volume fraction of the water loss;

$\rho_{backflow}$  is the density of the backflow grout;

$\rho_{28d}$  is the density of the backflow grout after 28 days after installation;

$\rho_w$  is the density of water;

Moreover, an estimation is made to see how much volume of sand is removed, the following equations are used. One can see from Table 5.6 and Figure 5.21 that for the W/B ratios used in this test, the mass fraction of sand in the backflow grout will be in the neighbourhood of 49% to 57%. However, it is also clear that flow rate has an impact on the volume of sand transported. Despite group D having a higher flow rate than group B, there was a sand mass fraction 10% higher for group B, which ended up leading to a similar sand transport for piles B1 and B3.

$$V_{bf} = V_{total} - V_{pile,annulus} \quad (5.3)$$

$$V_s = \frac{\%sand * (V_{bf} * \rho_{backflow})}{(1 - \%sand) * \rho_s} \quad (5.4)$$

Where:

$V_{total}$  is the total volume of injected grout during installation;

$V_{pile,annulus}$  is the volume of the annulus of the pile (the volume of the grout in between the concrete pile and the surrounding soil);

$V_s$  is the volume of transported sand;

$V_{gsi}$  is the volume of grout injected that reaches the surface level;

$\%sand$  is the mass fraction of the sand;

$\rho_s$  density of sand = 2650 [kg/m<sup>3</sup>];

Pile	$V_{total}$ injected in Sand Layer	W/B Ratio	$V_{gsl}$	$\%sand$	$V_s$
[-]	[L]	[-]	[L]	[%]	[L]
A2	1061	1.31	530	50	346
A3	1002	1.30	495	50	323
B1	1049	2.2	517	57	466
B2	911	3.57	315	57	284
B3	1018	3.03	468	57	421
D3	1419	1.92	846	49	500
E3	963	2.81	454	49	284

Table 5.5: This table shows properties obtained from the extraction of the piles and in the last column it shows the amount of sand transported out of the soil as a unit of volume (liters).

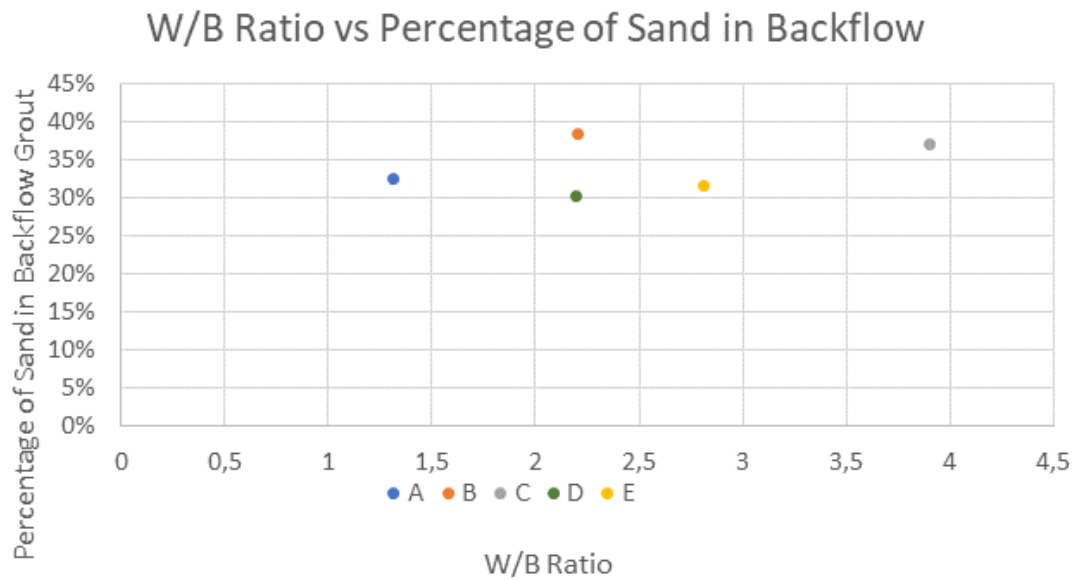


Figure 5.20: Percentage of sand in the backflow grout in relation to the W/B ratio.

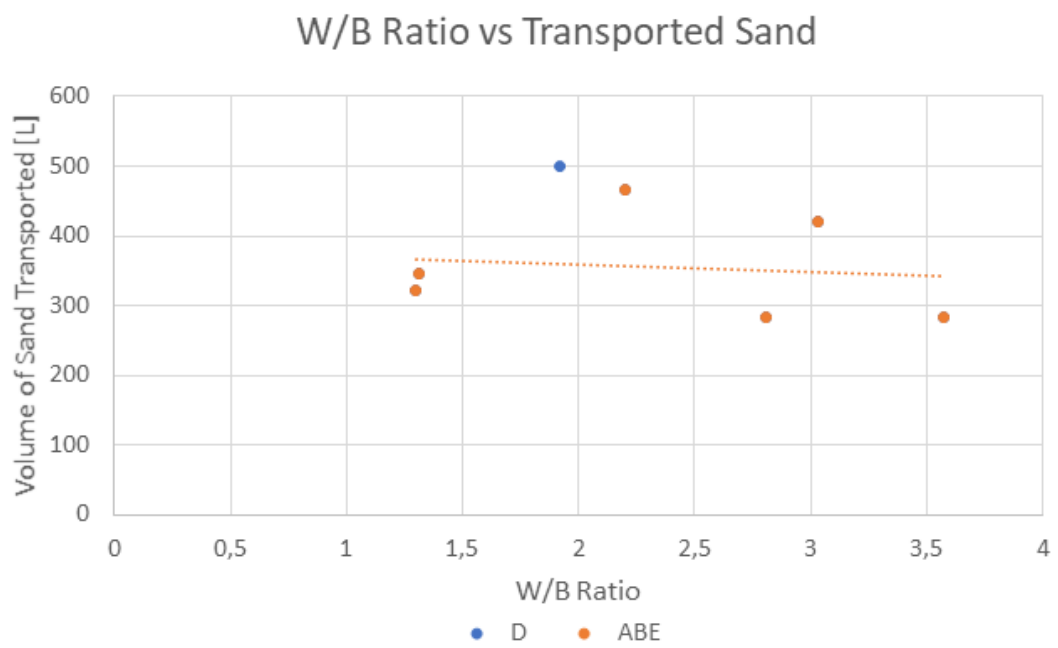


Figure 5.21: The relationship between the W/B ratio and the amount of sand transported out of the soil.

## 5.4. Grout Properties Analysis

In this section, a more in-depth analysis of the backflow grout is being done. This section includes the differences in grout material properties after installation, the relationship between said properties and the grout installation parameters, and an analysis of the shear stress analysis from data gathered from the UCS and Bending Test.

### 5.4.1. Change in Grout Material Properties

After the collection of the samples and of the data, certain patterns that can be identified. Looking at the water content of the freshly taken sample during the installation, the water content is nearing the 50% mark for all categories except for group C. Due to the high water content in group C, it was difficult to obtain reasonable samples, which resulted in peculiar situations, such as a water content of 111% for -6m NAP, which is impossible because that means that the weight of the water was greater than that of the dried sample, and for -9m NAP the water content was 27% which is the complete opposite of what was seen for category C at -6m NAP.

Backflow Grout Properties					
Pile Category	Water Content	Bleeding	$\rho_{inj}$	$\rho_{backflow}$	% of increase in $\rho$
[-]	[%]	[%]	[kg/m <sup>3</sup> ]	[kg/m <sup>3</sup> ]	[%]
-6m NAP					
A	50	4.5	1400.85	1761.75	25.76
B	45	9.67	1208.33	1792.67	48.36
C	111	12	1159	1709	47.45
D	65	13.67	1266.67	1643	29.71
E	57	6.67	1227.33	1699.67	38.49
-9m NAP					
A	52	3.67	1400.85	1764.67	26.0
B	47	3.33	1208.33	1813.33	50.07
C	27	8.33	1159	1742.67	50.36
D	43	15	1266.67	1693.67	33.71
E	49	3.67	1227.33	1748.67	42.48

Table 5.6: Shows multiple properties of the backflow grout, the water content and bleeding are expressed in percentage (weight of water over the weight of the dry sample, and bleeding is the percentage of the volume of the sample immediately after extraction and after 1 hour). The density of grout during injection and backflow is shown along with the percentage of increase in density.

### 5.4.2. Density Change vs Grout Installation Parameters

Furthermore, an analysis of the density change is also conducted. This is important because the grout material envelopes the pile, thus a more dense material at the interface of the pile gives a higher resistance at the pile-soil interface. As can be seen in Table 5.6, Groups A, B and C all have similar  $\rho_{backflow}$ , despite having very different  $\rho_{inj}$ . From this, the effect of the increase in density is analysed with respect to the installation parameters and with respect to shaft capacity, Group E is excluded since it is made from a different cement mixture. However, the difference between the A, B, C and E is not very large with

regards to B and D, for which the difference is 149.67 and 119.66 [ $kg/m^3$ ] for -6m and -9m NAP respectively. After that, the difference between B and C are 83.67 and 70.66 [ $kg/m^3$ ], and for B and E it is 93 and 64.66 [ $kg/m^3$ ]. Category B always ended up with a higher  $\rho_b$  and category D always with the lowest.

Figure 5.22 shows the relationship between the change in density and the W/C ratio. It can be seen that there is a clear trend that states that the higher the W/C ratio have higher increases in density but it is not a linear relationship.

The flow rate has negatively affected the density. An explanation for this is that the high pressure of the injected grout fluid has probably caused some wear of the soil particles. This would be consistent with what has been previously seen with the reduced torque, and the large decrease in cone resistance. Figure 5.23 shows the change in density vs the grout injection flow rate.

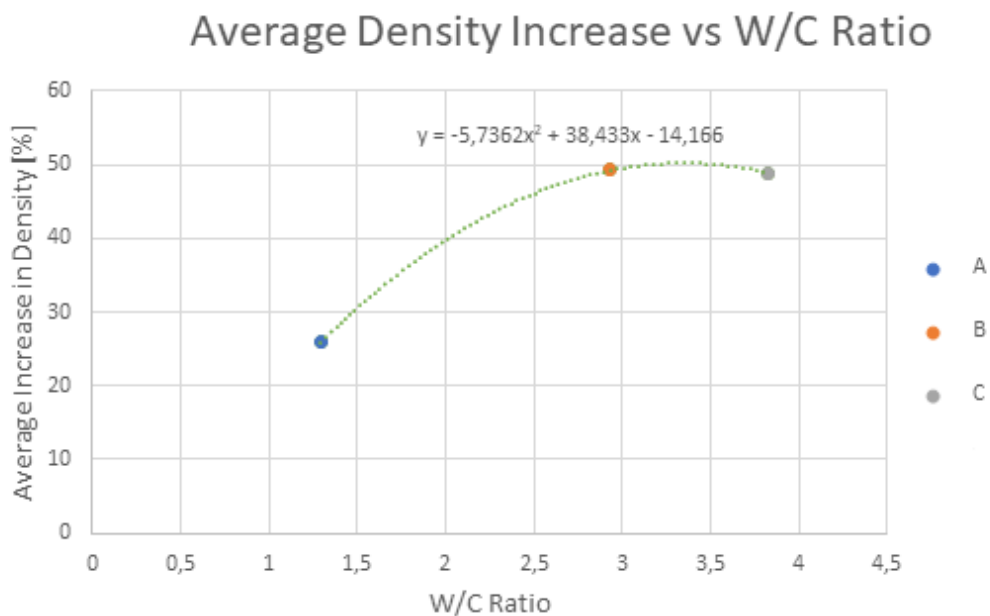


Figure 5.22: Average density increase between the injected grout and the collected backflow vs. W/C ratio of the injection grout fluid.

#### 5.4.3. Density Change vs Shaft Capacity

Figure 5.24 shows the relationship between the shaft capacity and the increase in density of the grout mixture. It can be seen that the percentage of increase in density does not show a clear trend and thus it can be concluded that the effect of change in density of the grout fluid is not a factor that will directly influence the shaft capacity prediction.

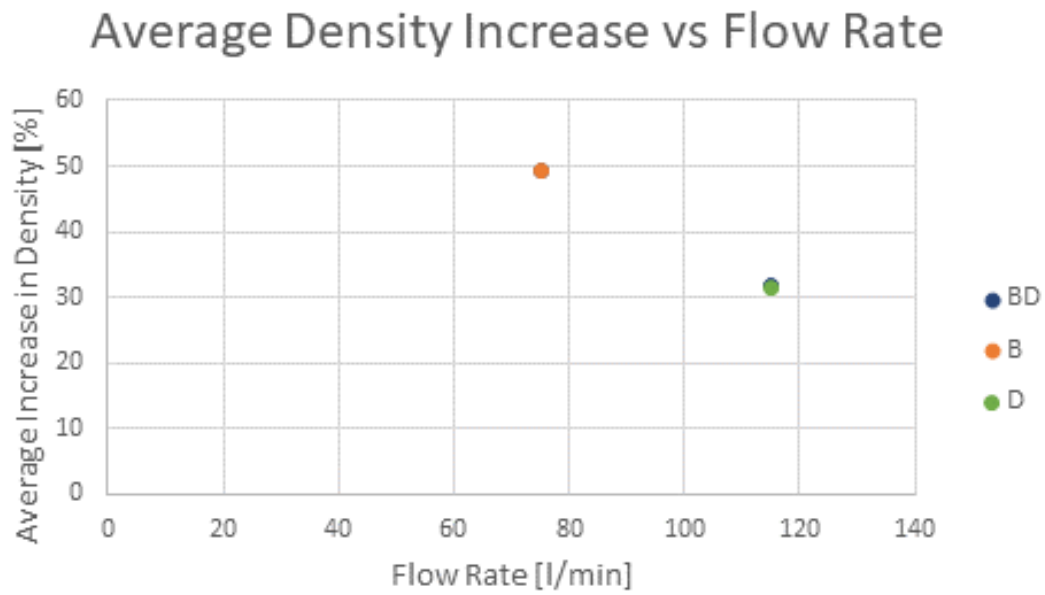


Figure 5.23: Average density increase between the injected grout and the collected backflow vs. flow rate of injection grout.

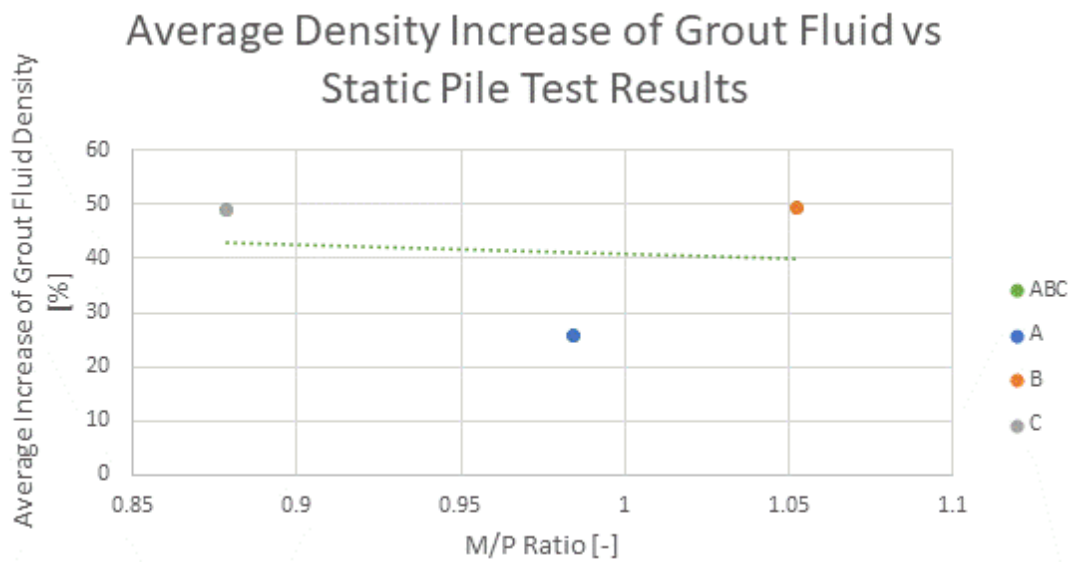


Figure 5.24: Average density increase between the injected grout and the collected backflow vs. M/P ratio.

#### 5.4.4. W/B ratio vs UCS Bending Test

Furthermore, two important research questions that can be answered in this section which is: Does injection W/B ratio have a significant influence on the shear strength after dissipation of the water after 28 days? And, does the shear strength of the grout mixture after 28 and 56 days have any significant impact on the shaft capacity? After 28 days of curing, the new W/B ratio was determined and two tests were performed: UCS tests, to determine the axial stress of the hardened grout, and a bending test, to determine the flexural strength of said grout. Table 5.7 shows the UCS test results for 28 and 56 days after pile installation, Table 5.8 shows the Bending test results for 28 and 56 days after pile installation.

Unconfined Compressive test			
Pile Category	$\sigma_{uc28Days}$	$\sigma_{uc56Days}$	% of increase $\sigma_{uc}$
[-]	[MPa]	[MPa]	[%]
-6m NAP			
A	9.15	12.35	35
B	4.9	6.53	33.3
C	1.42	2.1	47.9
D	4.78	6.78	41.8
E	2.17	3.12	43.8
-9m NAP			
A	10.37	14.23	37.2
B	5.32	7.22	35.7
C	2.05	2.72	32.52
D	4.77	6.62	36.7
E	2.33	3.02	29.6

Table 5.7: Stress tests for Unconfined Compressive Tests.

First, the relationship between the W/B ratio at injection and the  $\sigma_{uc}$  after 28 days is seen in Figures 5.25. The W/B ratio decreases after 28 days, the average new W/B ratios per group at both depths are: 1.25, 1.75, 2.83, 1.97, 2.63 for Groups A, B, C, D and E respectively. From Figure 5.25 it can be seen that there exists a relationship between  $\sigma_{uc}$  where the higher the W/B ratio is the lower the axial shear stress becomes, but when it reaches a W/B of approximately 2.81, the range of values of  $\sigma_{uc}$  becomes narrower than for lower W/B ratios. It is worth mentioning that pile group B suffers from a very large variation in  $\sigma_{uc}$ . The bending stress shows a very similar pattern to that of the UCS test, this is shown in Figure 5.26.

Bending Test			
Pile Category	$\sigma_{bt28Days}$	$\sigma_{bt56Days}$	% of increase $\sigma_{bt}$
[-]	[MPa]	[MPa]	[%]
-6m NAP			
A	2.1	2.2	4.76
B	1.23	1.57	27.6
C	0.33	1.13*	242
D	1.23	1.8	46.3
E	0.6	0.93	55.0
-9m NAP			
A	2.17	2.73	25.8
B	1.4	1.63	16.4
C	0.53	0.6	0.13
D	1.23	1.5	22.0
E	0.67	0.9	34.3

Table 5.8: Stress tests for Bending Tests. \*One of the samples for category C had the largest  $\sigma_{bt}$  recorded at 2.6 kN, thus drastically increasing the percentage of change of  $\sigma_{bt}$ .\*

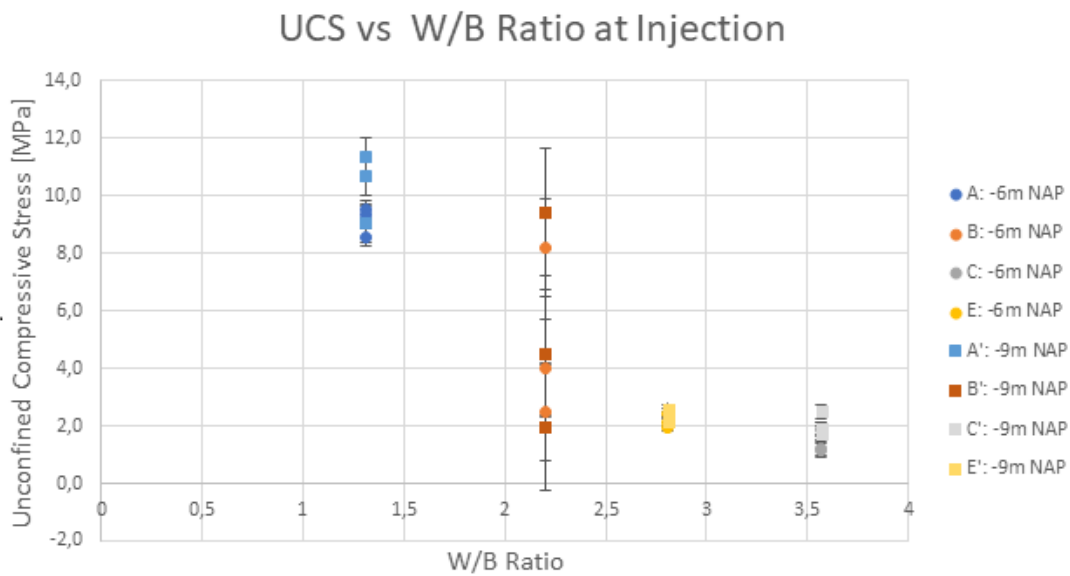


Figure 5.25: UCS vs W/B ratio at injection at both depths -6m and -9m NAP for all piles in Groups A,B, C, and E after pile installation.

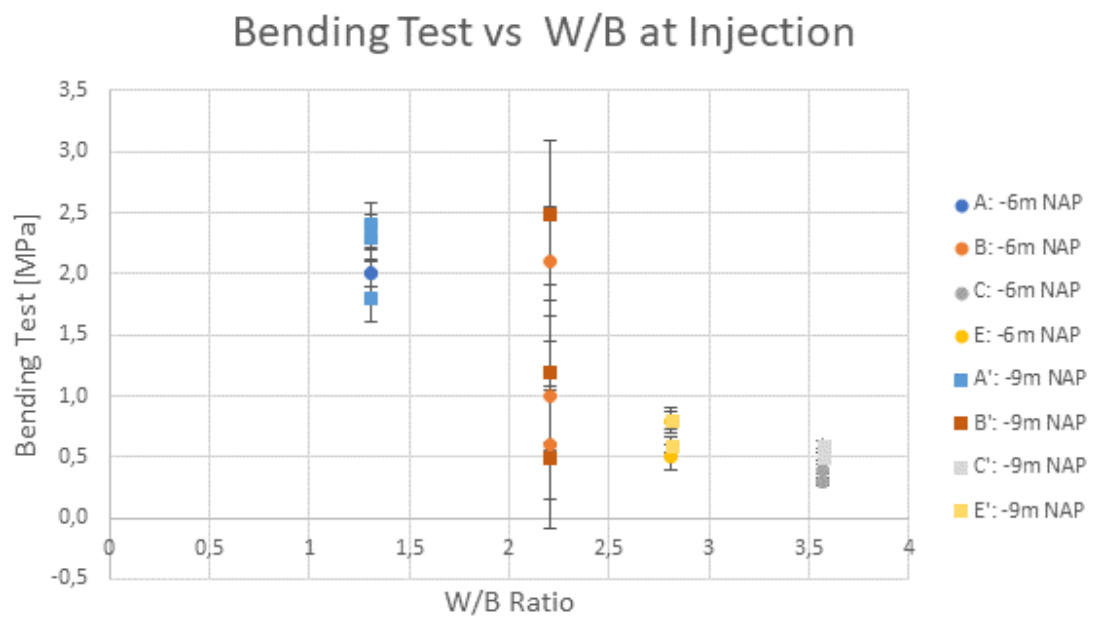


Figure 5.26: Bending stress vs average W/B ratio at injection at both depths -6m and -9m NAP for all piles in Groups A, B, C, and E after pile installation.

### 5.4.5. Flow Rate vs UCS Bending Test

Figure 5.27 shows the effect of different flow rates on  $\sigma_{uc}$ . It can be seen that in terms of variability, the range of values of axial stress is lower for Group D (115 l/min) compared to Group B (75 l/min). Yet, the general trend shows that a lower flow rate has a higher  $\sigma_{uc}$  on average than a higher flow rate.

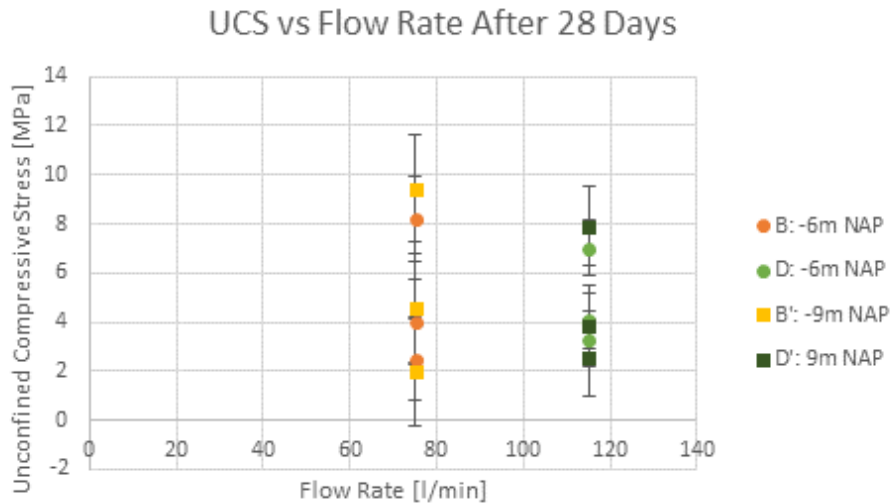


Figure 5.27: Average density increase between the injected grout and the collected backflow vs. flow rate of injection of grout.

As seen in the case of the W/B ratio relationship, the flow rate relationship trend between the UCS and Bending test is similar.

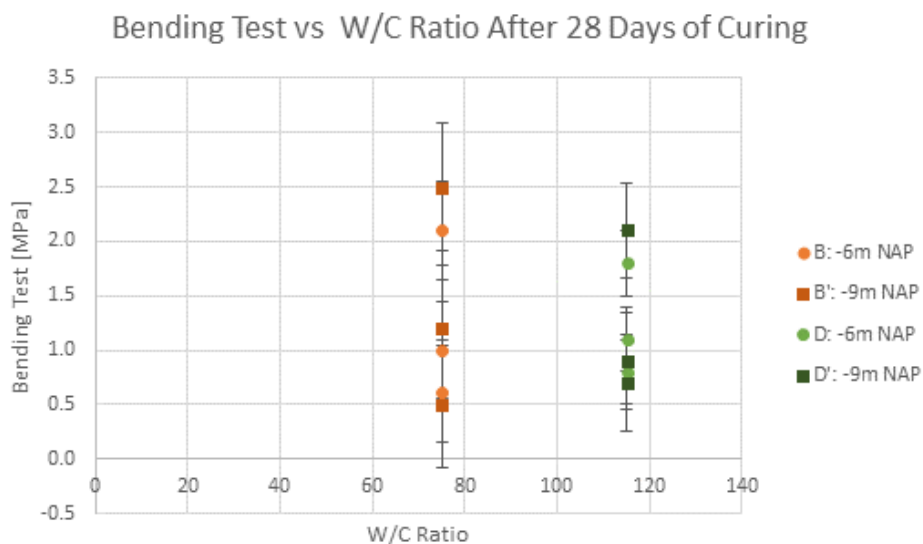


Figure 5.28: Average density increase between the injected grout and the collected backflow vs. flow rate of injection of grout.

### 5.4.6. Shear Stress of Grout vs Shaft Capacity

It was seen that the UCS and Bending test plots vs grout installation parameters were very similar, this is the same case with the shaft capacity. There is a clear and almost identical trend. Looking at category A, B, C and E, it can be seen that high values of  $\sigma_{bt}$  and  $\sigma_{uc}$  are closer to M/P of 1. Comparing Groups B and D, the  $\sigma_{bt}$  and  $\sigma_{uc}$  are not very different yet the M/P ratio is lower for Group D.

It is important to determine whether the failure is purely geotechnical or also structural. According to the DIN4043 and EC7-3, the shear stress of the grout can be expressed by equation 5.5, then the shear stress of the soil can be expressed by equation 5.6.

$$\tau_f = 2 * f_t \quad (5.5)$$

$$\tau_f > \alpha_t * q_c \quad (5.6)$$

There are two ways that the force of tension can be determined, which are taking 10% of the  $\sigma_{uc}$  or just taking the  $\sigma_{bt}$ . Table 5.9 shows the shear stress of the grout vs the shear stress of the soil. It can be seen that in both ways to determine the shear stress that the failure is purely geotechnical as the shear stress of the soil is lower in every case than that of the grout, even for the very high W/B ratio of pile C2 (W/B = 3.9 at injection). It can be concluded that the shear stress of the grout will not be higher than the shear stress of the soil for W/B ratios lower than 3.9. This in turn means that there is no influence of the shear stress of the grout with the shaft capacity of the piles.

Pile Name	$\tau_f = \alpha_t q_c$	$\tau_f$ using UCS	$\tau_f$ using BT
[-]	[MPa]	[MPa]	[MPa]
A2	0.13	2.3	4.6
B1	0.14	1.20	2.92
C2	0.17	0.41	1.3
D1	0.17	1.15	2.88
E3	0.16	0.53	1.55

Table 5.9: Shear stress of the grout and shear stress of the soil.

Group A, B and E have different W/B ratios and show a very large range of  $\sigma_{uc}$  and  $\sigma_{bt}$  whilst still showing very similar M/P ratios. For Group D, nothing can be said directly about these shear strength properties and shaft capacity.

## 5.5. Pile Shape Analysis

The piles were extracted several months after their installation with the purpose of recording the increase in diameter due to the grout enveloping the concrete pile. This is an important part of the analysis as it is expected that a higher average diameter of the pile leads to a higher shaft capacity due to the fact that there is more area of the pile in contact with the surrounding soil. Only 7 piles were extracted due to possible problems with surrounding structures that could arise from extracting the other 8. This, unfortunately, means that no piles from Group C were extracted. From Figure 5.29 it can be seen that no irregular patterns can be seen in the grout around the concrete, the grout formed a thicker bulb around the tip and becomes thinner at the middle of the length of the pile.



Figure 5.29: Photograph of the extracted piles from the test site in Lemmer, Friesland.

### 5.5.1. Pile Volume Increase

The diameter was measured for every 1m, the increase in diameters along the length of the pile was recorded and can be seen in Figure 5.30. The volume around the pile is calculated by taking the volume of the pile with the new diameters along its length minus the cylindrical volume of the original pile (with a diameter of the casing + crown = 0.380m). It can be seen that a higher W/B ratio at injection leads to a higher grout volume increase. The higher flow rate reduces the grout volume around the pile.

As mentioned at the beginning of this pile shape analysis, the higher the volume/diameter of the pile, the more area of contact there is at the pile-soil interface, leading to a higher shaft capacity. Figure 5.33 shows that there is a clear trend that pile volume increases with

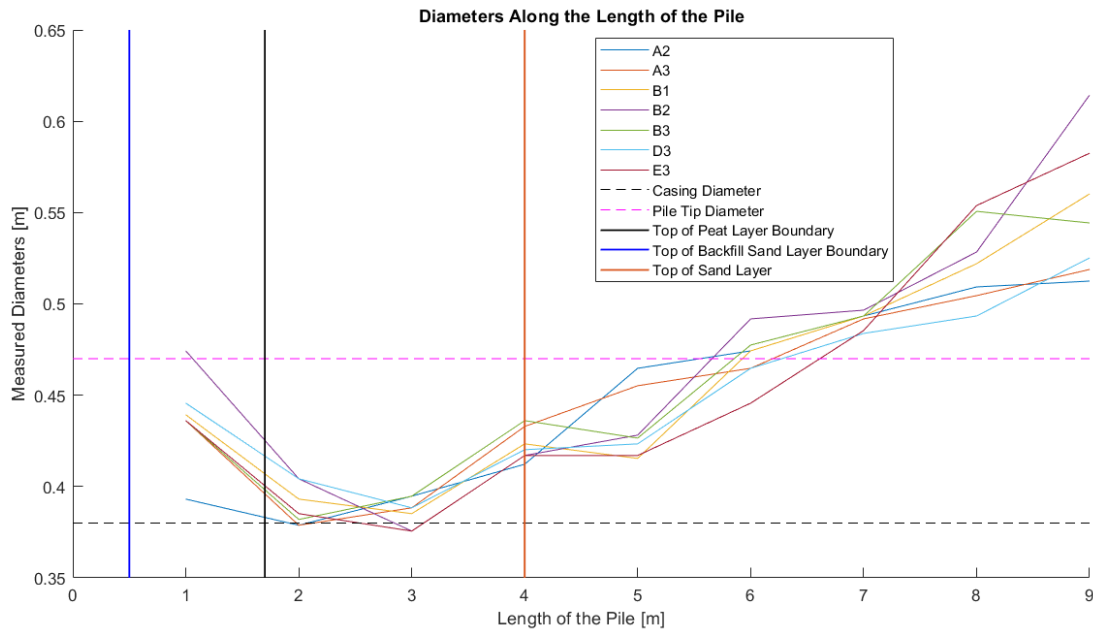


Figure 5.30: Size of diameters along the pile length.

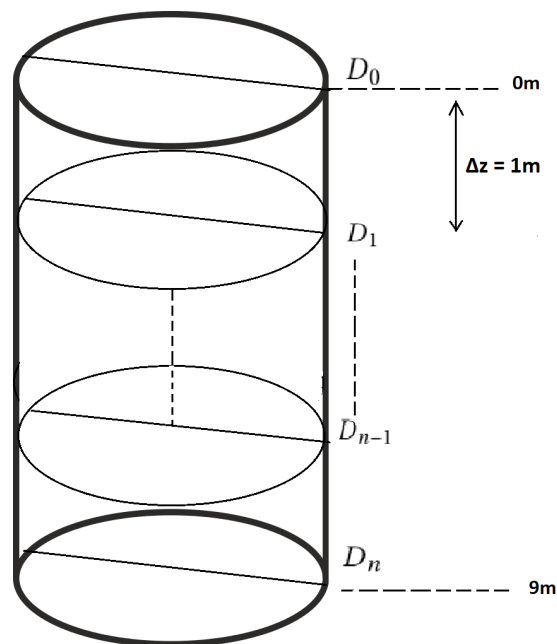


Figure 5.31: Discretization of the pile after extraction into nodes in the diameter positions.

W/B ratio. Consequently, Figure 5.34 shows that there is another clear trend that relates to the increase in diameter and an increase in M/P ratio (and is almost perfectly consistent with the W/B ratio).

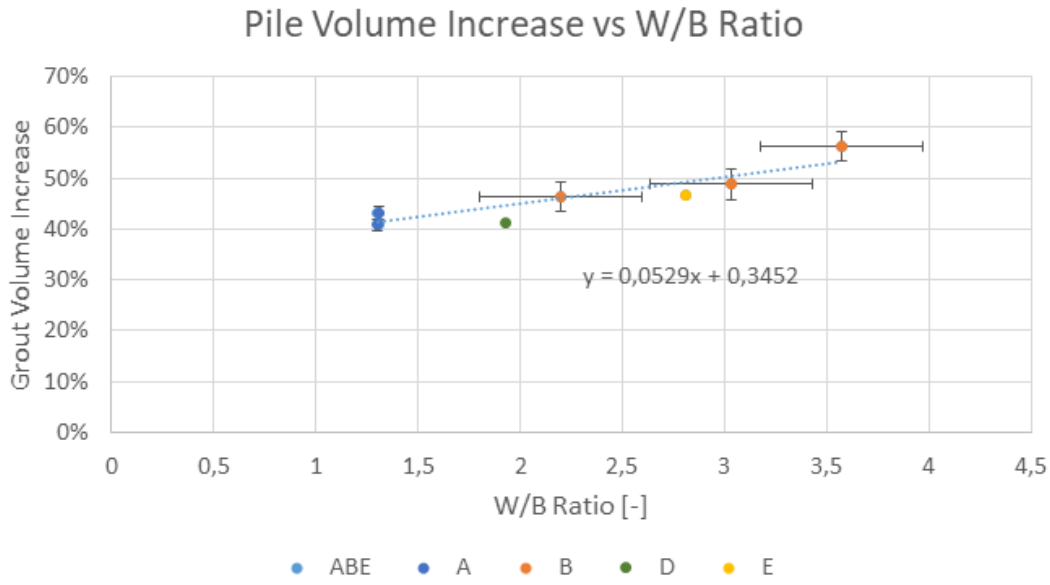


Figure 5.32: Pile volume increase vs W/B ratio at injection.

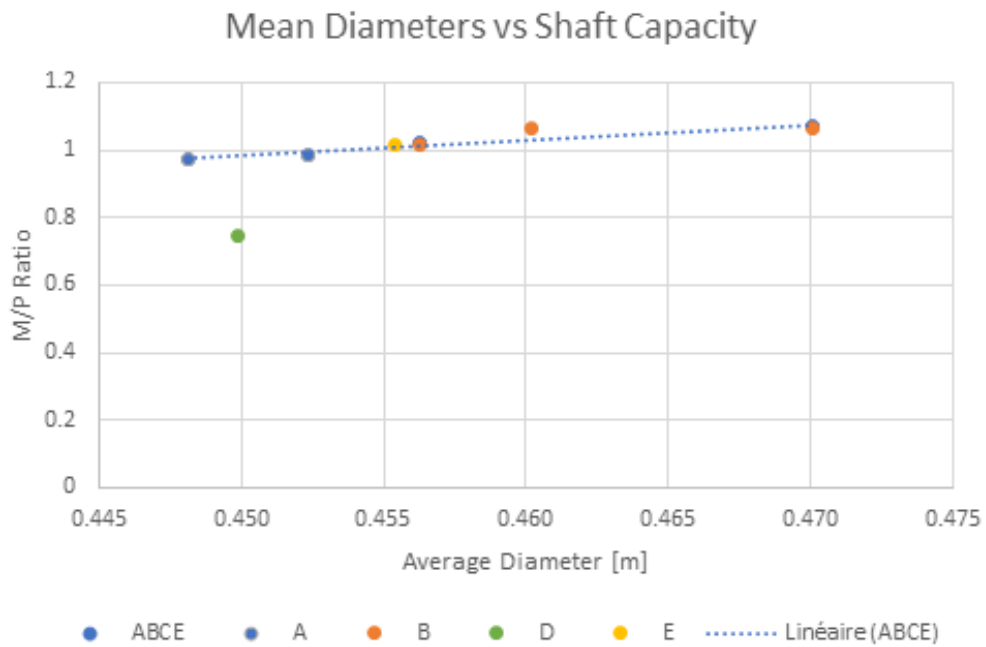


Figure 5.33: Average diameter size vs M/P ratio.

## 5.6. Final Analysis

This section of the analysis is where the research objectives are addressed and summarised. The two main research objectives can be summarised here. First: **Observe the influence on load-settlement behaviour changes in the W/C ratio and high injection flow rate.** Second: **Compare measurements on piles to the predictions of bearing capacity with multiple pile installation properties.** The findings from the analysis are summarized in Figure 5.35.

W/B Ratio	Flow Rate
<ul style="list-style-type: none"> <li>• <math>\uparrow W/B = \downarrow \text{Torque}</math></li> <li>• <math>\uparrow W/B = \downarrow V_{s, \text{Transported}}</math></li> <li>• <math>\uparrow W/B = \downarrow \text{UCS} \ \&amp; \ \downarrow \text{Bending Stress}</math></li> <li>• <math>\uparrow W/B = \downarrow V_{gsl}</math></li> <li>• <math>\uparrow W/B \neq \downarrow \Delta q_c</math></li> <li>• <math>\uparrow W/B = \uparrow \text{Mean Diameter of Pile}</math></li> </ul>	<ul style="list-style-type: none"> <li>• <math>\uparrow \text{FR} = \downarrow \text{M/P Ratio}</math></li> <li>• <math>\uparrow \text{FR} = \downarrow \Delta q_c</math></li> <li>• <math>\uparrow \text{FR} = \downarrow \text{Torque}</math></li> <li>• <math>\uparrow \text{FR} = \uparrow V_{s, \text{Transported}} \ \&amp; \ V_{gsl}</math></li> <li>• <math>\uparrow \text{FR} = \downarrow \Delta \text{Density}</math></li> <li>• <math>\uparrow \text{FR} \approx \downarrow \text{UCS} \ \&amp; \ \downarrow \text{Bending Stress (slightly)}</math></li> </ul>
M/P Ratio	Other
<ul style="list-style-type: none"> <li>• <math>\uparrow \Delta q_c = \uparrow \text{M/P}</math></li> <li>• <math>\uparrow \text{Torque} = \uparrow \text{M/P}</math></li> <li>• M/P not influenced by density change</li> <li>• M/P not influenced by shear stress of grout</li> <li>• <math>\uparrow \text{Mean Diameter} = \uparrow \text{M/P}</math></li> </ul>	<ul style="list-style-type: none"> <li>• <math>\uparrow \text{Torque} = \uparrow \Delta q_c</math></li> </ul>

Figure 5.34: Summary of research findings. **Note:** for  $V_{gsl}$  we do not know the transport data for piles of Group C.

Moreover, from all of the information collected two cases that can be described. In each of these cases, one can see the order of events and their corresponding effect with one another, starting from the installation parameters to the shaft capacity determination.

### Case 1: Flow rate = 75 [l/min]; $1.26 \leq W/B \text{ at injection} \leq 4.01$ :

1. Decrease in torque with high W/B ratio, causing easier propagation of grout, facilitating the pile installation.
2. Reduced transport of sand with higher W/B ratio. Yet  $\rho_{backflow}$  is very similar for all W/B ratios in Case 1.
3. A higher W/B ratio does not lead to higher sand content in the backflow grout.
4. No consistent relationship between higher W/B ratios leading to a decrease in the change in  $q_c$  between post- and pre-installation.

5. After 28 days after installation: Reduction in shear stress properties, these include the UCS,  $\sigma_{uc}$ , the Bending stress,  $\sigma_{bt}$ , and the shear stress of the grout,  $\tau_{f,grout}$ . Significant reduction observed at W/B ratio  $\geq 2.81$
6. Extraction of the pile: Less transport of grout out of the system means more stays in. Higher W/B ratios increase the pile volume; this increases the area of contact between the pile and the surrounding soil which in turn increase the M/P ratio.

**Case 2: Flow rate = 115 [l/min];  $1.92 \leq W/B$  at injection  $\leq 2.34$ :**

1. The highest decrease in torque recorded; more flow of grout lubricant facilitates installation a lot.
2. The lowest density of backflow grout was recorded; this is due to the high amount of flow coming out of the ground compared to the other cases.
3. The highest volume of sand transported out of the soil.
4. Drastic reduction in  $q_c$ , possibly due to the large amount of transport of in-situ material and also probably the high grout pressure could have caused some wear on the soil body.
5. Insignificant decrease in the shear properties (UCS, Bending stress, and shear stress of grout).
6. The W/B ratio is the dominant factor when looking at the new pile diameter. The flow rate did not seem to influence it (however there is only one data point to suggest this).



# 6

## Conclusion and Recommendations

### 6.1. Conclusion

This research focused on the effects of variation of grout fluid used during the installation of SI-piles onto the shaft capacity of the piles. The research objective was to determine whether, and if so, to what extent a difference exists in the shaft bearing capacity in tension for screw-injection piles made with grout lubrication where the two main variables are the grout injection rate, and the composition of the grout, notably the W/C (and W/B) ratio. The effects on shaft capacity of these varying grout parameters were explored by performing full-scale static pile load tests. These tests were performed in tension in order to eliminate the influence of the pile base resistance, thus focusing on the shaft resistance of the pile only. Five variations of the grout mixture were tested, four different W/B ratios with an injection rate of 75 l/min (pile groups A, B, C, and E) and variation with the same W/B ratio as group B but with a higher injection rate of 115 l/min (group D). The cement mixtures used for the tests were CEMIII B and GM42 (for pile group E only). There was a total of 15 piles installed, thus 3 piles per group category. In addition, this research also focuses on how the variations on the grout fluid affect other properties that are related to the shaft capacity of the piles. These include the changes in cone resistance after the installation of the pile, the effects recorded during installation (torque and sand transported out of the soil), the shear stress properties of the grout, and the final pile shape. The preliminary design for the predictions of the shaft capacity was in accordance with the NEN 9997-1 code, with a single deviation which is not to limit the cone resistance to a maximum value of 15 MPa, instead, the real values seen on the field were utilized.

The results of the measured failure load from the test were similar to those of the preliminary calculations in general, but especially for pile groups A, B, and E which had average W/B ratios of 1.29, 2.93, and 2.52 respectively. Pile groups C and E had high water-cement ratios (group C had a W/C ratio average of 3.83), whilst not having the same W/B ratio. It cannot be concluded that there is a direct relationship between the composition of the grout and the shaft capacity of the SI-piles. There is a striking difference noticed when looking at piles B2 and C1 which both have the same W/C ratio of 3.57 but a very different Measured/Predicted ratio, a difference of approximately 21%. However, for group D, the group with the flow rate of 115 l/min, the M/P ratio was on average the lowest of all categories and extremely low compared to group B, which had similar W/C and W/B ratios.

Thus it can be concluded that having a high grout injection flow rate of 115 l/min does significantly affect the shaft capacity of the pile.

Moreover, the indirect effects of the grout variations on the shaft capacity are studied. From the preliminary equation, it is known that the cone resistance, the pile diameter and the friction coefficient,  $\alpha_t$ , are the parameters needed to determine shaft resistance. First, cone resistance was assessed before and after the pile installation. The results of this analysis show that there is not a consistent relationship that shows that the W/B ratio of the grout mixture influences the change in cone resistance,  $\Delta q_c$ . However, the higher flow rate significantly decreases  $\Delta q_c$ , and for two piles the cone resistance is decreased. For pile D1 the recorded decrease was approximately 16.6%. A possible explanation for this is that the higher pressure of the injected grout must be causing some wear on the soil in addition to the fact that with more grout flow rate leads to a higher volume of grout injected which transports more sand particles out of the soil body, which also reduces the cone resistance.

Second, the analysis of the torque during installation. This analysis shows that there exists a linear trend where the higher the W/B ratio and grout injection flow rate, the lower the torque during installation. Comparing the torque to the M/P ratio, it can be concluded that there is a tendency that shows that the lower the torque, the higher the M/P ratio tends to be. The data is very consistent for all pile groups except for group E which has a much larger variation in torque, but it is also the pile group for which W/C  $\neq$  W/B ratio because it is not made from the same grout mixture as the others that are fully composed of water and cement. Third, the sand transported out of the soil. For this, the data of the extracted piles was considered in combination with the total grout inserted into the soil and the analysis done on the collected samples of the backflow grout. Having all of these parameters in mind, what can be concluded is that a higher W/B ratio leads to less transport of sand particles. Additionally, a higher flow rate resulted in a higher transport of sand particles.

Fourth, the shear stress properties of the grout. For this two tests were performed on samples after 28 and 56 days after the installation of the piles, after the grout has hardened and some water has evaporated out. While there is a clear trend that the shear stress of the grout decreases with increasing W/B ratios, the most important aspect is that even for a high W/C ratio of 3.90, the shear stress of the grout is never lower than that of the soil, which suggests that failure is purely geotechnical, thus it does not affect the measured shaft capacity. A higher grout flow rate showed a decrease in the shear stress of the grout but it is negligible. Lastly, the pile shape analysis. In this section, a relationship is drawn between the pile volume and the varying grout parameters. Only 7 out of the 15 piles were extracted and no piles from group C were extracted. But out of this limited data, one can see that the diameters of the piles were very similar, and there was a tendency that the diameters got larger when getting closer to the pile tip. From this data, one can see that there is a linear relationship between the W/B ratio and the grout volume surrounding the pile; this consequently means that there is a tendency of a higher mean diameter with higher W/B ratios. This leads to an even clearer relationship that is almost perfectly linear between the mean diameter and the shaft capacity of the piles.

An additional objective in this thesis was to determine if there is a need to adjust the  $\alpha_t$

factor depending on the W/B ratio and the different grout injection flow rates. There is an issue relating to the fact that there is an inherent variability that comes with working with soils, and only having three data points per group is meagre. With that in mind, one cannot conclude that there exists a solid relationship between the W/B ratio and the  $\alpha_t$ . However, for flow rate it can be the difference between group B and D are striking, therefore if a higher grout flow rate is used, a lower value of  $\alpha_t$  should be used. According to the data in this research, this factor should be in the neighbourhood of 0.0079.



# 7

## Discussion

This chapter shows the discussion on the topics touched upon in chapter 5. This discussion includes a section about collection and processing of the data and a section concerning the reliability and validity of the obtained results of the analysis.

### **7.1. Evaluation on Data Processing and Collection**

#### **7.1.1. Static Pile Load Test**

The first and foremost point that needs to be addressed here is about the negative pile head rise that was seen in pile categories A and B during the static pile load test. In this test the pile is subjected to tension, thus a pulling force is being applied, and a negative pile head rise signifies that the pile has been pushed downwards. An external company was hired in order to complete this static pile test but no explanation was found as to why these pile head rises occurred. It was speculated that perhaps piles B1 and A2 could have an inclined Gewi bar (pull-out rod in the concrete pile), thus explaining the negative displacements. However this was proven to not be the case and the inclination of said piles was between  $0^{\circ}$  -  $2^{\circ}$  max for pile A2 and  $0^{\circ}$  for pile B1. Nonetheless, despite that strange measurement of the pile head rise, the values of shaft bearing capacity were very close to those predicted according to the Dutch NEN method.

#### **7.1.2. Installation Process and Sample Collection**

There were no major inconveniences during the installation process of the piles except for one that the original position for pile A1 was CPT position 10, but due to installation error at that position. This is important to address as the original CPT positions were carefully chosen so that the pile categories would have as similar soil conditions as possible to each other. Even though the CPT profiles were not extremely different from each other, it can be seen that a difference is indeed present and that affected the results for pile A1.

Another point to address is that the grout mixtures were prepared on site during the installation and the mixer did not measure density automatically so that had to be done manually which creates a certain level of error. Additionally, in the first couple of seconds pressure of

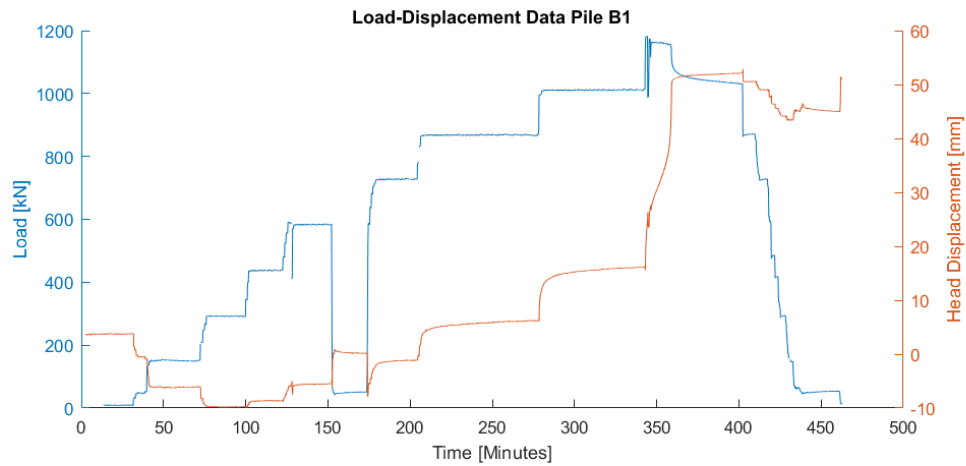


Figure 7.1: Load-Displacement plot for pile B1, for which one can see the negative pile head rise.



Figure 7.2: Inclination of Pile B1

the injection of the grout mixture needed to be regulated until the correct flow rate would be reached. Both of these create a certain level of error and small deviations in what the perfect conditions could be for this test, yet this is rather negligible when looking at the bigger picture because in the end the intended input parameters were always achieved.

### 7.1.3. Pre- and Post-Installation Data

There is an ongoing discussion about whether the mean of the two post CPT data should be used or the minimum value between two CPT positions per pile location (the East and

West post shown in Figure 5.1). The minimum value is a more conservative approach as it would prevent from overestimating the cone resistance. However from section 5.1.2 one can see that the contour plot with the mean cone resistance values is slightly more uniform in terms of the distribution of the values across the field, but in terms of range, so the distance between the highest and lowest value, is almost the same in both situations. Although an important point to consider is that during the installation of the post-CPT probing some of the CPTs suffered from a certain degree of inclination, some more than others and to significant extent, Figure 6.2 shows an example of said inclination. In this figure, it can be seen that the tip of the cone was displaced to about 1m off of its initial trajectory during penetration. It becomes unclear to conclude that the contour plot with the minimum cone resistance is a good representation of the situation in the field, and this is because of how interpolation works. Even if interpolation with more data points is more precise in theory, the fact that some of the data points contain information of cone resistance of an erroneous (x,y) position in the field, thus the interpolation does lack accuracy in that regard. These variations are extreme as can be seen in Figures 5.18 5.19 and not very representative of the true situation. Therefore the representation of the average or mean cone resistance contour plot should not be discarded as a valid representation of the field in 2D.

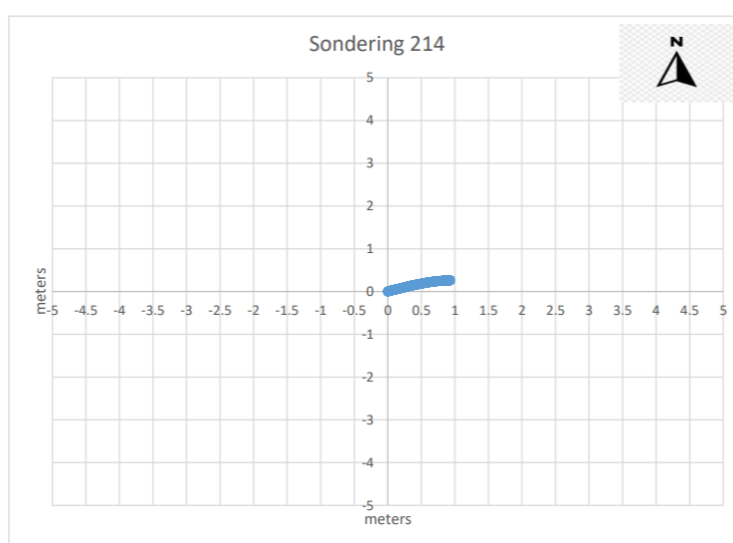


Figure 7.3: Inclination of Post CPT 14 (East)

Furthermore, another point of discussion is the applicability of using post-installation CPTs as means for predictability of the shaft bearing capacity. Currently, the Dutch method states that only the pre-installation CPTs are to be used in order to estimate the shaft bearing capacity, but what if we could use the post-installation data in order to define a prediction. The current method applies an  $\alpha_t$  factor of 0.009 for SI-piles with grout injection but this general term disregards the effect of variations of W/C ratio and injection flow rate. A similar  $\alpha_t$  parameter analysis is conducted for a possible "post-installation  $\alpha_t$  parameter". In order to obtain this parameter equation 4.2 is rearranged in order to solve for  $\alpha_t$ ,  $F_t$  being the measured shaft bearing capacity, and  $q_c$  being the average post-installation cone re-

sistance. The full set of 15 piles is analysed for the pre-installation, post-installation and minimum ( $q_c$ )  $\alpha_t$  factors. Table 6.2 shows the mean, standard deviation and the coefficient of variation of these variations of  $\alpha_t$  and ultimately proves that the pre-installation  $\alpha_t$  suffers from the least variation (lowest CoV), which means that  $\alpha_t = 0.009$  for the pre-installation situation is most likely to reach a more accurate prediction,  $\frac{F_{t,measured}}{F_{t,predicted}} \rightarrow 1$ .

Pile	Mean $q_c$ Pre	Mean $q_c$ Post Average	$\alpha_{t,pre}$	$\alpha_{t,post,avg}$	$\alpha_{t,post,min}$
1	18.12	13.10	0.0079	0.0096	0.012
2	14.22	15.71	0.0088	0.0073	0.0083
4	19.11	18.31	0.0078	0.0073	0.0085
5	17.77	17.26	0.0083	0.0074	0.0079
6	18.42	19.94	0.0083	0.0065	0.0075
7	19.06	18.30	0.0077	0.0069	0.0073
8	18.31	16.99	0.0082	0.0072	0.0083
9	13.52	11.39	0.0090	0.0072	0.0075
11	16.82	17.36	0.0092	0.0081	0.0086
12	15.30	13.45	0.0092	0.0084	0.0096
13	15.13	14.13	0.0096	0.0084	0.010
14	18.14	14.51	0.0074	0.0081	0.0083
15	16.12	15.00	0.0096	0.0083	0.0085
17	13.60	14.35	0.0088	0.0063	0.0071
18	15.03	16.17	0.0089	0.0062	0.0079
	Mean		0.0086	0.0075	0.0085
	Standard Deviation		0.00069	0.00090	0.00117
	CoV*		0.08	0.12	0.14

Table 7.1: Assessment of  $\alpha_t$  parameters, \*CoV = Coefficient of variation

A probability density function was plotted in order to have a visual representation of why the pre-installation  $\alpha_t$  value is best, this is shown in Figure 7.4. It is important to remember that in a PDF the area under the curve must be equal to 1, thus since the standard deviation is so low the probability values become very high, but this is just a tool to compare the three different scenarios.

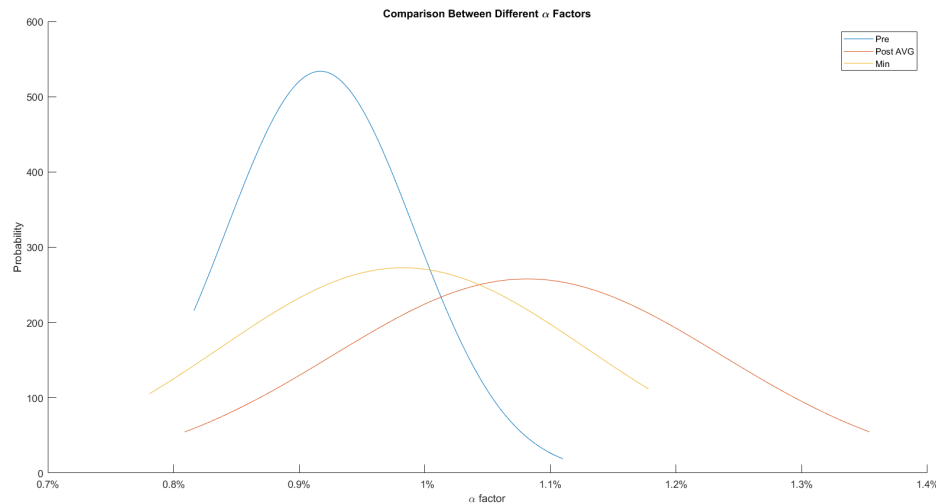


Figure 7.4: Inclination of Pile B1

## 7.2. Deviation from the NEN 9997-1

The one aspect of this research that deviates from the Dutch code NEN 9997-1 is the fact the cone resistance was not limited to  $q_c \leq 15$  MPa. If this limit would have been implemented, then the results of the M/P ratio would have been less conservative. Table 7.2 shows the difference in M/P ratio with and without the cone resistance limit specified in the Dutch code. What can be derived from the table is that for group A there is not much difference but for the other groups the difference is striking, especially for group D piles. where the deviation to the perfect ratio of M/P = 1 for this pile group D is 0.16 without a limit and 0.06 with the limit. Additionally, a major difference can be seen for pile group C, where setting a limit decreases severely the predicted failure load which lead to group C to having the largest M/P ratio of all the pile groups. But looking at all the 15 piles, the M/P ratio has been closest to 1, therefore having a more correct prediction, when no limit was set. Only for piles A3, D1, and D3 that was not the case. This leads to the conclusion that for the set of piles used in this experiment, not setting a limit yields more accurate shaft capacity. However, this also shows that for shaft capacity calculations including the conservative limit of  $q_c \leq 15$  MPa, than you could perfectly have much higher W/B ratios and flow rates and still have very good M/P ratios.

### 7.3. Observations on the Validity of Obtained Results

There exists a problem with the quantity of data points per variation in this research. Each variation, or pile category, only consists of 3 piles and thus 3 data points that can be obtained. This is extremely restricted and makes it very difficult to draw major conclusions. Nonetheless, certain conclusions can be drawn and these can then set the path for further research on specific subjects. One of the notable conclusions and with a rather clear result is that the pre-installation CPT  $\alpha_t$  factor is more likely to predict the shaft bearing capacity observed in the field. In Dutch practice the  $\alpha_t$  factor utilised is in the bounds of 0.009 to 0.012 (as an upper limit), and this is consistent with the results obtained in this research, where ultimately the average of all the piles for  $\alpha_t = 0.0089$  and the maximum value observed is less than that upper limit.

Additionally, while the analysis in Chapter 5 focuses on attempting to understand the direct and indirect effects that the grout installation parameters have on the shaft capacity, there is an important observation to point out. The M/P ratio had high accuracy ( $M/P > 0.970$ ) for piles that had a predicted pullout force  $F_t < 1300$  [kN]. For any pile with a higher prediction the M/P ratio would decrease far beyond 0.970. It could be interesting for further research to explore the possible effect of the initial cone resistances and the influence it has on the M/P ratio afterwards. Perhaps it would also be great to try to observe the mechanism that occurs with the penetration of the grout fluid in the soil pores and seeing if there is any wear that occurs that could such observed results.

[5] [15] [17] [4] [23] [25] [20] [22] [9] [14] [10] [11] [18] [16] [1] [13] [24] [8] [7] [12] [2] [19] [6] [27] [3] [26] [21]

Pile Name	Measured Failure Load [kN]	Predicted Failure Load (No Limit) [kN]	Predicted Failure Load (Limit) [kN]	Ratio [M/P] (No Limit) [-]	Ratio [M/P] (Limit) [-]
A1	965	972	957	0.993	1.01
A2	972	999	957	0.973	1.02
A3	1117	1132	1063	0.987	1.05
B1	1182	1159	1063	1.020	1.11
B2	1210	1132	1076	1.069	1.12
B3	1302	1219	1110	1.068	1.17
C1	1319	1532	1103	0.86	1.20
C2	1321	1438	1110	0.919	1.19
C3	1272	1485	1083	0.857	1.17
D1	1247	1432	1143	0.870	1.09
D2	1244	1372	1103	0.907	1.13
D3	1077	1432	1123	0.752	0.96
E1	1102	1125	1010	0.980	1.09
E2	1319	1432	1116	0.921	1.18
E3	1250	1225	1056	1.020	1.18

Table 7.2: Comparison of the measured and predicted shaft capacity with and without the limit of  $q_c \leq 15$  MPa

# Bibliography

- [1] Mohammad Reza Azadi, Ali Taghichian, and Ali Taheri. Optimization of cement-based grouts using chemical additives. *Journal of Rock Mechanics and Geotechnical Engineering*, 9(4):623–637, 2017.
- [2] SK Bagui, SK Puri, Venkat Rao, BC Dinesh, and Atasi Das. Estimation of base grout quantity for cast in situ piles based on field test results. *Advances in Bridge Engineering*, 1(1):1–15, 2020.
- [3] Imad A Basheer. Selection of methodology for neural network modeling of constitutive hystereses behavior of soils. *Computer-Aided Civil and Infrastructure Engineering*, 15(6):445–463, 2000.
- [4] Prasenjit Basu and Monica Prezzi. Design and applications of drilled displacement (screw) piles. 2009.
- [5] Prasenjit Basu, Monica Prezzi, and Dipanjan Basu. Drilled displacement piles—current practice and design. *DFI Journal-The Journal of the Deep Foundations Institute*, 4(1):3–20, 2010.
- [6] M Bustamante and L Gianceselli. Installation parameters and capacity of screwed piles. In *Deep foundations on bored and auger piles BAP III*, pages 95–108, 1998.
- [7] Ryen Caenn, Henry CH Darley, and George R Gray. Composition and properties of drilling and completion fluids. Gulf professional publishing, 2017.
- [8] Danielle Collins. Shafts in torsion: Mechanical properties of materials, 2019. URL [www.linearmotiontips.com/mechanical-properties-of-materials-shafts-in-torsion/](http://www.linearmotiontips.com/mechanical-properties-of-materials-shafts-in-torsion/).
- [9] Harry M Coyle and Lymon C Reese. Load transfer for axially loaded piles in clay. *Journal of the soil mechanics and foundations division*, 92(2):1–26, 1966.
- [10] P Dayakar, K Venkat Raman, and KVB Raju. Study on permeation grouting using cement grout in sandy soil. *Journal of Mechanical and Civil Engineering*, 4(4):5–10, 2012.
- [11] Vahidoddin Fattahpour, Béatrice Anne Baudet, and James Wang-Cho Sze. Laboratory investigation of shaft grouting. *Proceedings of the Institution of Civil Engineers-Geotechnical Engineering*, 168(1):65–74, 2015.
- [12] Henry Green et al. *Industrial rheology and rheological structures*. 1949.
- [13] John Ross Jeffrey, Michael John Brown, Jonathan Adam Knappett, Jonathan David Ball, and Karlis Caucis. Chd pile performance: part i—physical modelling. *Proceedings of the Institution of Civil Engineers-Geotechnical Engineering*, 169(5):421–435, 2016.

- [14] Adam Krasiński and Mateusz Wiszniewski. The mechanism of grouting action under the base of bored pile. 2018.
- [15] Martin Larisch. Behaviour of stiff, fine-grained soil during the installation of screw auger displacement piles. 2014.
- [16] Zhipeng Li, Lianzhen Zhang, Yuntian Chu, and Qingsong Zhang. Research on influence of water-cement ratio on reinforcement effect for permeation grouting in sand layer. *Advances in Materials Science and Engineering*, 2020, 2020.
- [17] All Answers LTC. Effect of embedment ratio on load-transfer and failure mechanisms of helical screw piles, 2019. URL <https://ukdiss.com/examples/embedment-ratio-load-transfer-failure-mechanisms.php>.
- [18] Mamdouh A. Nasr. Method for installing ascrew pile, 4 2008. URL <https://patentimages.storage.googleapis.com/4e/ed/40/21add1f8a202fe/US7338232.pdf>. US Patent 7,338,232 B2.
- [19] Willie M NeSmith. Static capacity analysis of augered, pressure-injected displacement piles. In *Deep Foundations 2002: An International Perspective on Theory, Design, Construction, and Performance*, pages 1174–1186. 2002.
- [20] Ruwan Abey Rajapakse. *Geotechnical engineering calculations and rules of thumb*. Butterworth-Heinemann, 2015.
- [21] Mark Randolph and Susan Gourvenec. *Offshore geotechnical engineering*. CRC press, 2017.
- [22] AS Ritonga et al. Shear strength parameters of peat soil of district of asahan by direct shear test. In *IOP Conference Series: Materials Science and Engineering*, volume 801, page 012013. IOP Publishing, 2020.
- [23] E. Smienk and L. de Quelerij. *Handboek funderingen: Deel B - 4430*. SBR, 2010.
- [24] Cristina de Hollanda Cavalcanti Tsuha and Nelson Aoki. Relationship between installation torque and uplift capacity of deep helical piles in sand. *Canadian Geotechnical Journal*, 47(6):635–647, 2010.
- [25] GJC Van Gorp. *Optimization of modeling pile foundations*. 2014.
- [26] JC Van Mierlo and AW Koppejan. Lengte en draagvermogen van heipalen. *Bouw*, 3: 1952, 1952.
- [27] Miao Yu, Chenhui Wei, Leilei Niu, Shaohua Li, and Yongjun Yu. Calculation for tensile strength and fracture toughness of granite with three kinds of grain sizes using three-point-bending test. *PloS one*, 13(3):e0180880, 2018.

# A

## Appendix A: Pre- Post-Installation Changes

### A.1. CPT Profiles

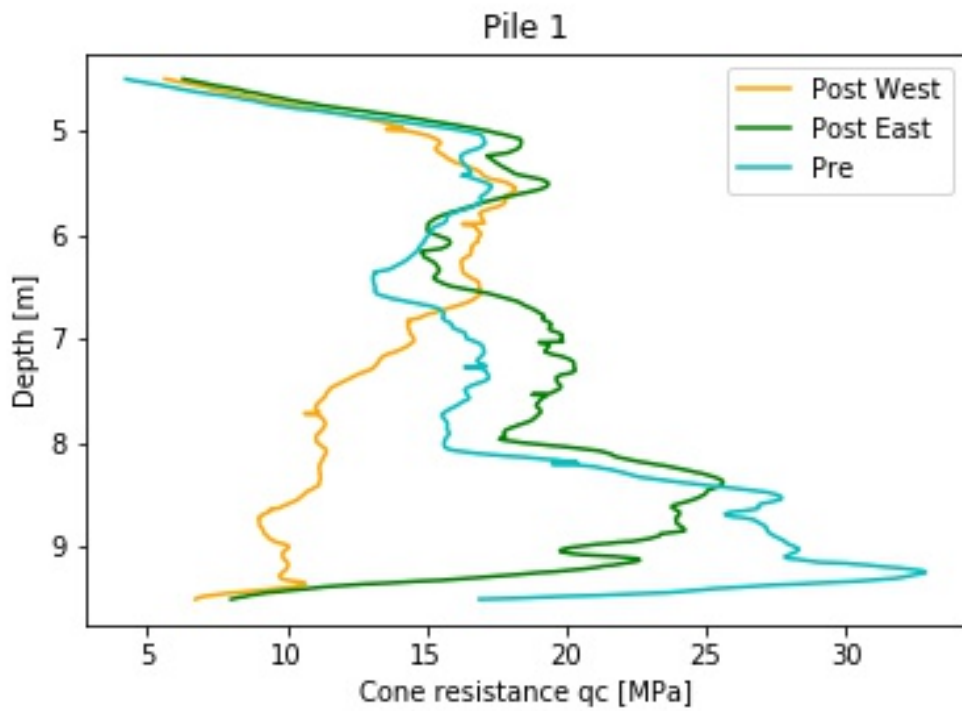


Figure A.1: Pile D1: Pre-installation vs (average) Post-installation Cone Resistance

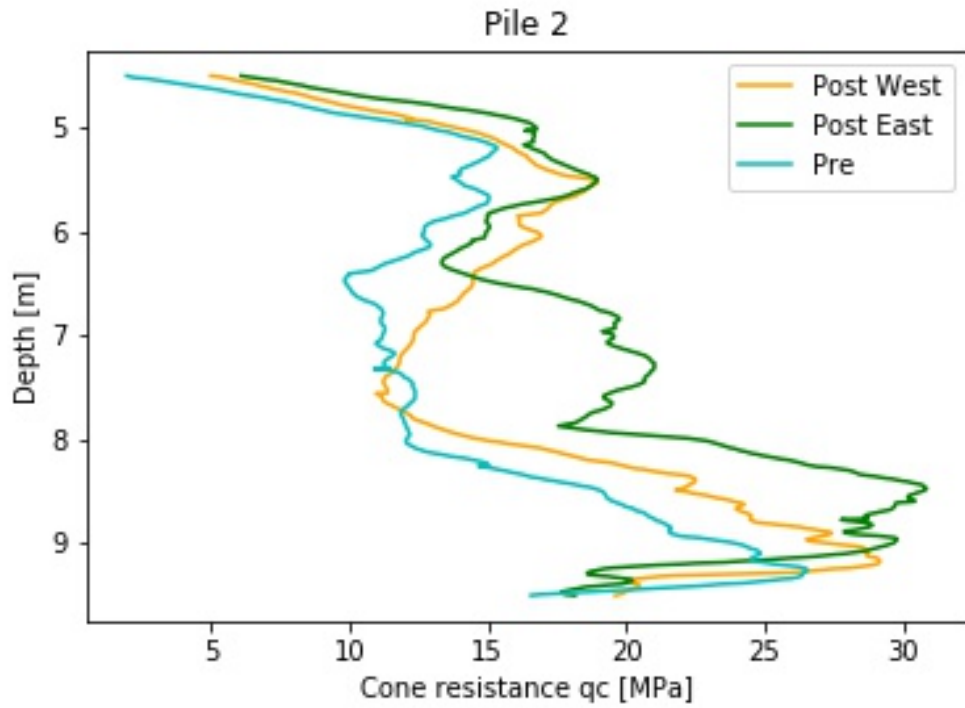


Figure A.2: Pile E1: Pre-installation vs (average) Post-installation Cone Resistance

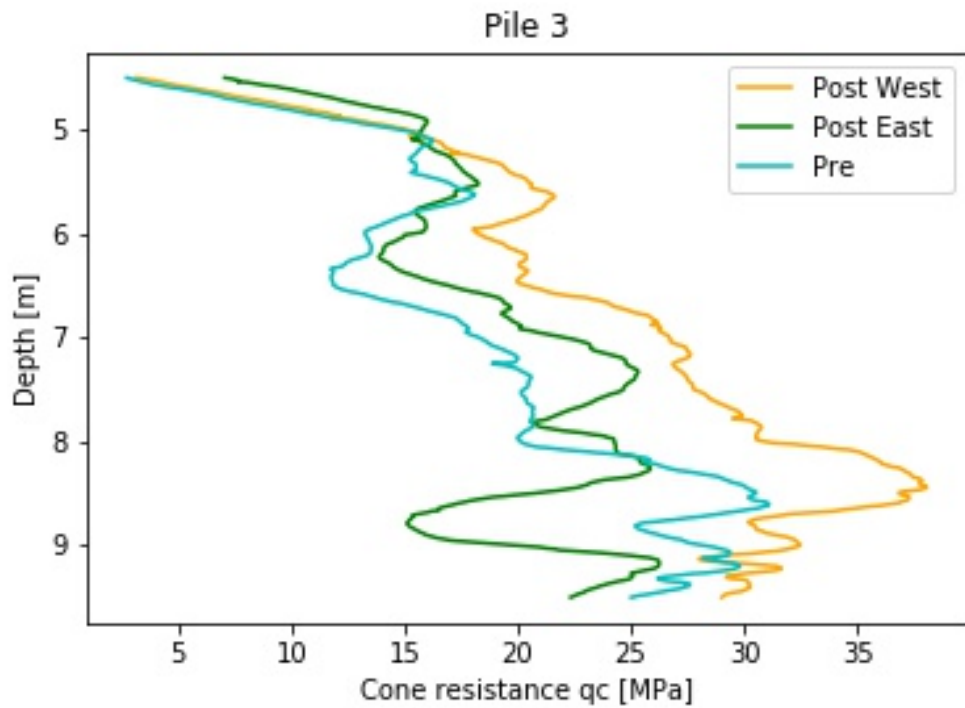


Figure A.3: Pile C1: Pre-installation vs (average) Post-installation Cone Resistance

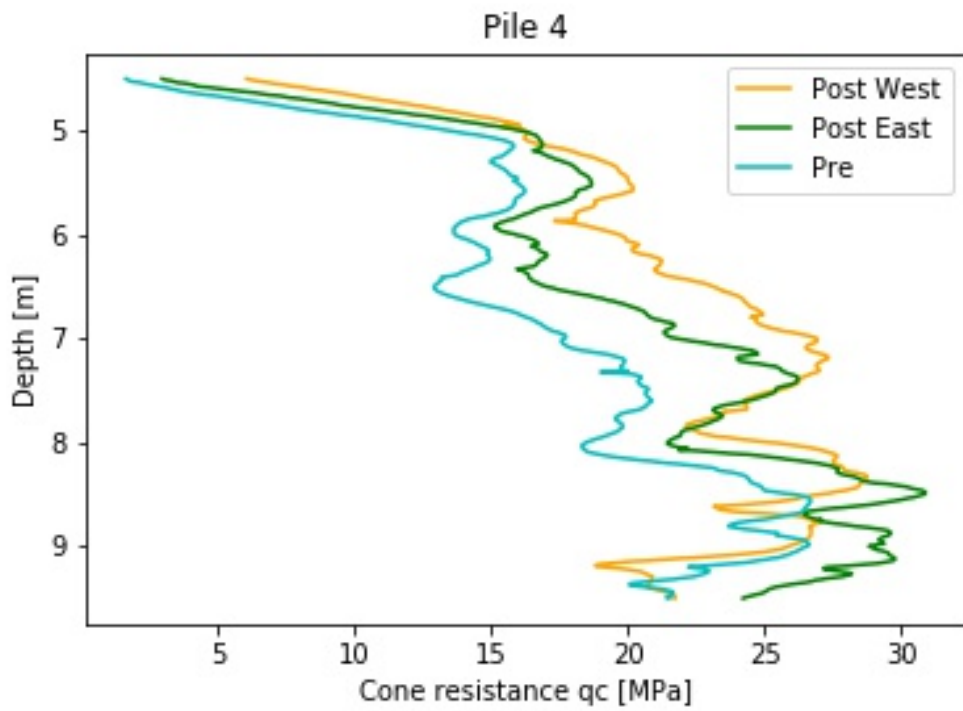


Figure A.4: Pile E2: Pre-installation vs (average) Post-installation Cone Resistance

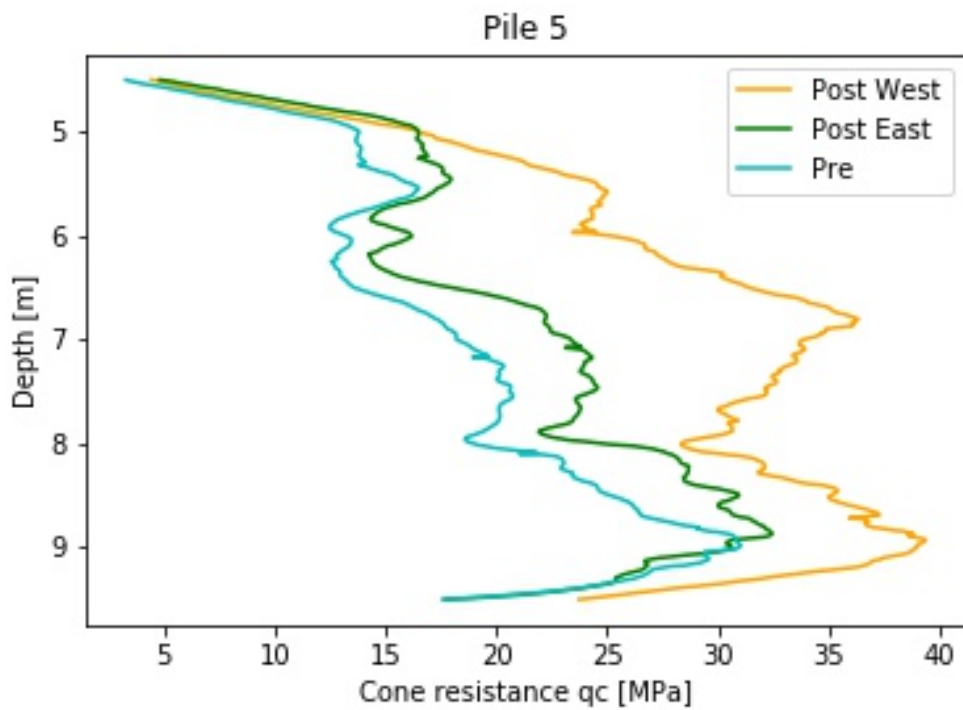


Figure A.5: Pile C2: Pre-installation vs (average) Post-installation Cone Resistance

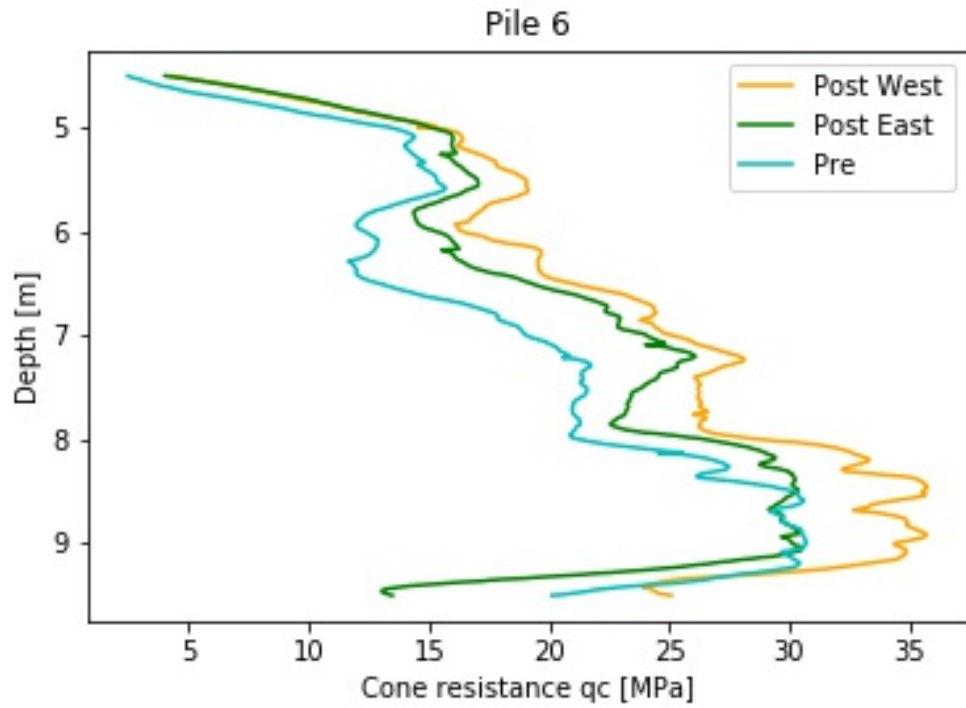


Figure A.6: Pile C3: Pre-installation vs (average) Post-installation Cone Resistance

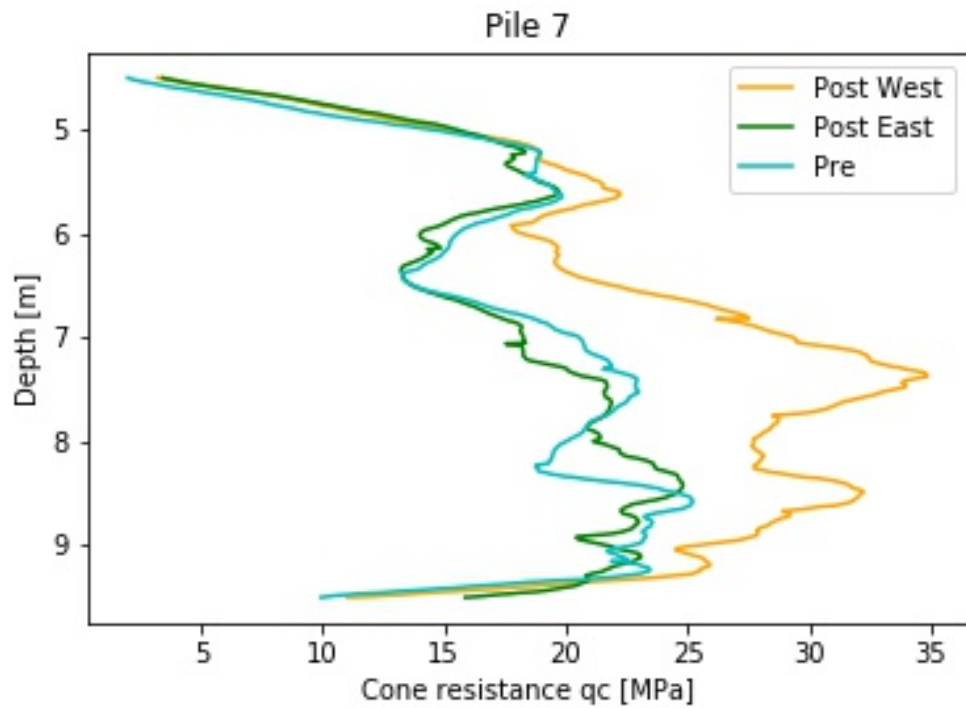


Figure A.7: Pile D2: Pre-installation vs (average) Post-installation Cone Resistance

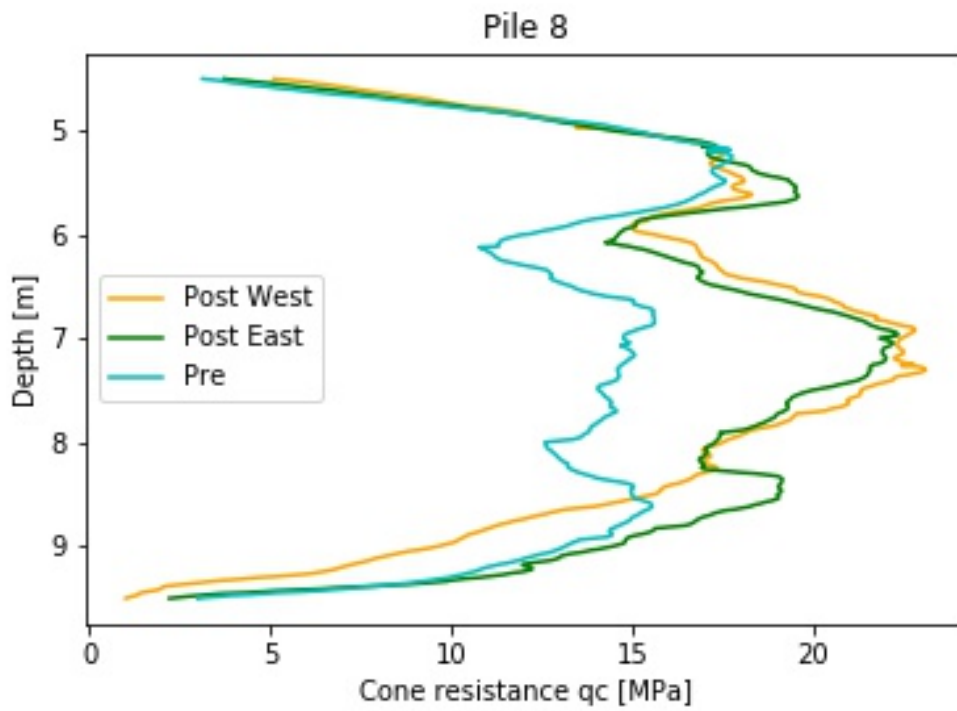


Figure A.8: Pile A1: Pre-installation vs (average) Post-installation Cone Resistance

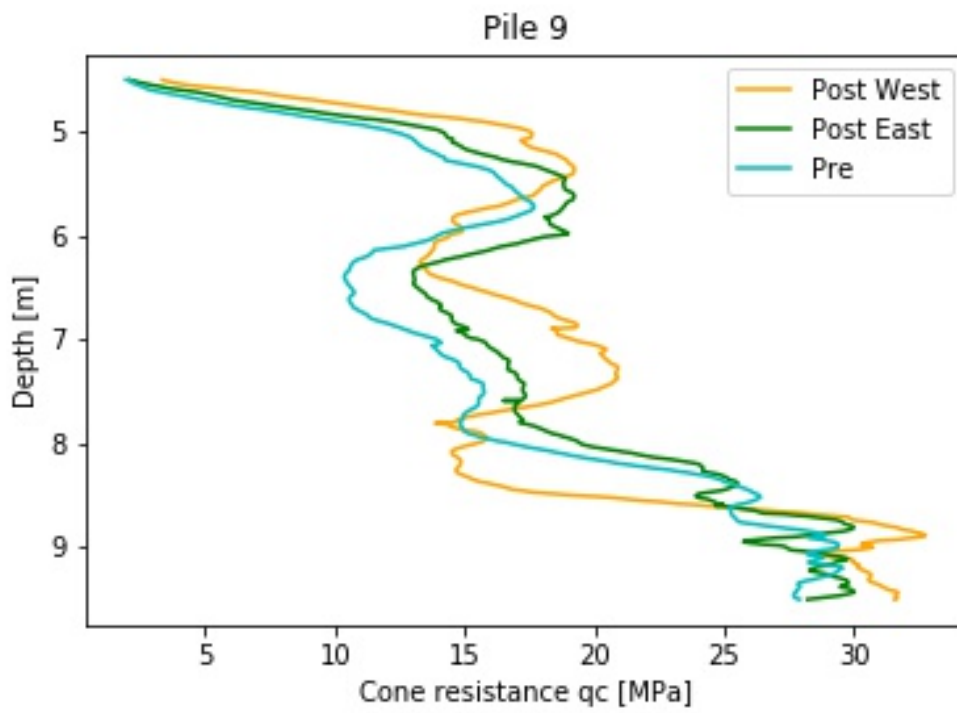


Figure A.9: Pile E3: Pre-installation vs (average) Post-installation Cone Resistance

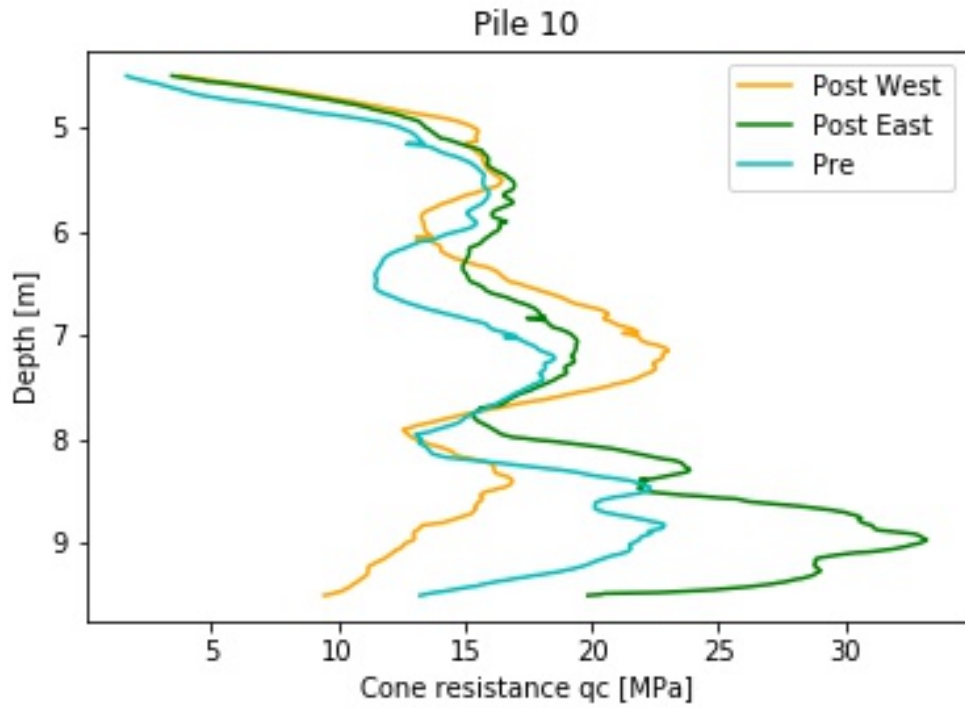


Figure A.10: Pile B1: Pre-installation vs (average) Post-installation Cone Resistance

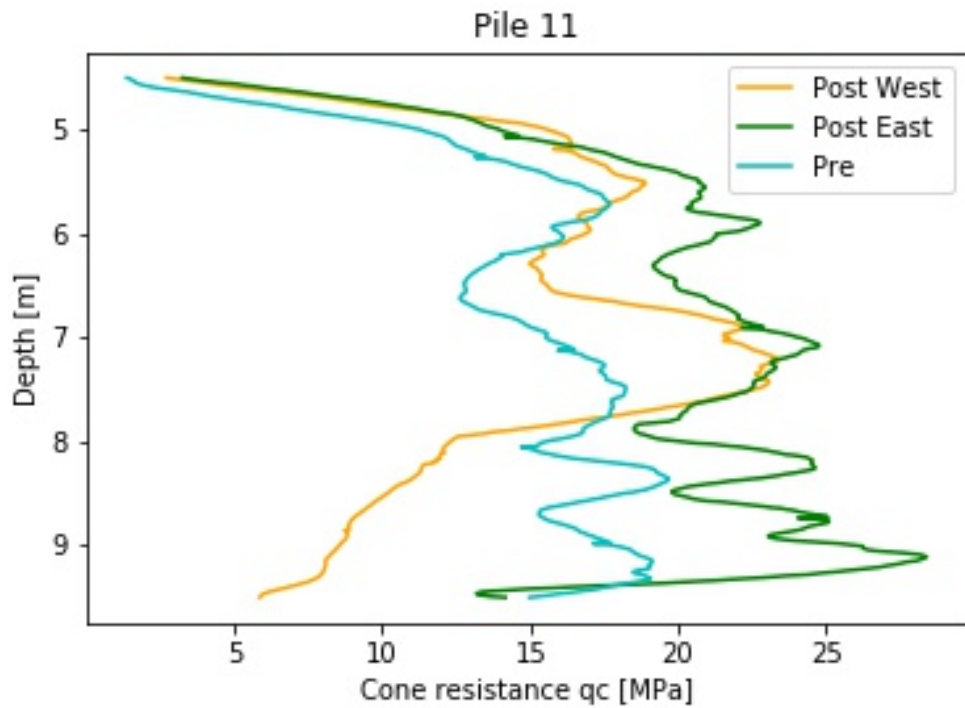


Figure A.11: Pile B2: Pre-installation vs (average) Post-installation Cone Resistance

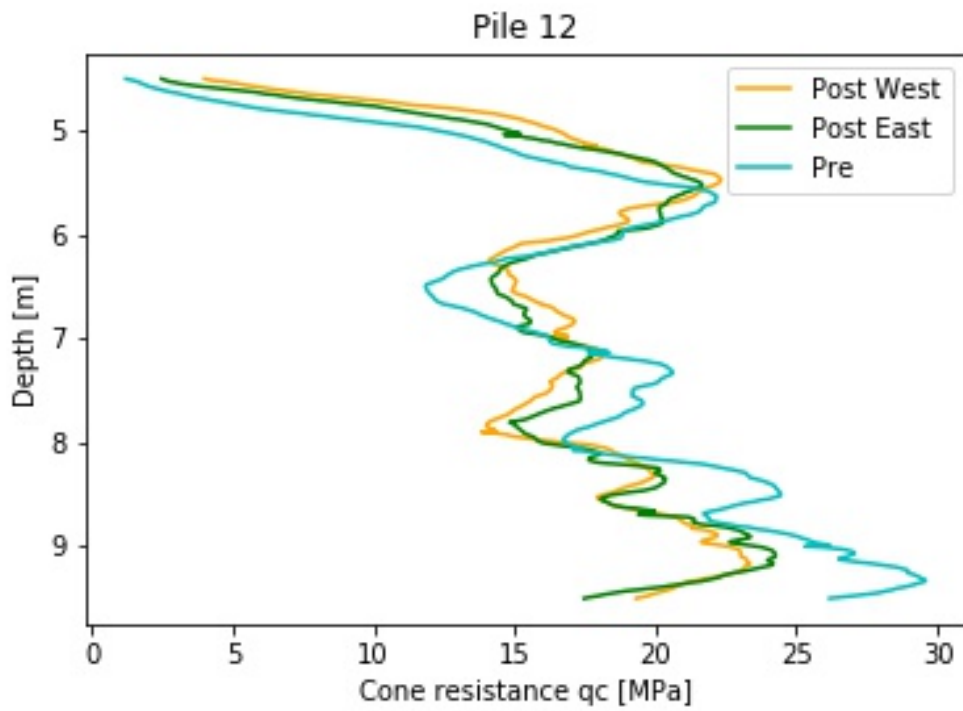


Figure A.12: Pile D3: Pre-installation vs (average) Post-installation Cone Resistance

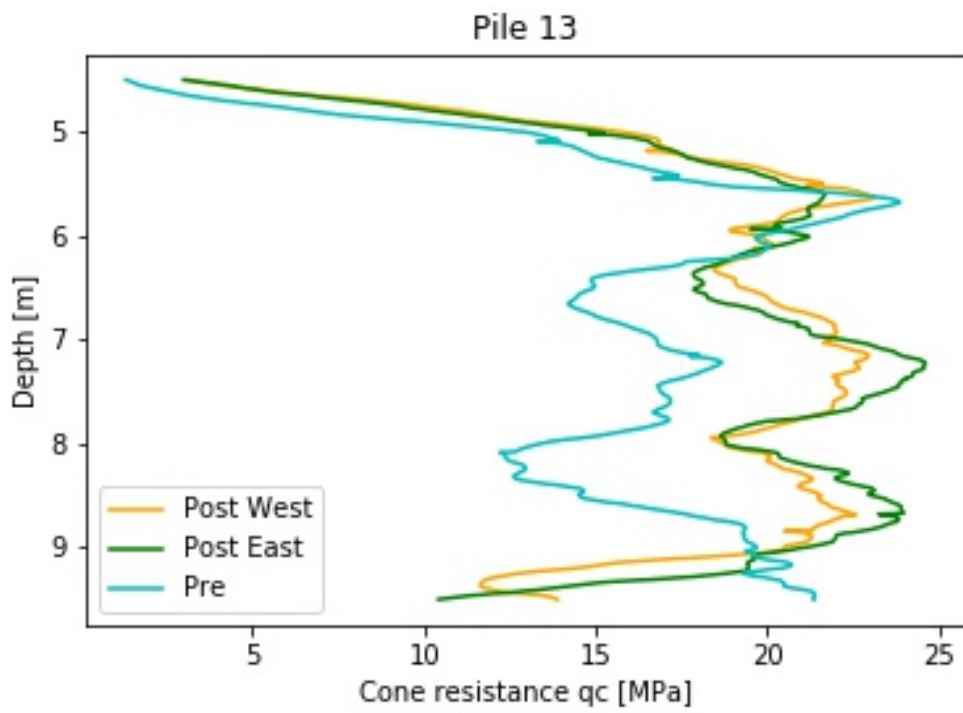


Figure A.13: Pile B3: Pre-installation vs (average) Post-installation Cone Resistance

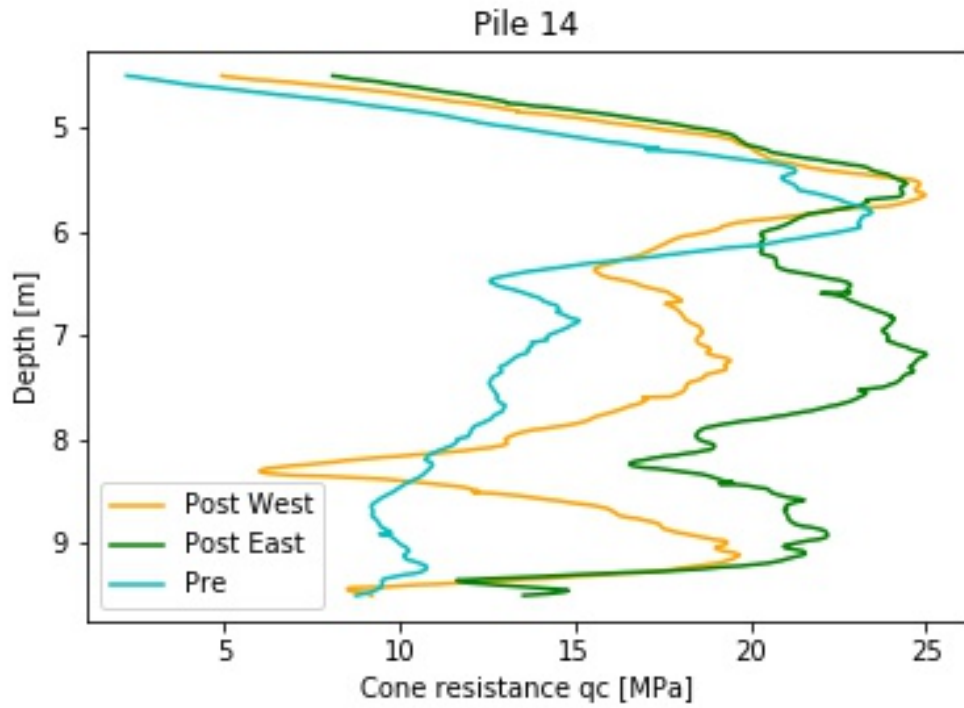


Figure A.14: Pile A2: Pre-installation vs (average) Post-installation Cone Resistance

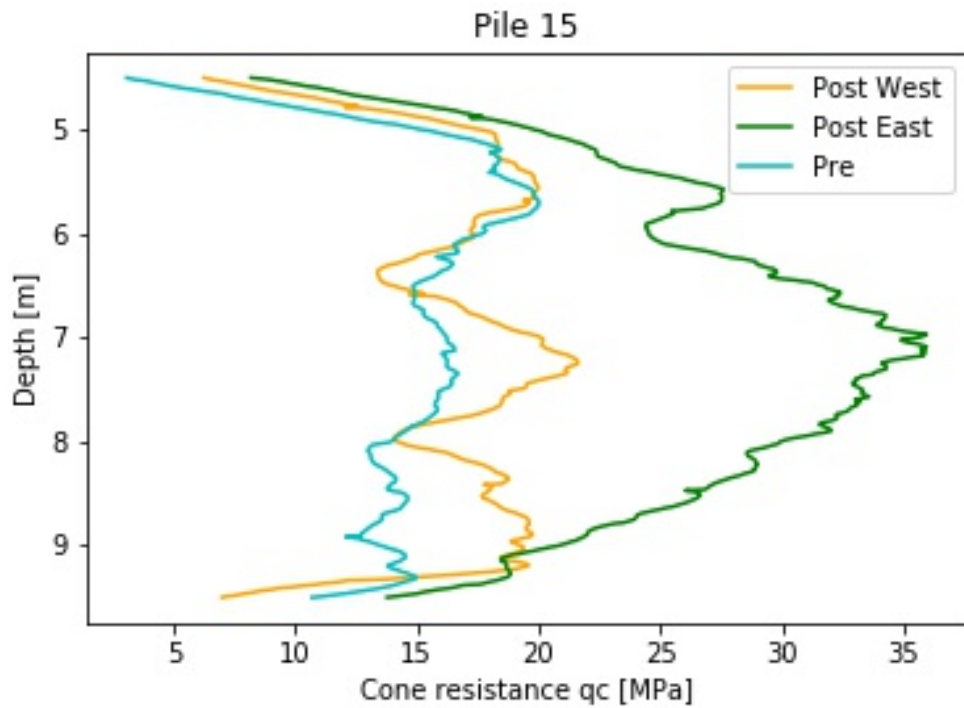


Figure A.15: Pile A3: Pre-installation vs (average) Post-installation Cone Resistance

## A.2. Ratio of Increment

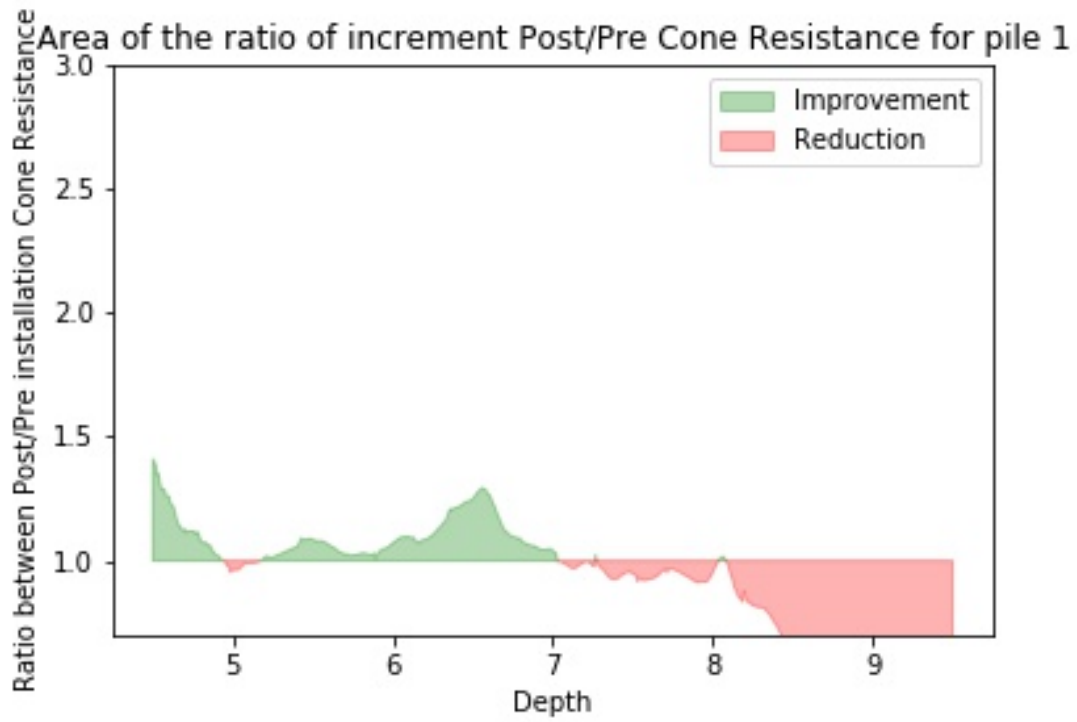


Figure A.16: Pile D1: Pre-installation vs (average) Post-installation Cone Resistance

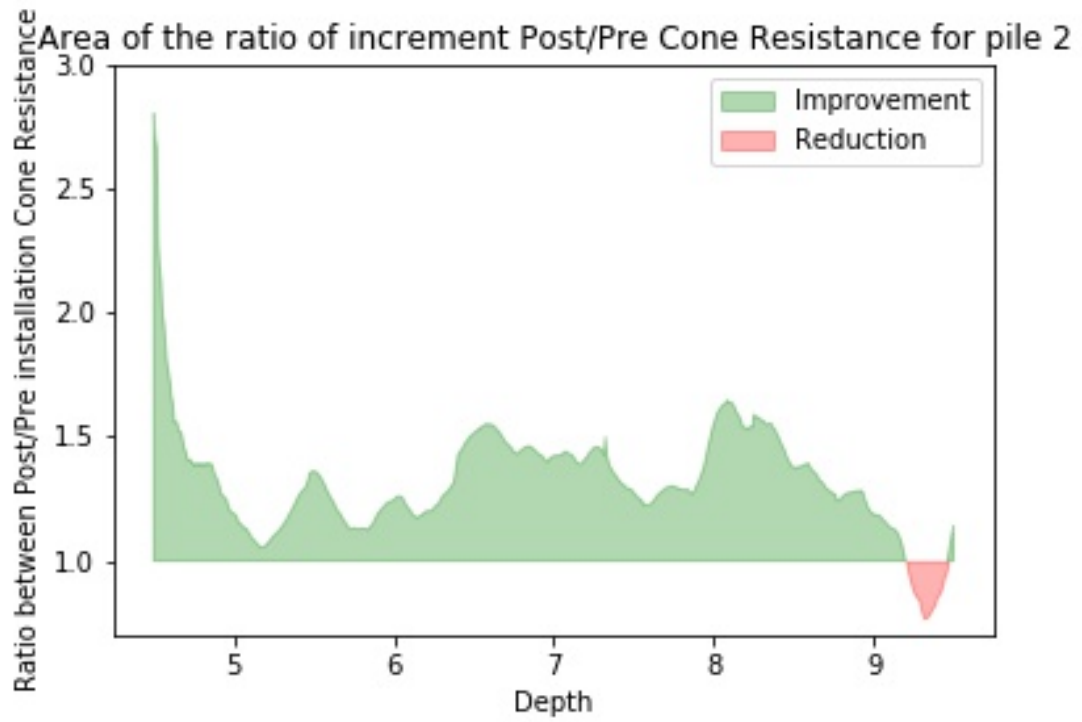


Figure A.17: Pile E1: Pre-installation vs (average) Post-installation Cone Resistance

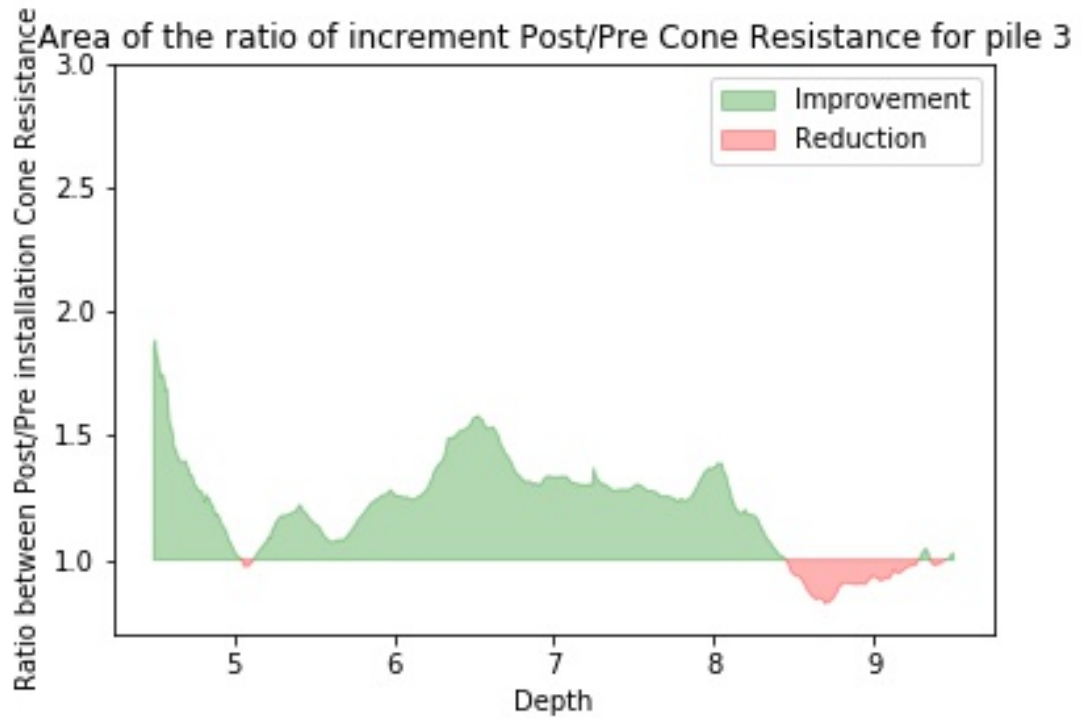


Figure A.18: Pile C1: Pre-installation vs (average) Post-installation Cone Resistance

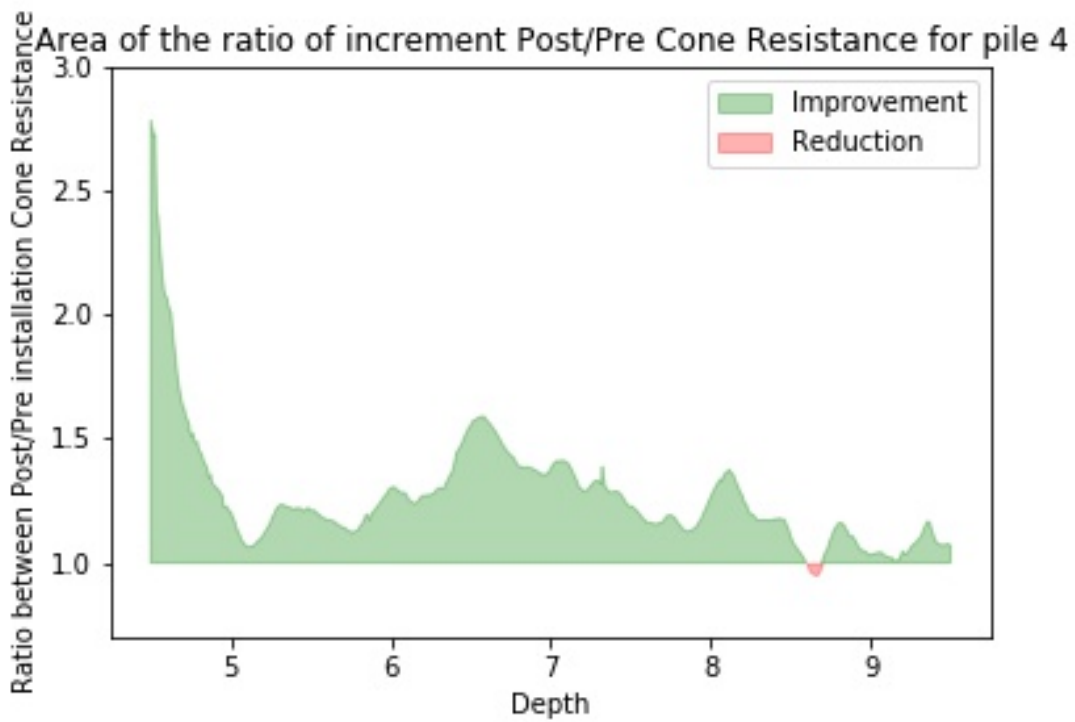


Figure A.19: Pile E2: Pre-installation vs (average) Post-installation Cone Resistance

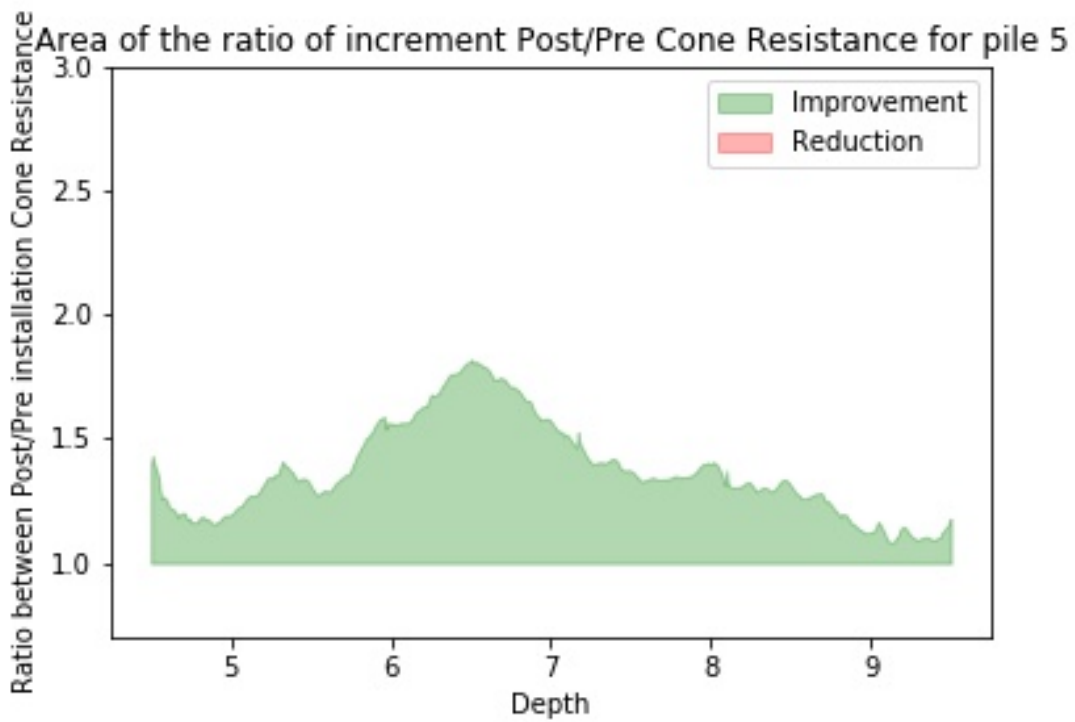


Figure A.20: Pile C2: Pre-installation vs (average) Post-installation Cone Resistance

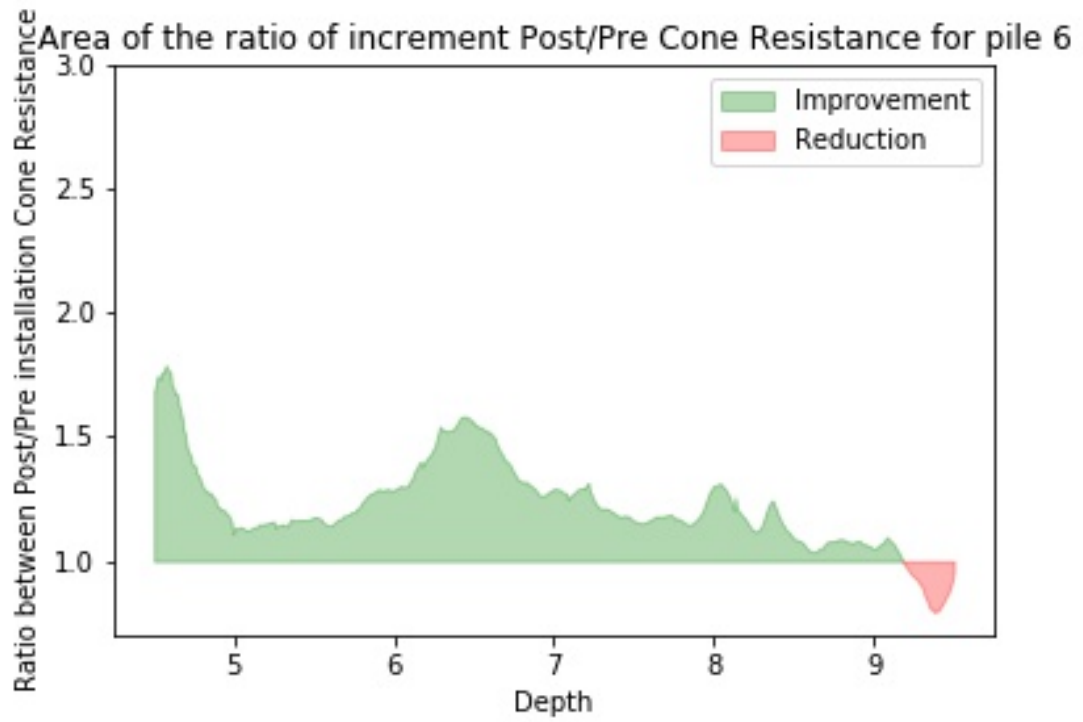


Figure A.21: Pile C3: Pre-installation vs (average) Post-installation Cone Resistance

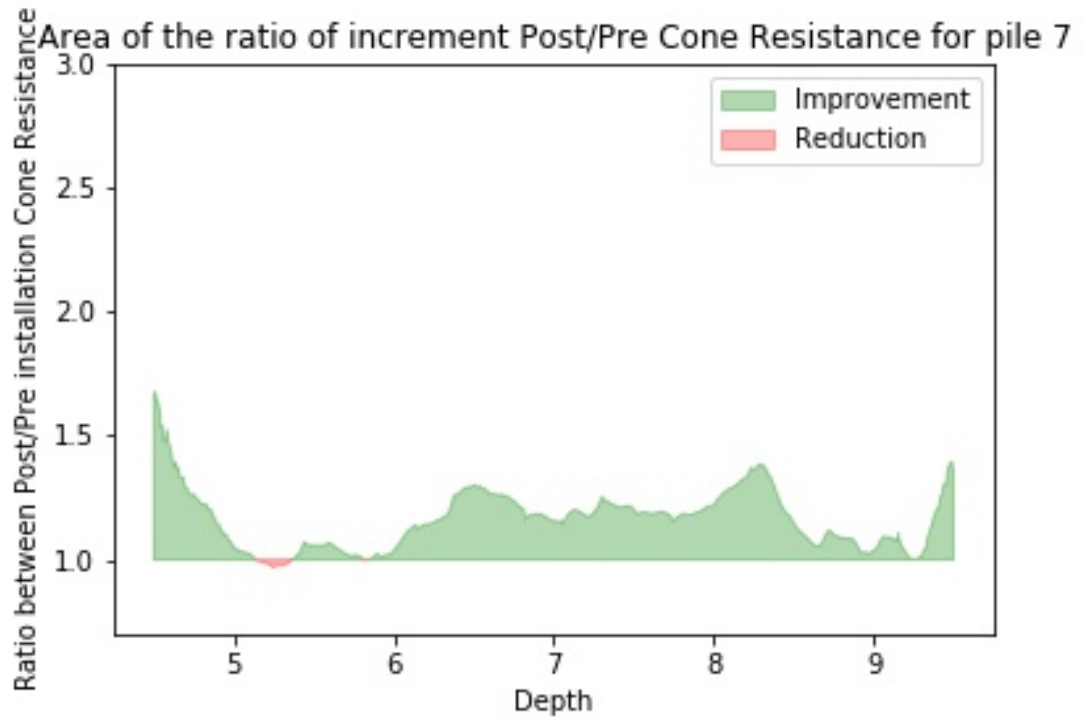


Figure A.22: Pile D2: Pre-installation vs (average) Post-installation Cone Resistance

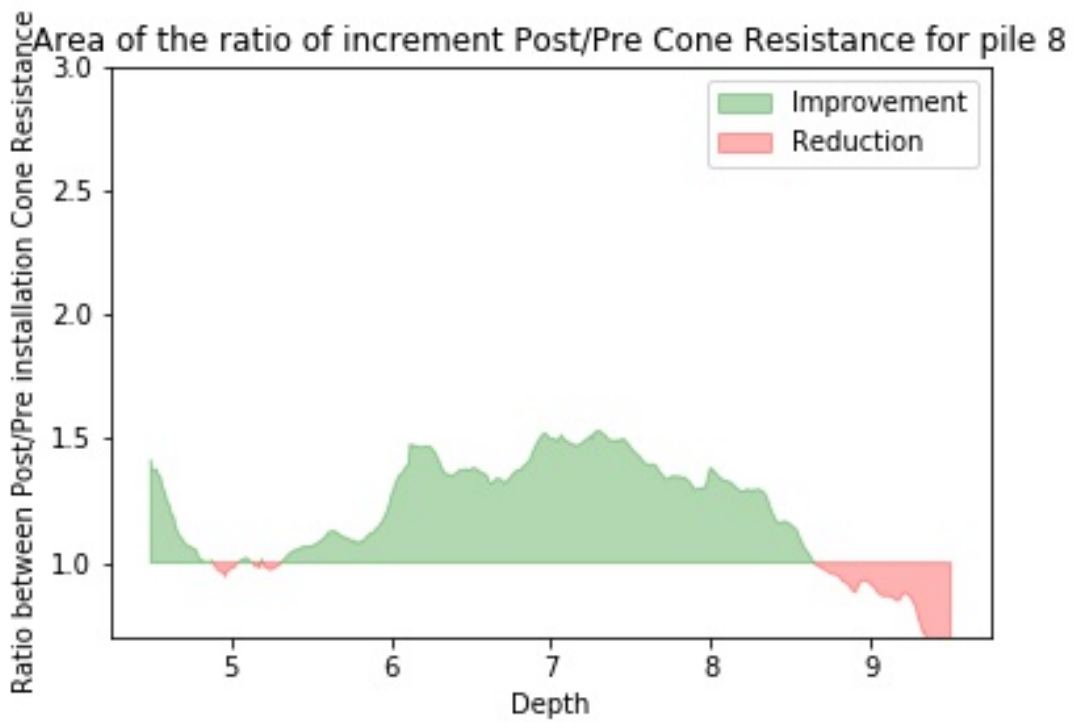


Figure A.23: Pile A1: Pre-installation vs (average) Post-installation Cone Resistance

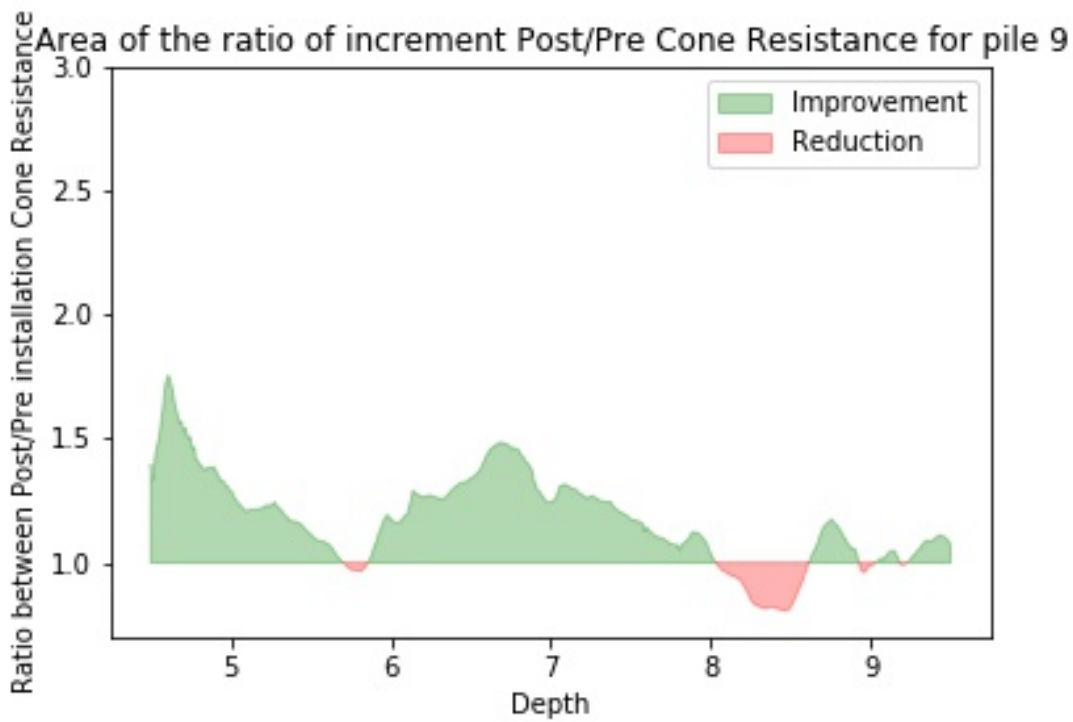


Figure A.24: Pile E3: Pre-installation vs (average) Post-installation Cone Resistance

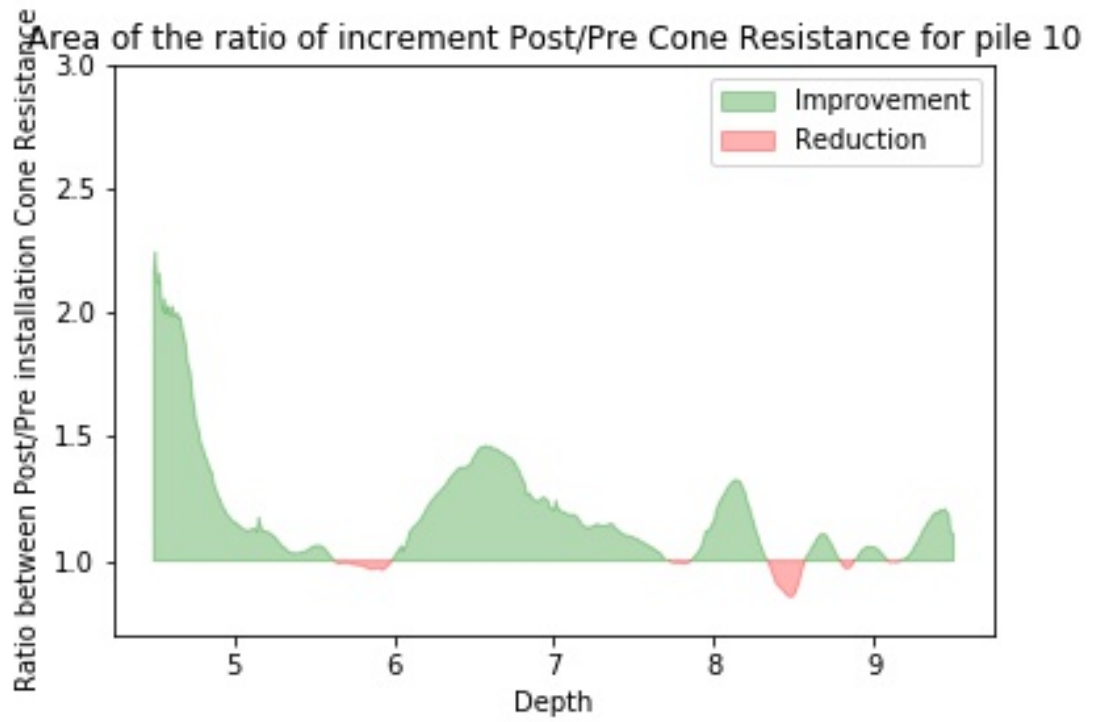


Figure A.25: Pile B1: Pre-installation vs (average) Post-installation Cone Resistance

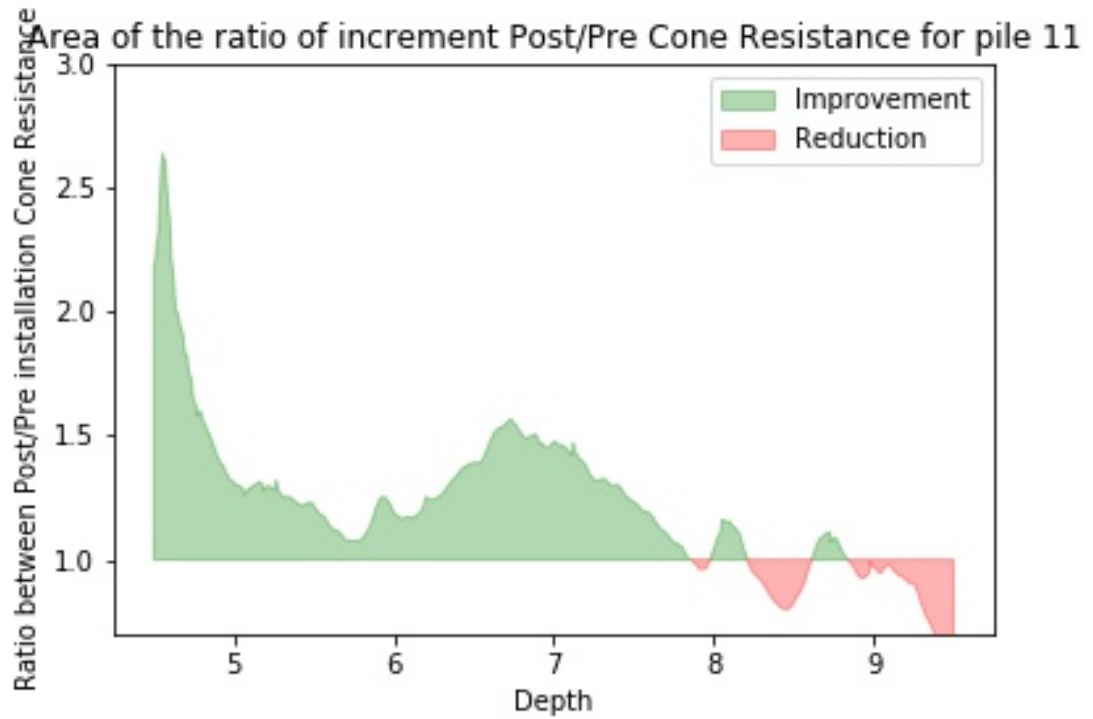


Figure A.26: Pile B2: Pre-installation vs (average) Post-installation Cone Resistance

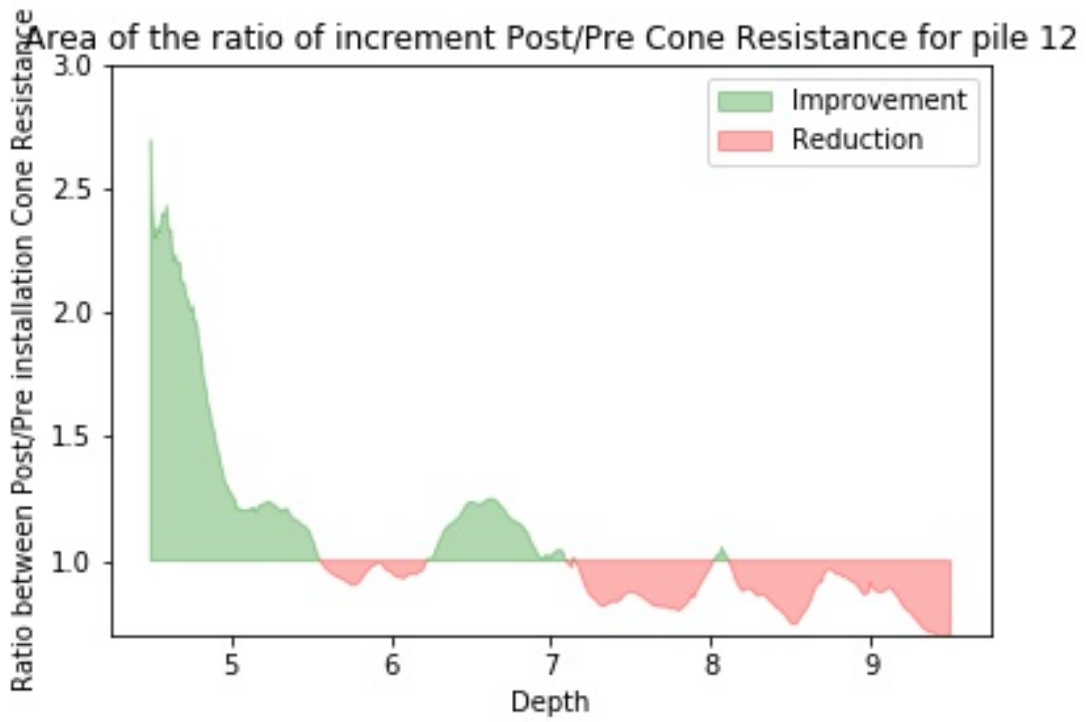


Figure A.27: Pile D3: Pre-installation vs (average) Post-installation Cone Resistance

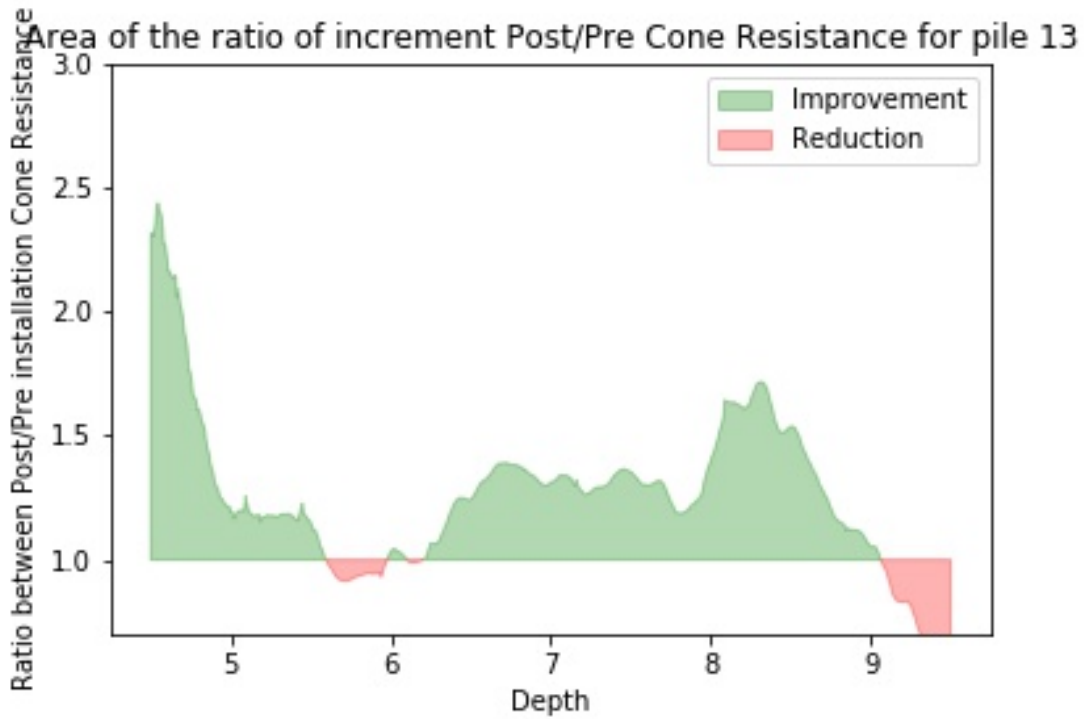


Figure A.28: Pile B3: Pre-installation vs (average) Post-installation Cone Resistance

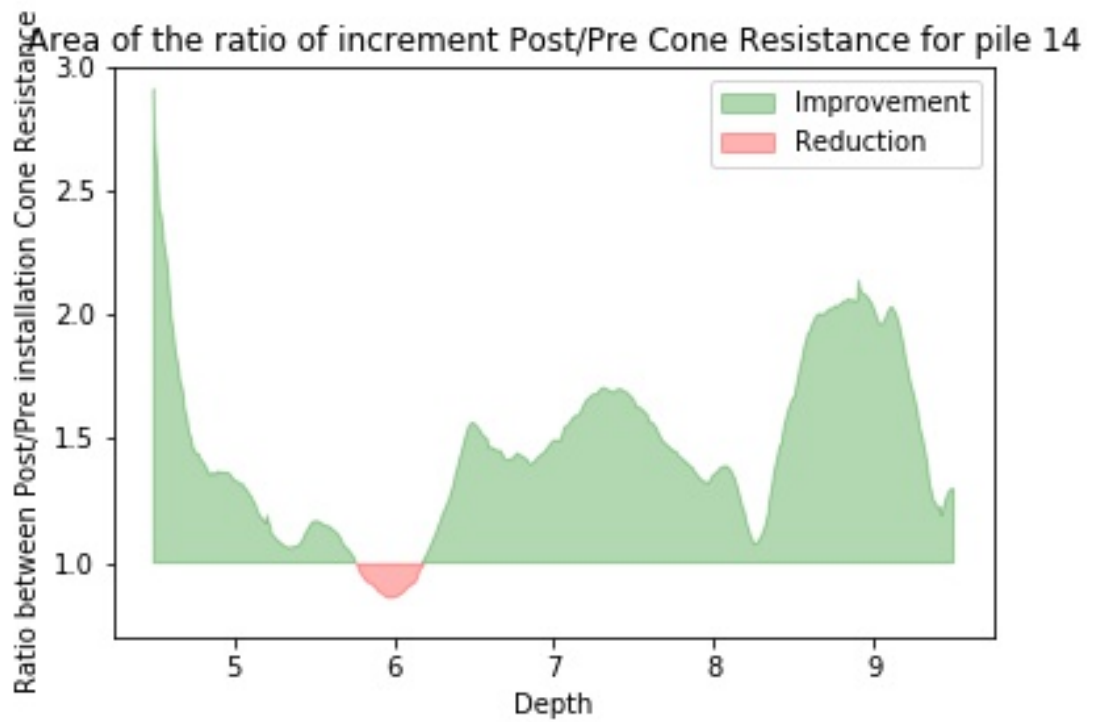


Figure A.29: Pile A2: Pre-installation vs (average) Post-installation Cone Resistance

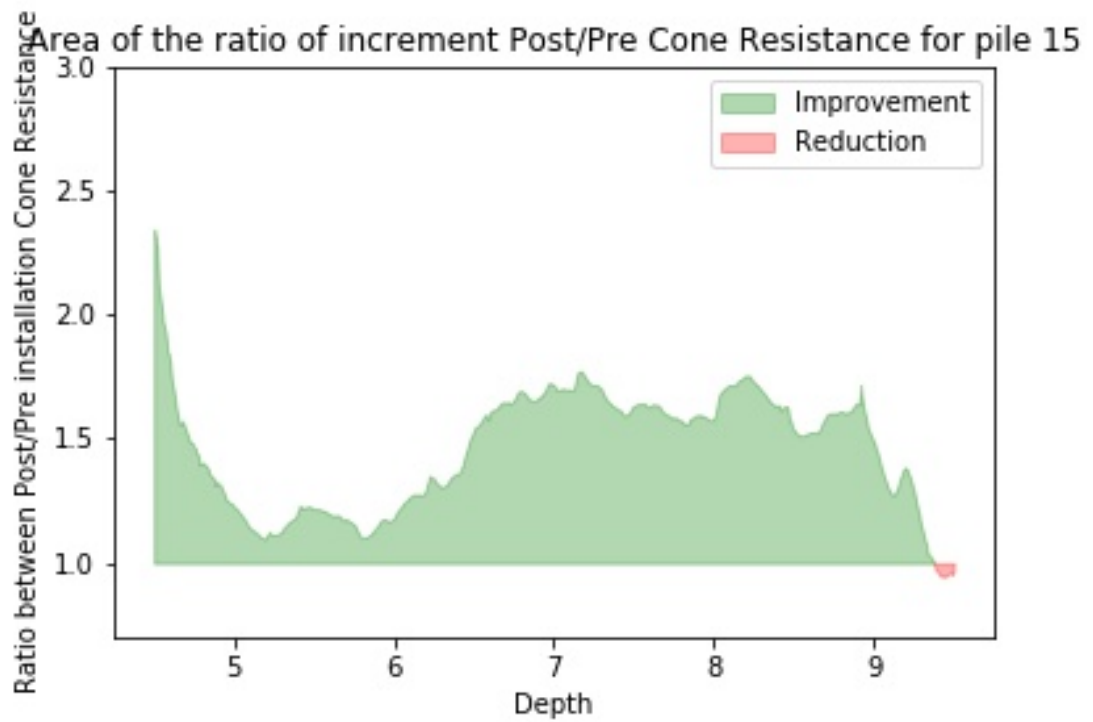


Figure A.30: Pile A3: Pre-installation vs (average) Post-installation Cone Resistance

# B

## Appendix B: Contour Plots

### B.1. Contour Plots of the Mean Post-Installation CPT Average Post-Installation CPT Contour Plots

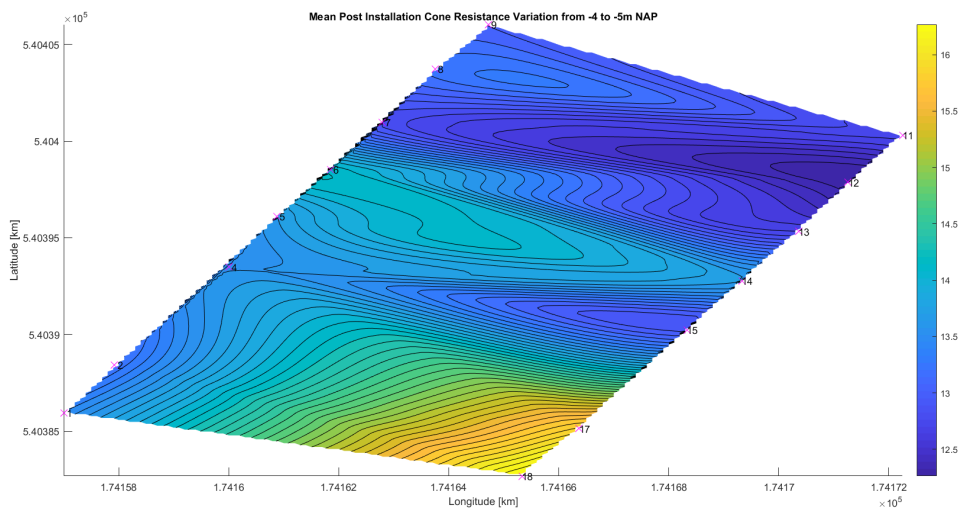


Figure B.1: 2D Contour Plot of depth -4m to -5m NAP

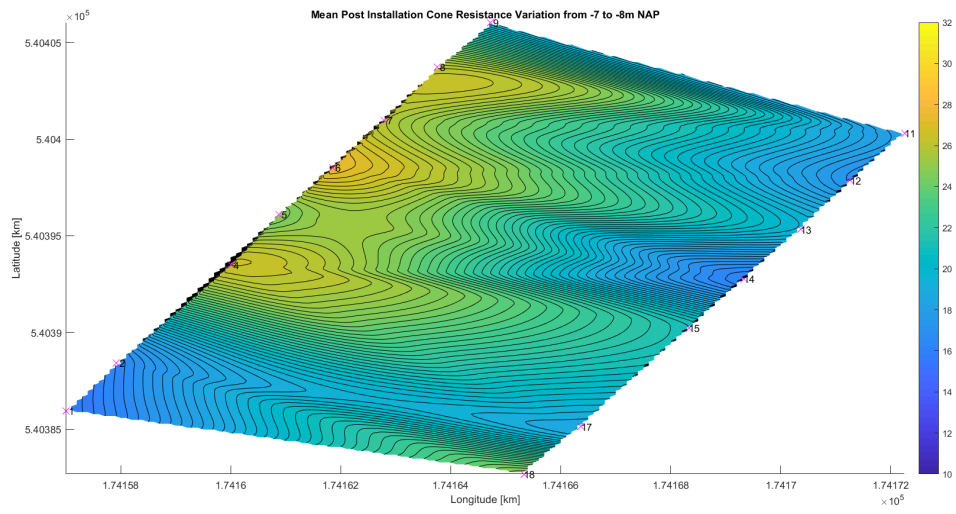


Figure B.2: 2D Contour Plot of depth -4m to -5m NAP

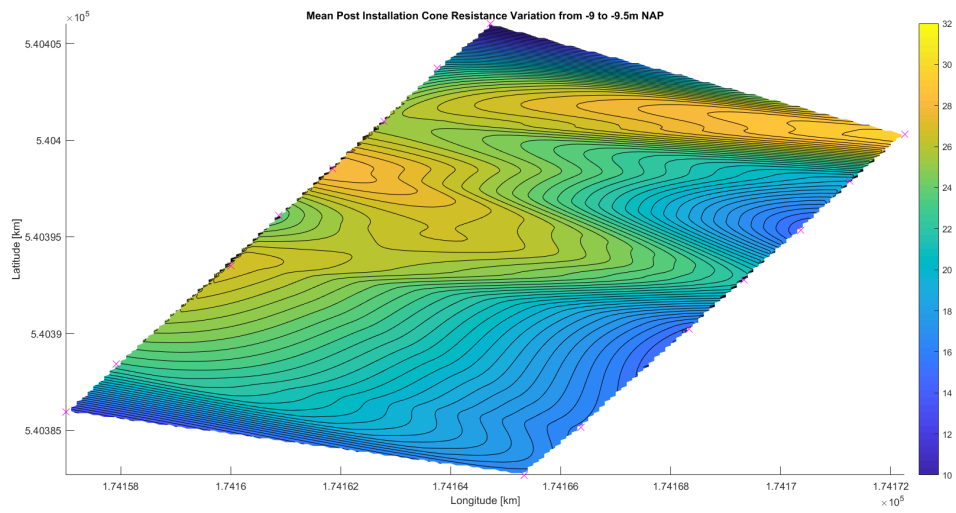


Figure B.3: 2D Contour Plot of depth -4m to -5m NAP

**Minimum Post-Installation CPT Contour Plots**

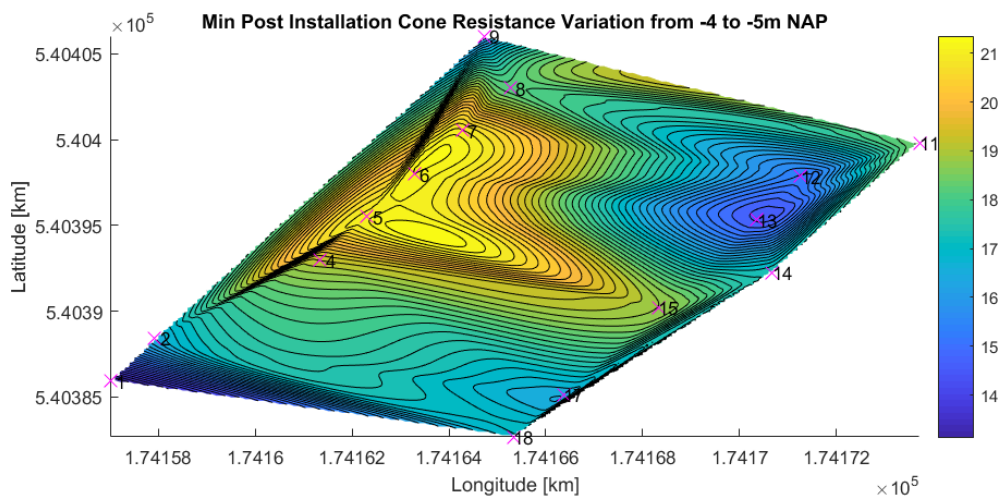


Figure B.4: 2D Contour Plot of depth -4m to -5m NAP

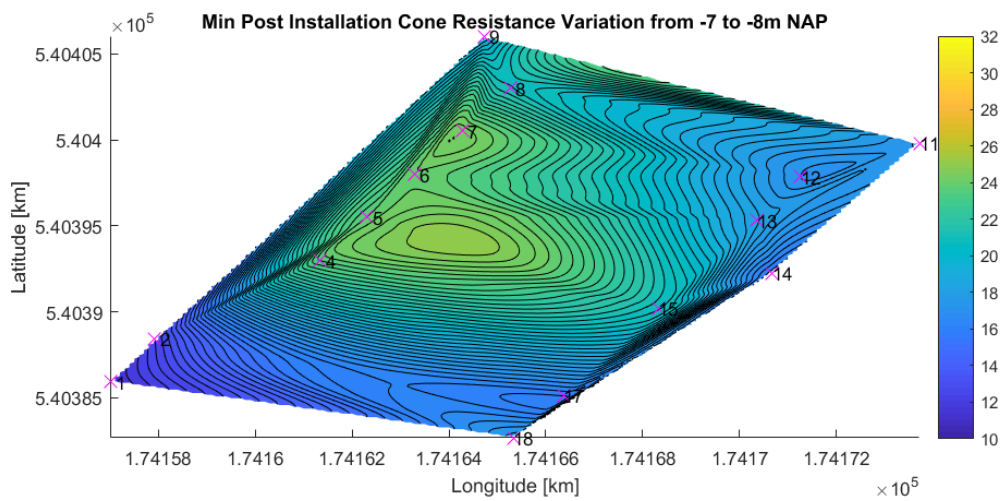


Figure B.5: 2D Contour Plot of depth -7m to -8m NAP

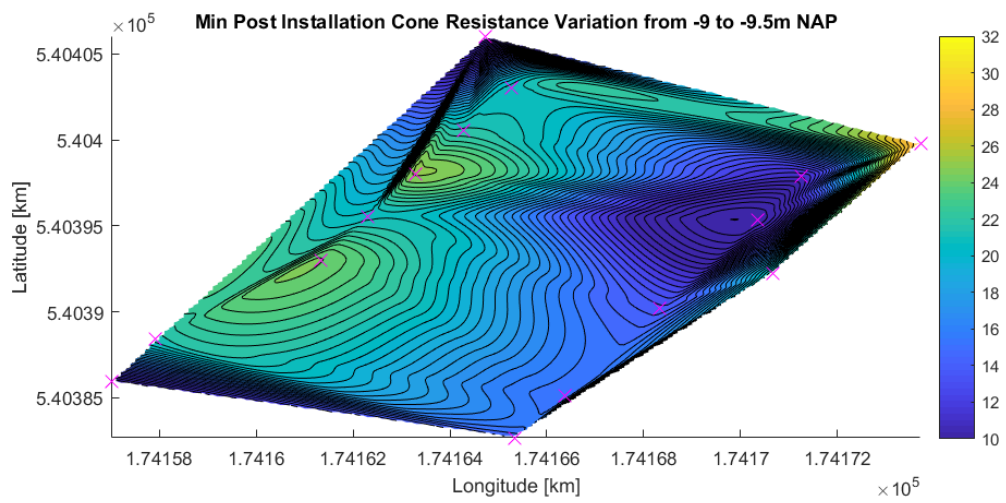


Figure B.6: 2D Contour Plot of depth -9m to -9.5m NAP

**Pre-Installation CPT Contour Plots**

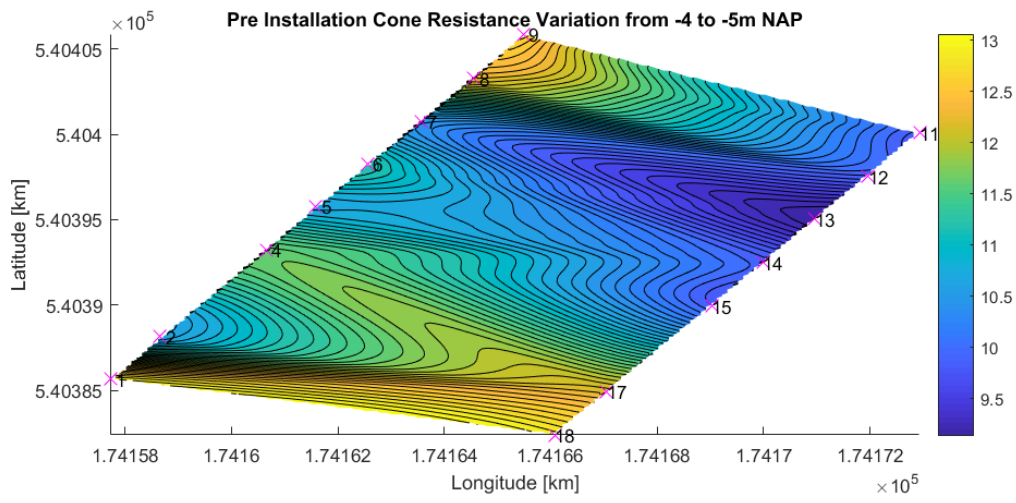


Figure B.7: 2D Contour Plot of depth -4m to -5m NAP

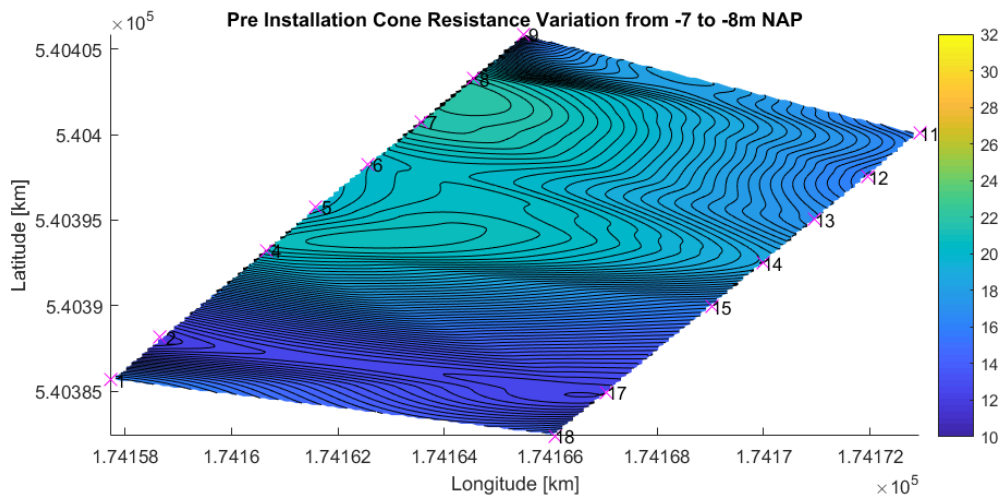


Figure B.8: 2D Contour Plot of depth -7m to -8m NAP

**Difference Between Mean Post- and Pre-Installation Cone Resistance**

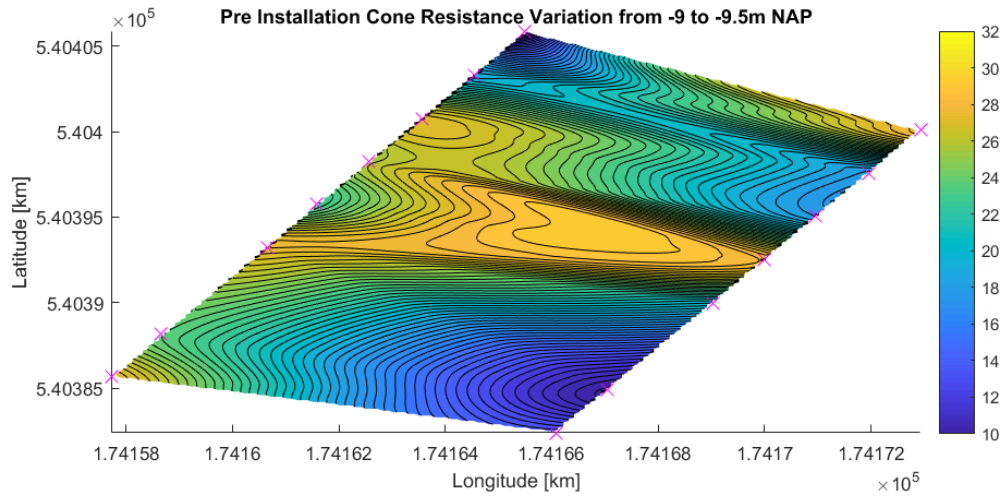


Figure B.9: 2D Contour Plot of depth -9m to -9.5m NAP

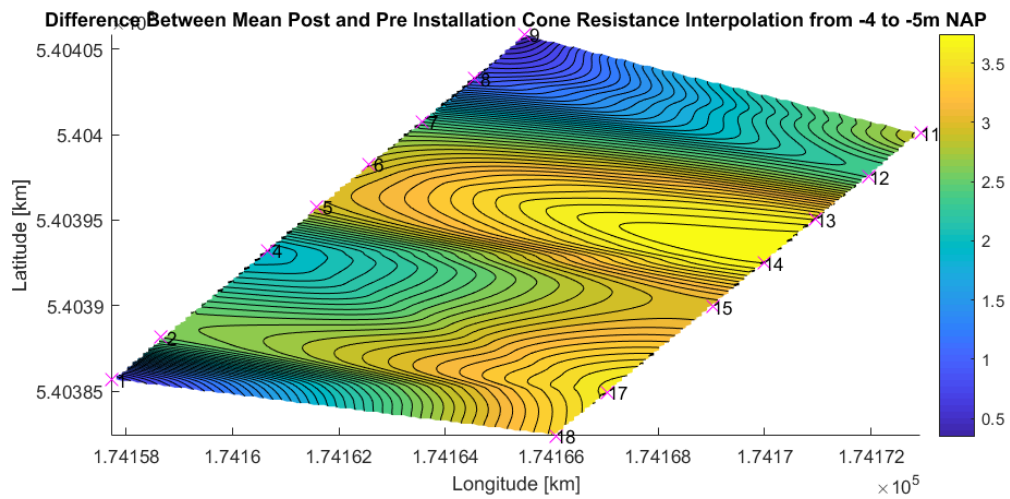


Figure B.10: 2D Difference Contour Plot post- vs pre-installation of depth -4m to -5m NAP

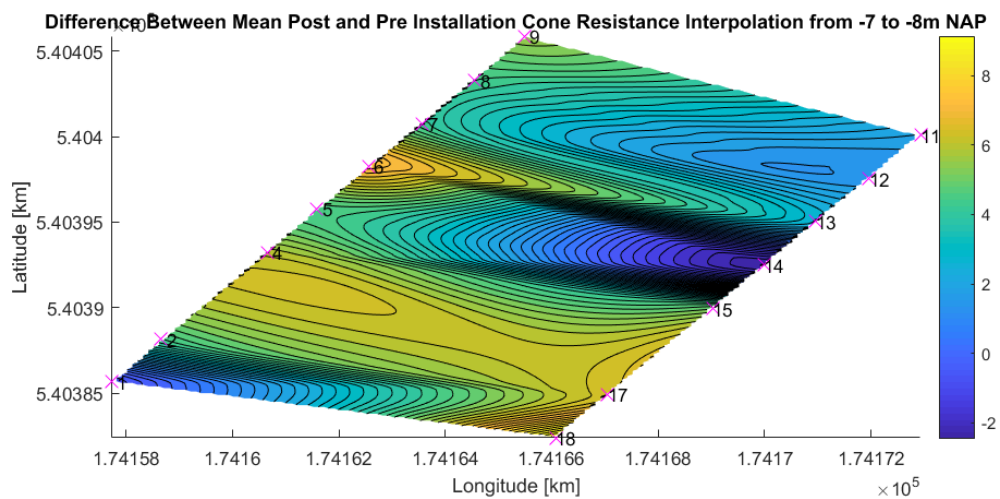


Figure B.11: 2D Difference Contour Plot post- vs pre-installation of depth -7m to -8m NAP

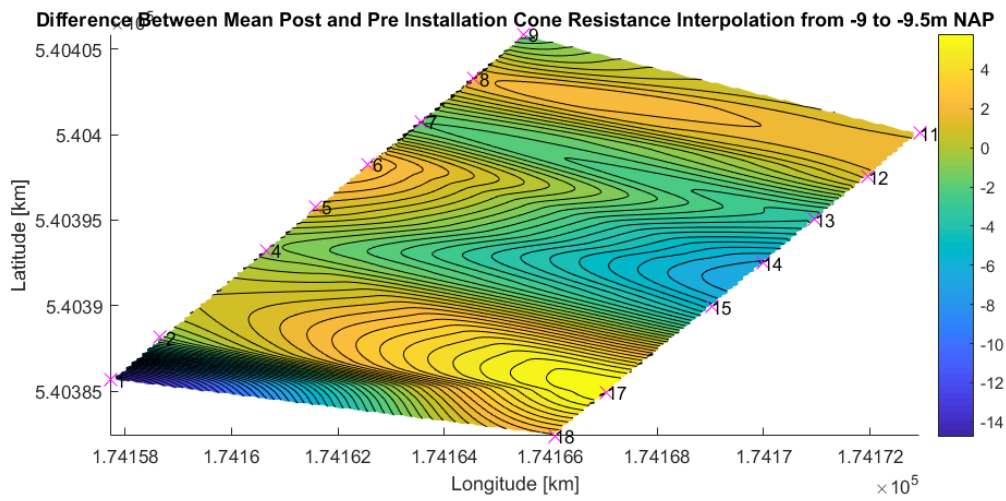


Figure B.12: 2D Difference Contour Plot post- vs pre-installation of depth -9m to -9.5m NAP



# C

## **Appendix C: Installation Parameters**

**Torque**

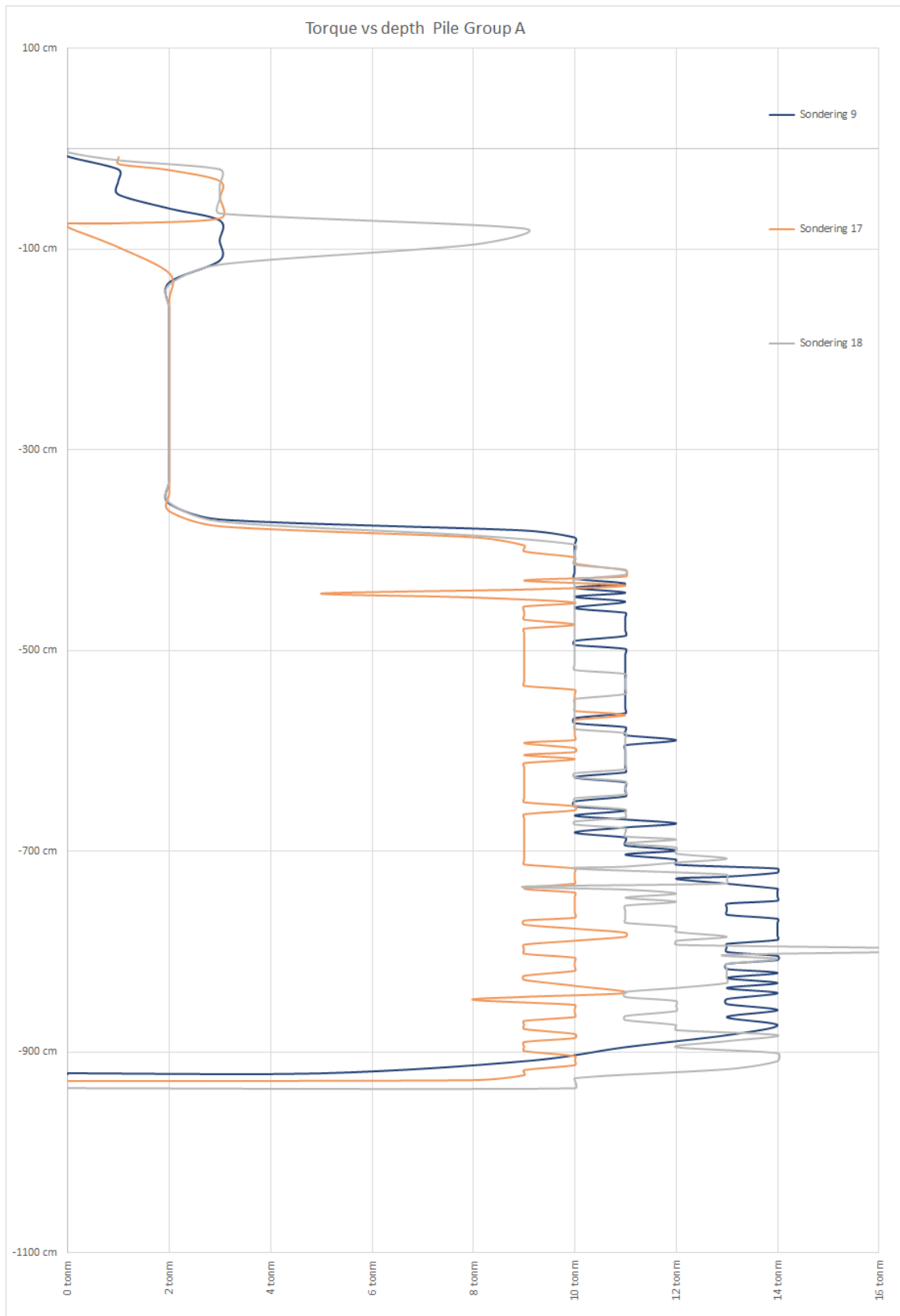


Figure C.1: Torque for pile category A

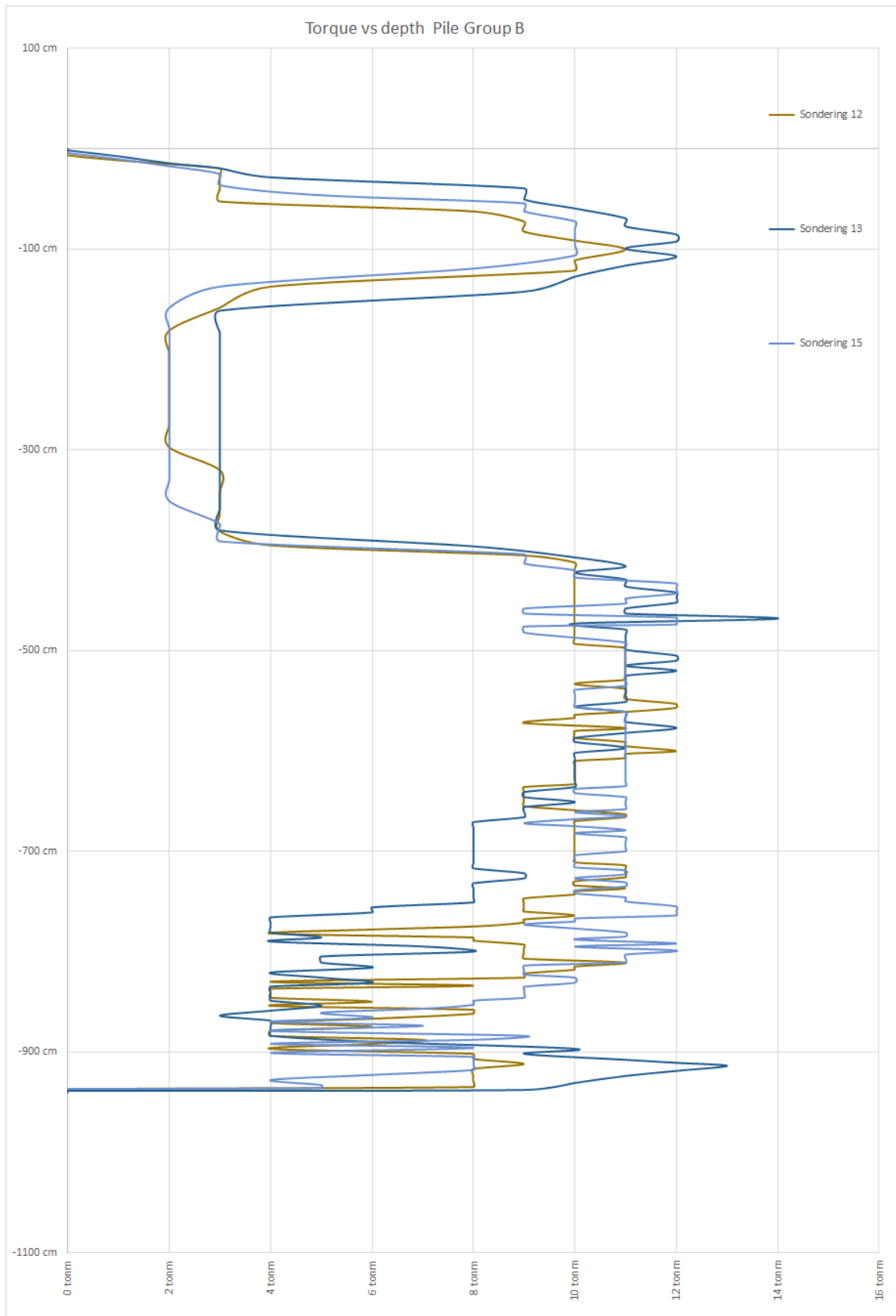


Figure C.2: Torque for pile category B

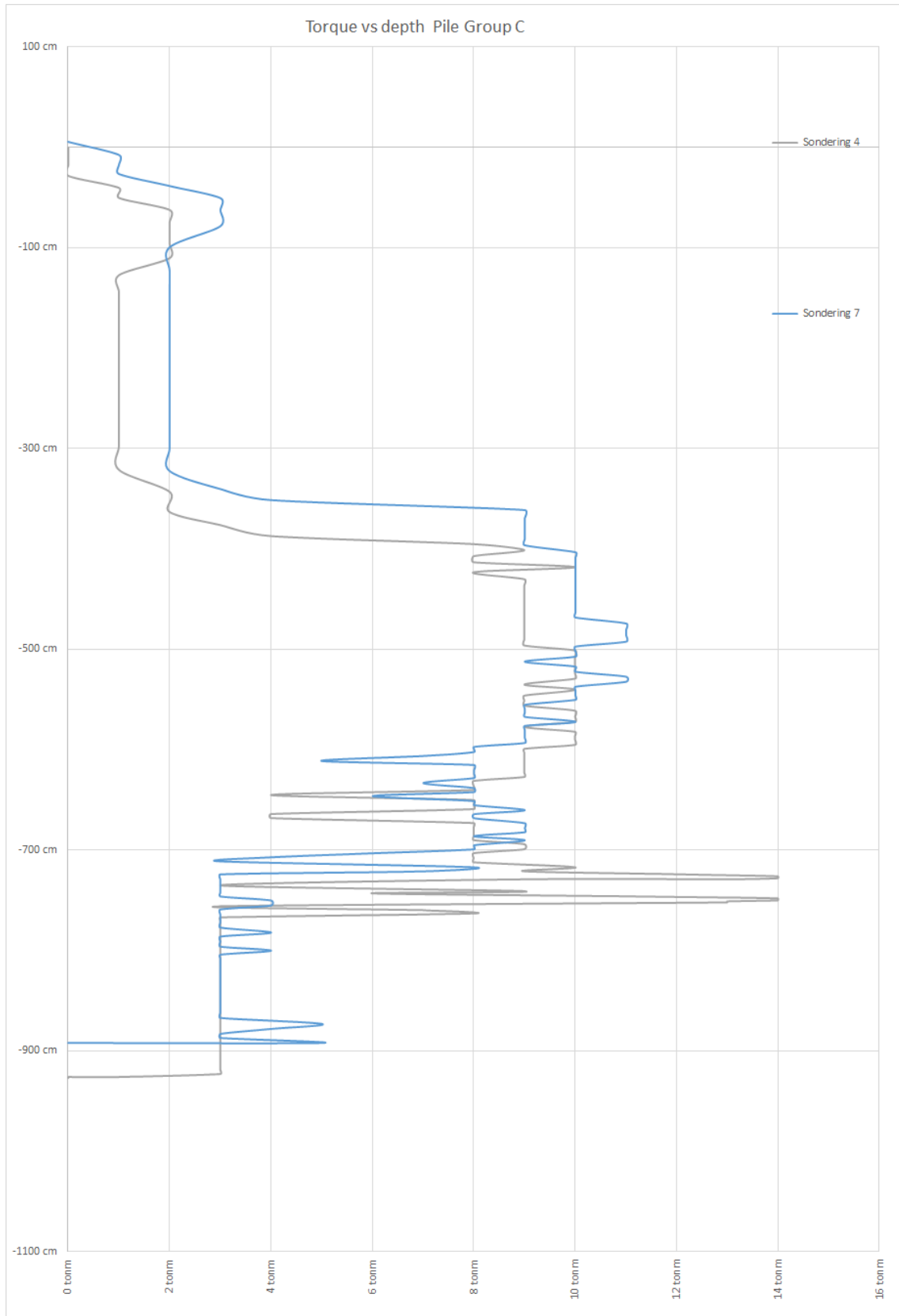


Figure C.3: Torque for pile category C

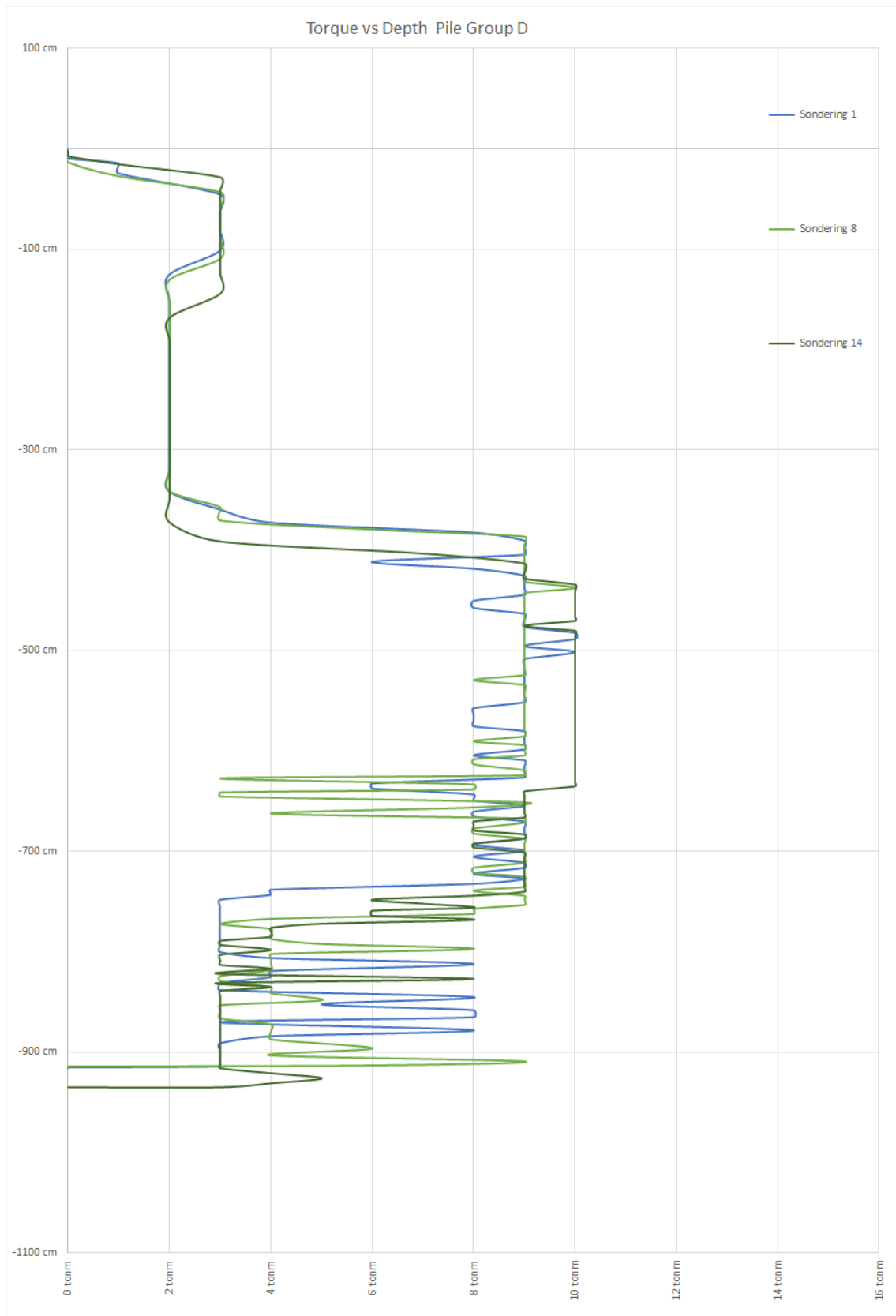


Figure C.4: Torque for pile category D

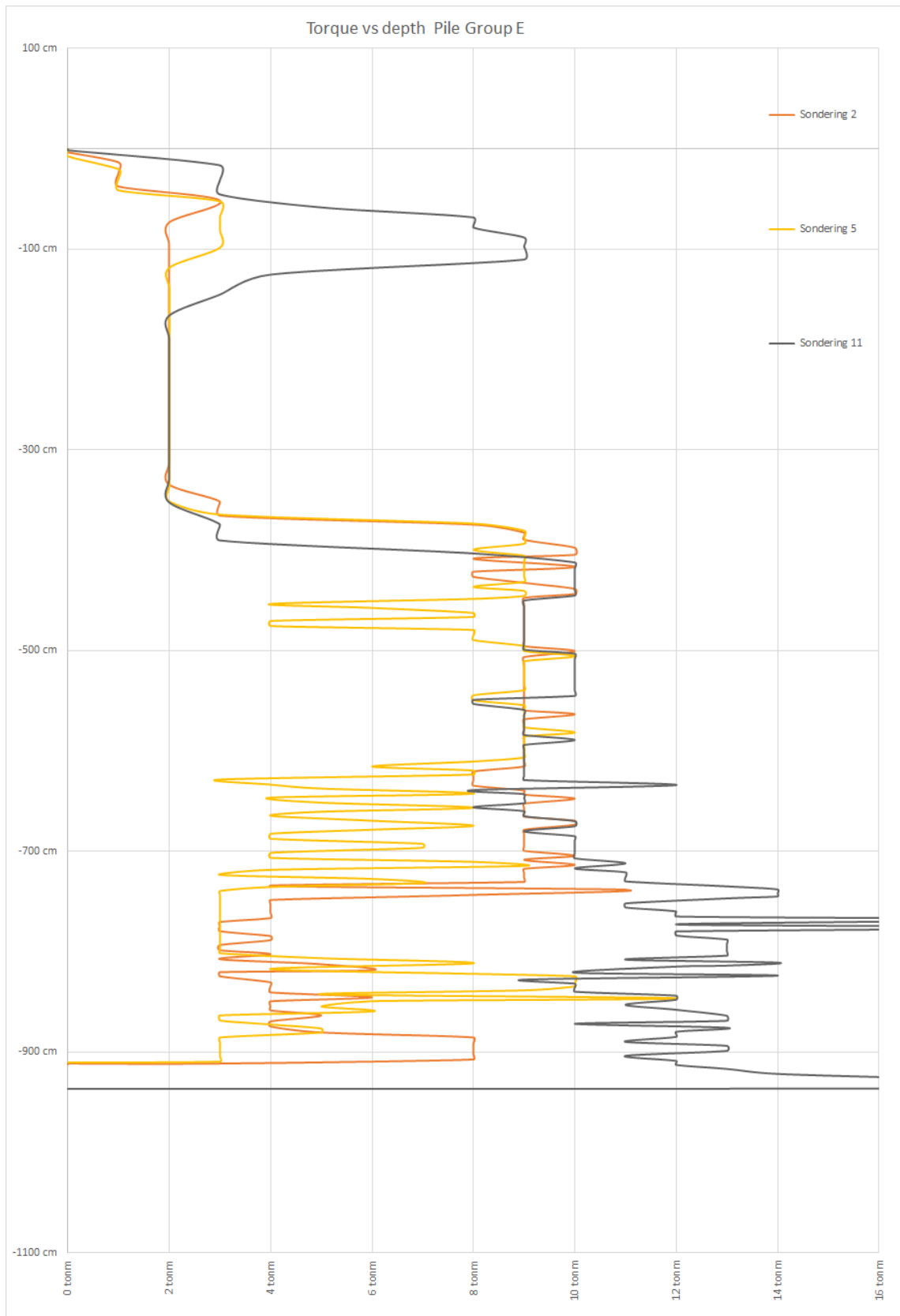


Figure C.5: Torque for pile category E

# D

## Appendix D: Load-Settlement Data

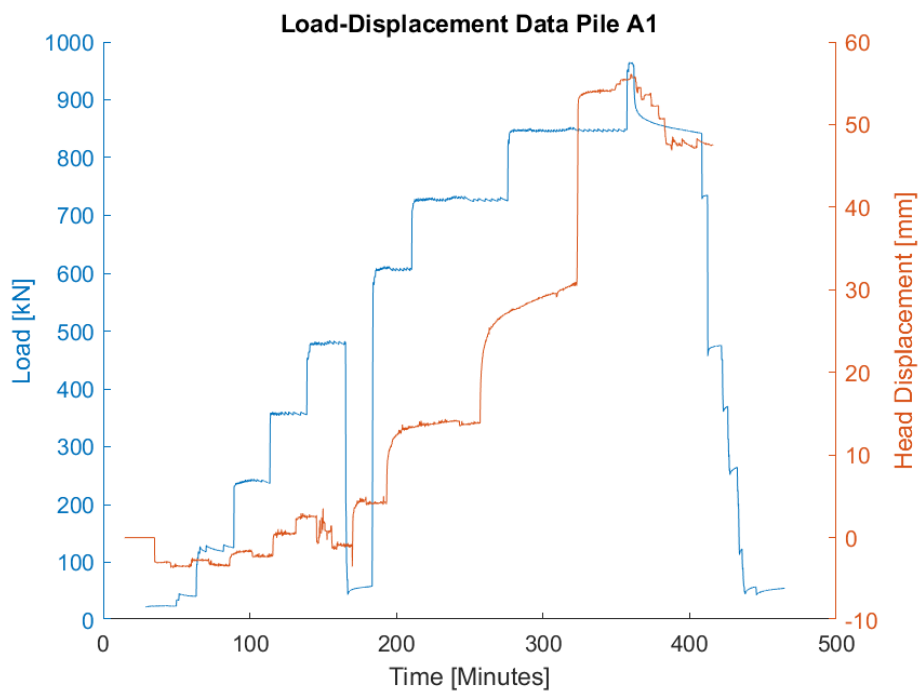


Figure D.1: Load vs pile head settlement for pile A1

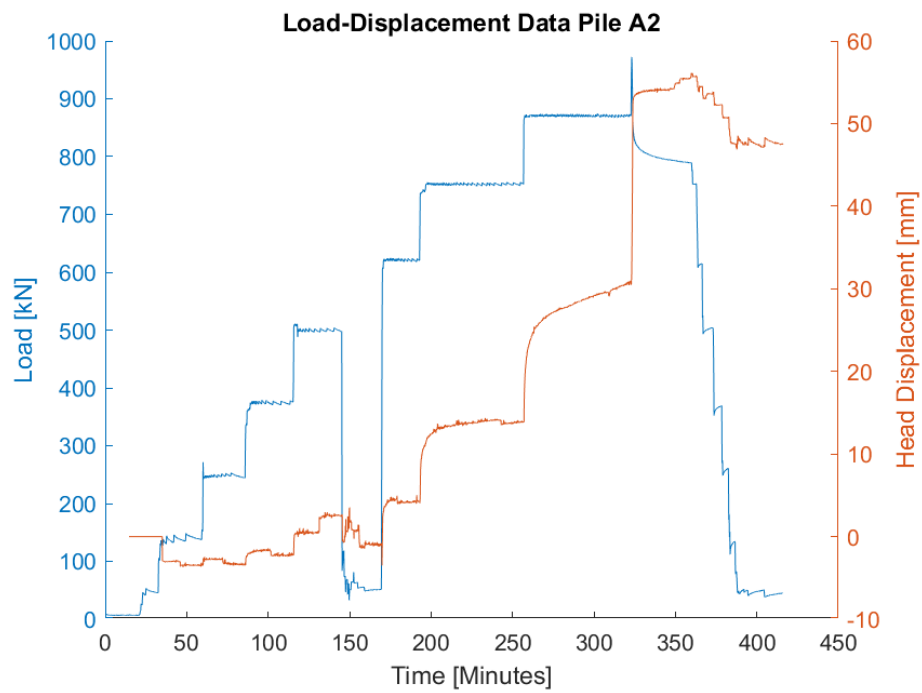


Figure D.2: Load vs pile head settlement for pile A2

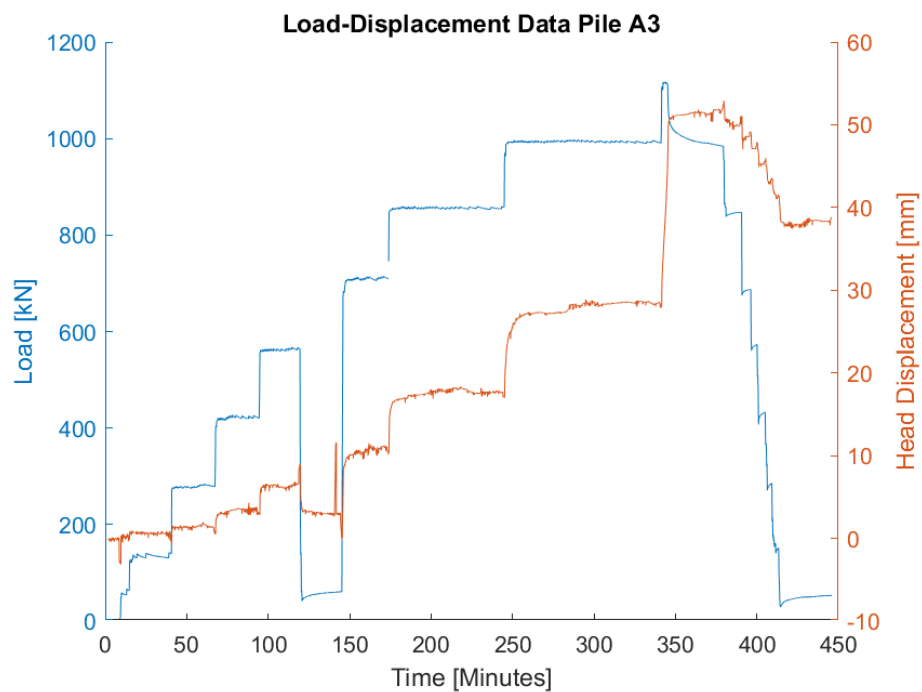


Figure D.3: Load vs pile head settlement for pile A3

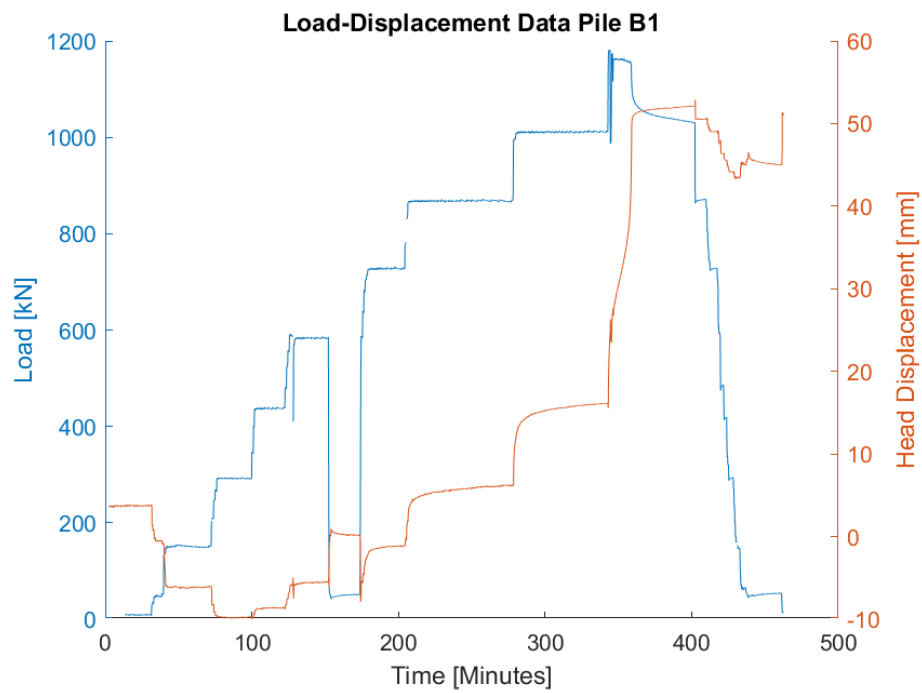


Figure D.4: Load vs pile head settlement for pile B1

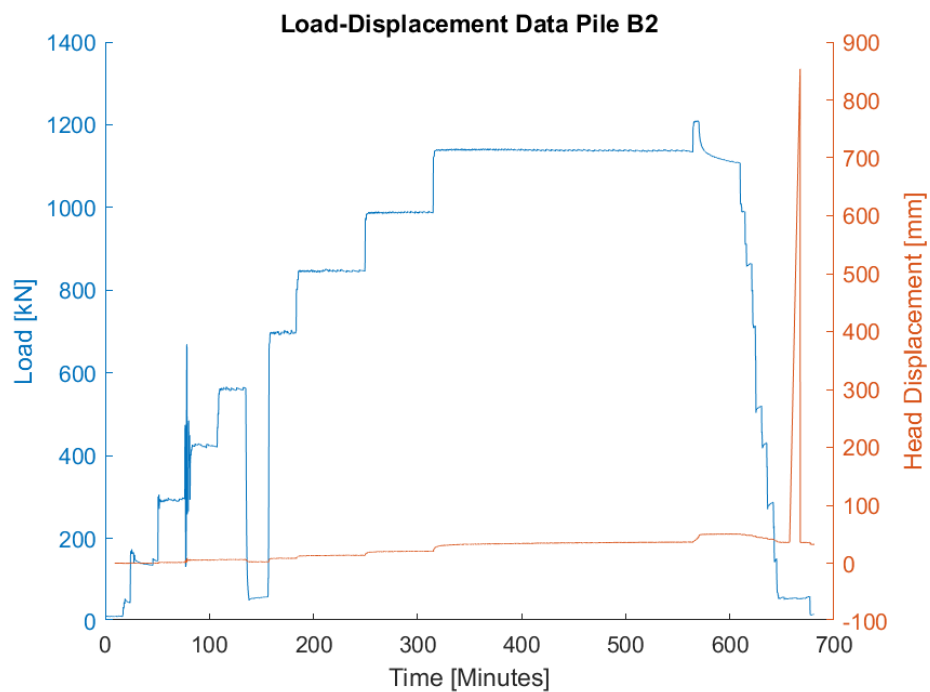


Figure D.5: Load vs pile head settlement for pile B2

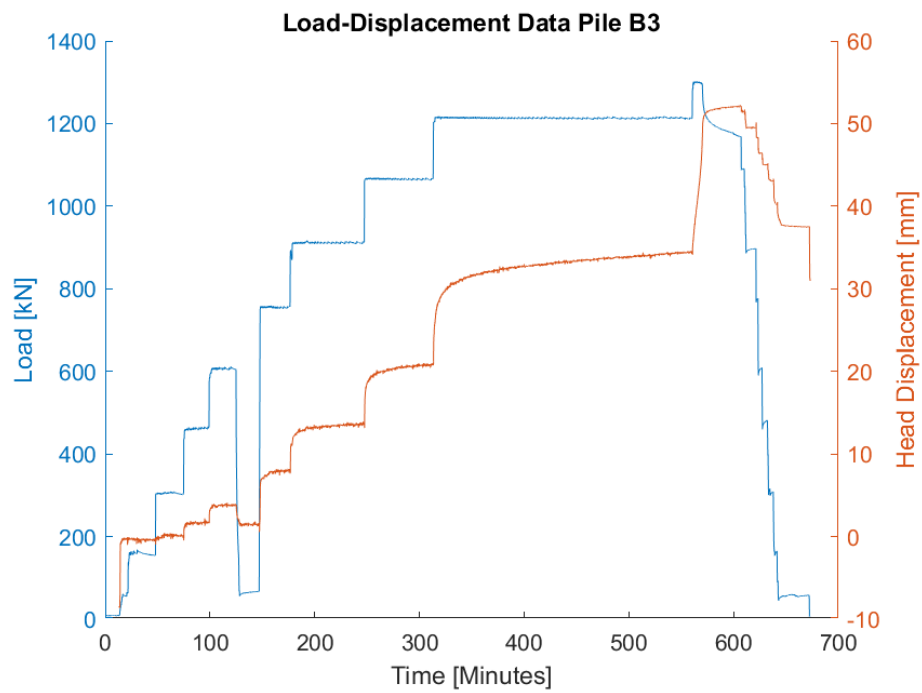


Figure D.6: Load vs pile head settlement for pile B3

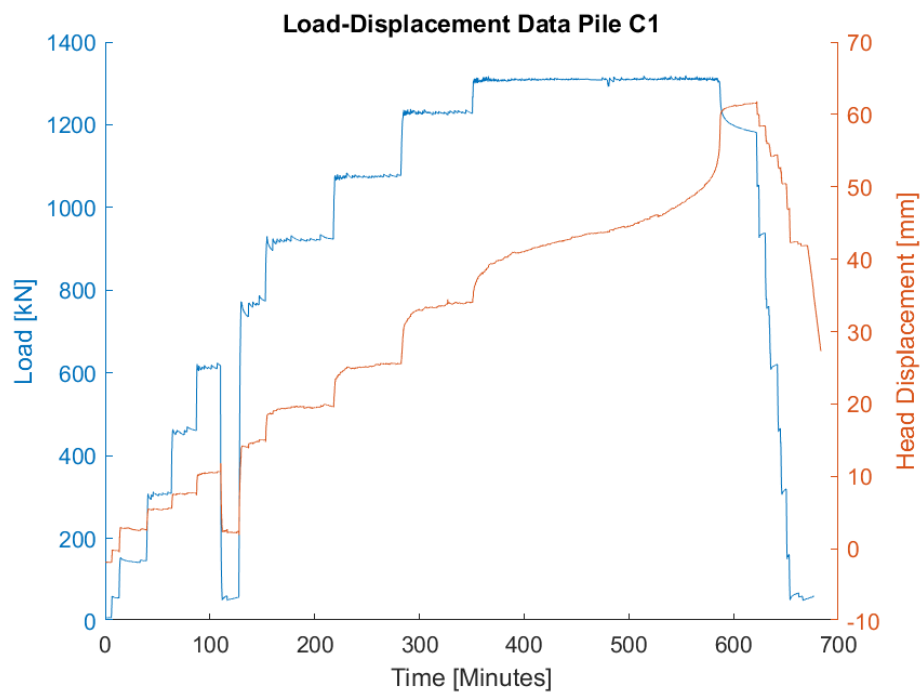


Figure D.7: Load vs pile head settlement for pile C1

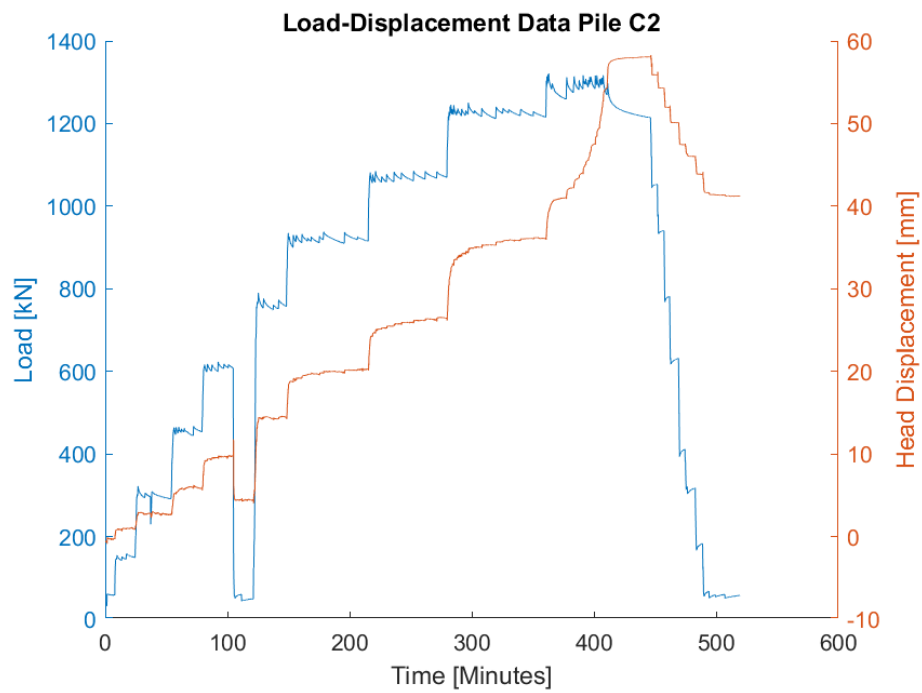


Figure D.8: Load vs pile head settlement for pile C2

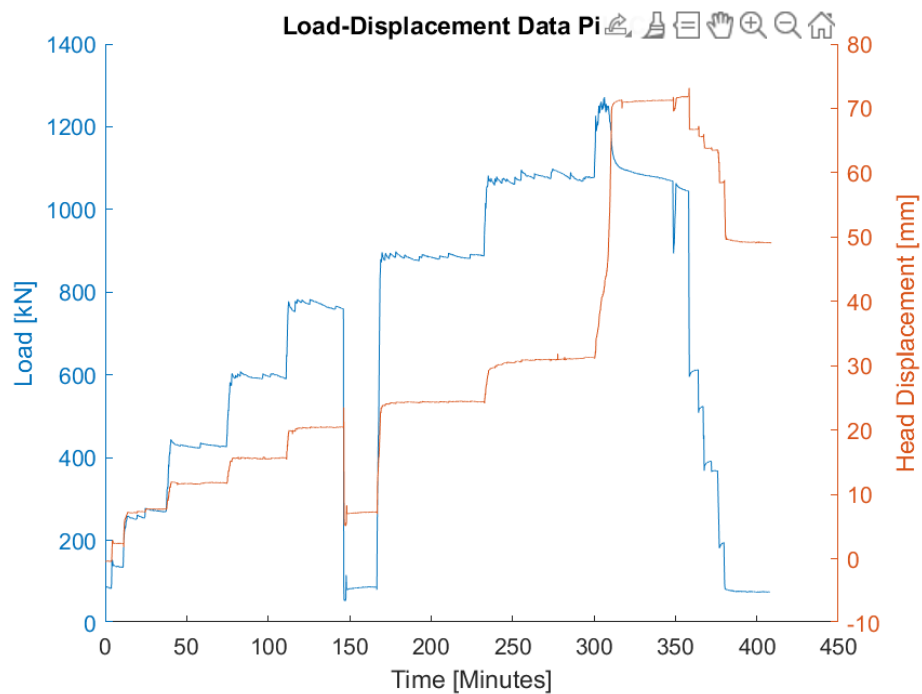


Figure D.9: Load vs pile head settlement for pile C3

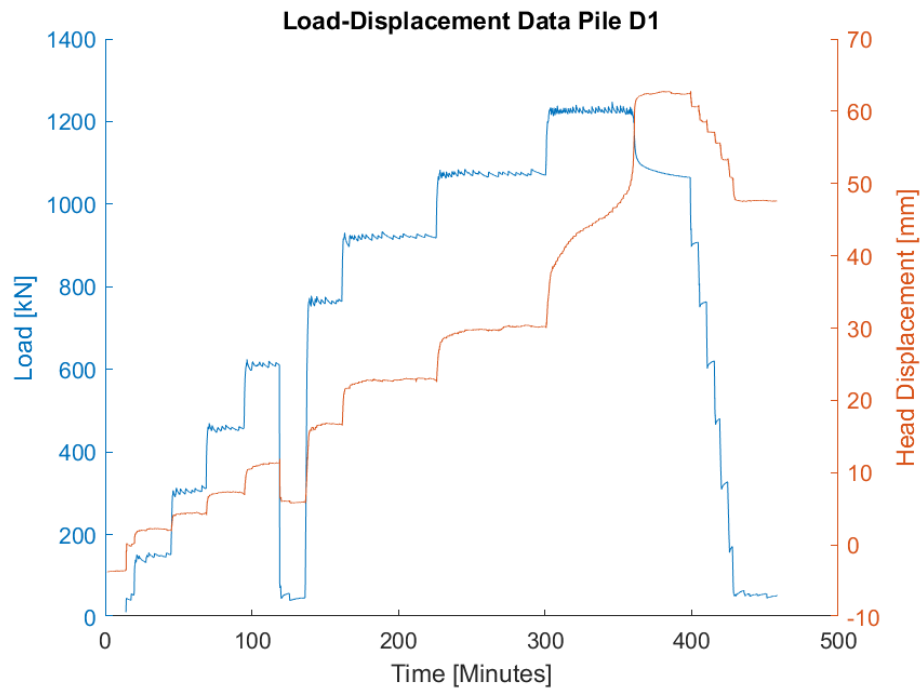


Figure D.10: Load vs pile head settlement for pile D1

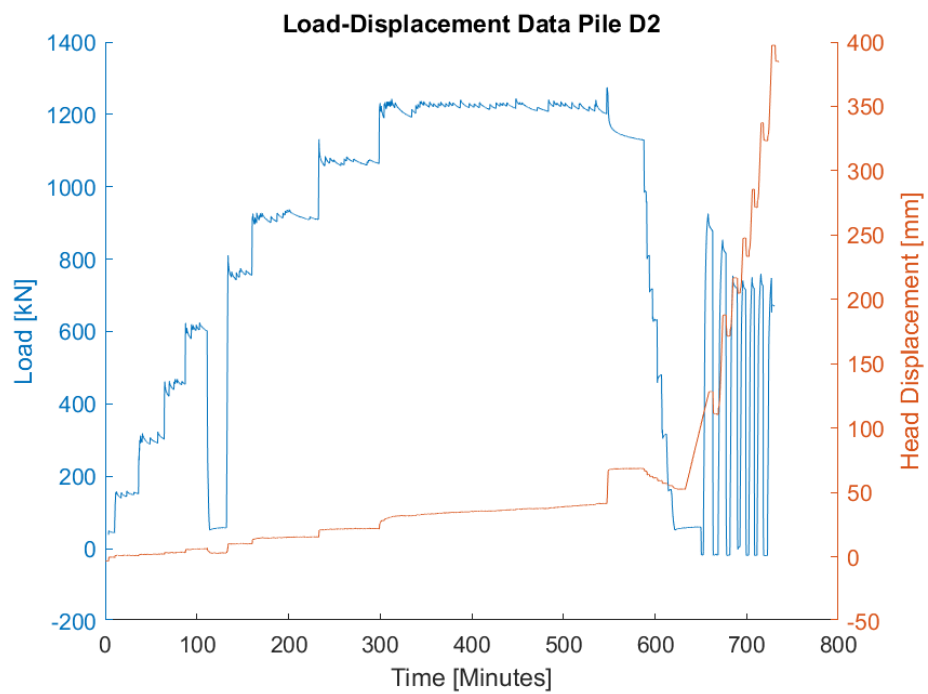


Figure D.11: Load vs pile head settlement for pile D2

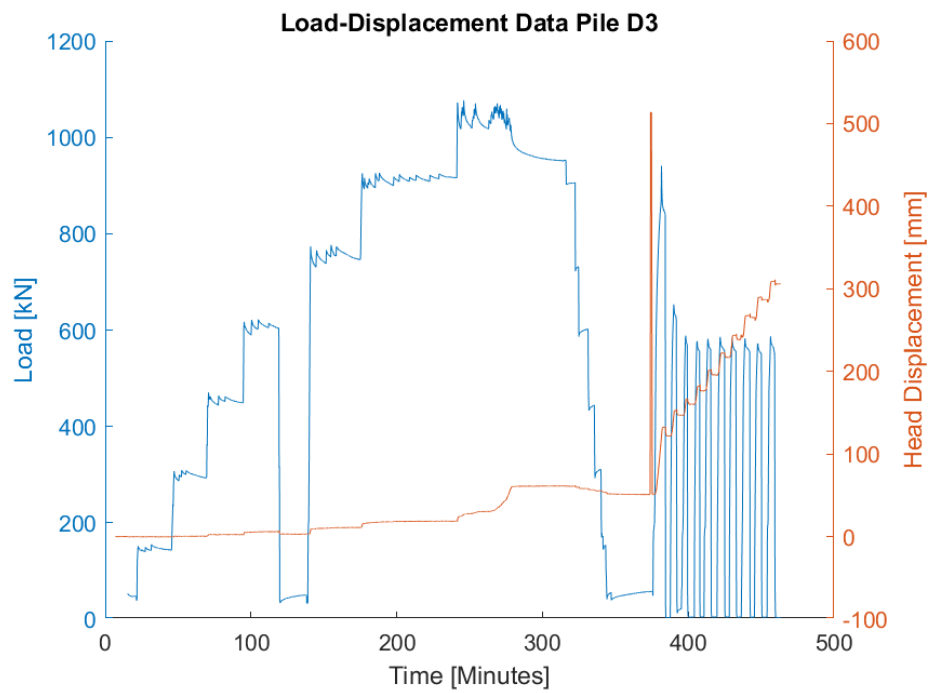


Figure D.12: Load vs pile head settlement for pile D3

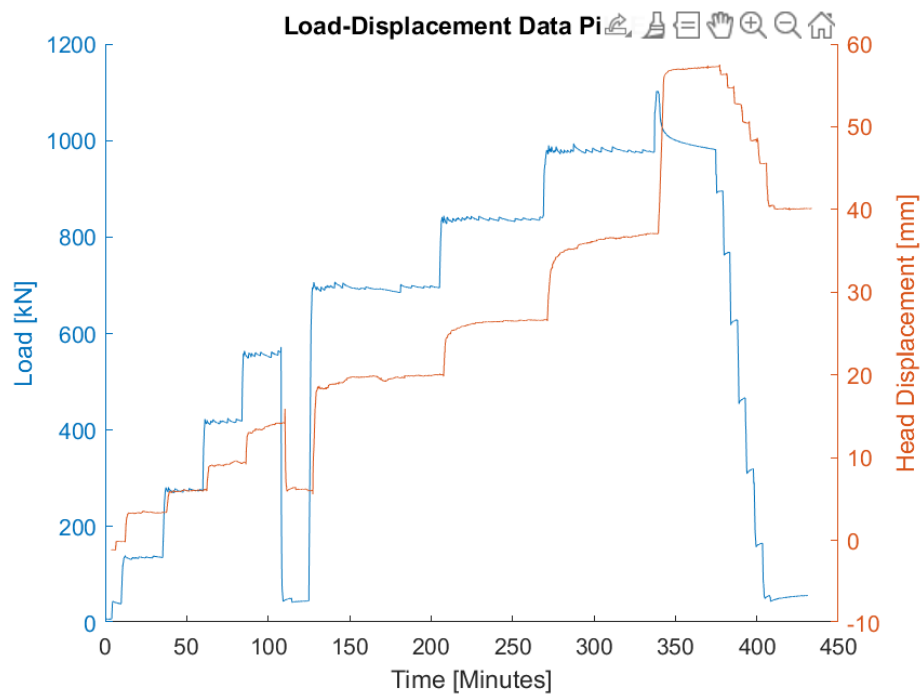


Figure D.13: Load vs pile head settlement for pile E1

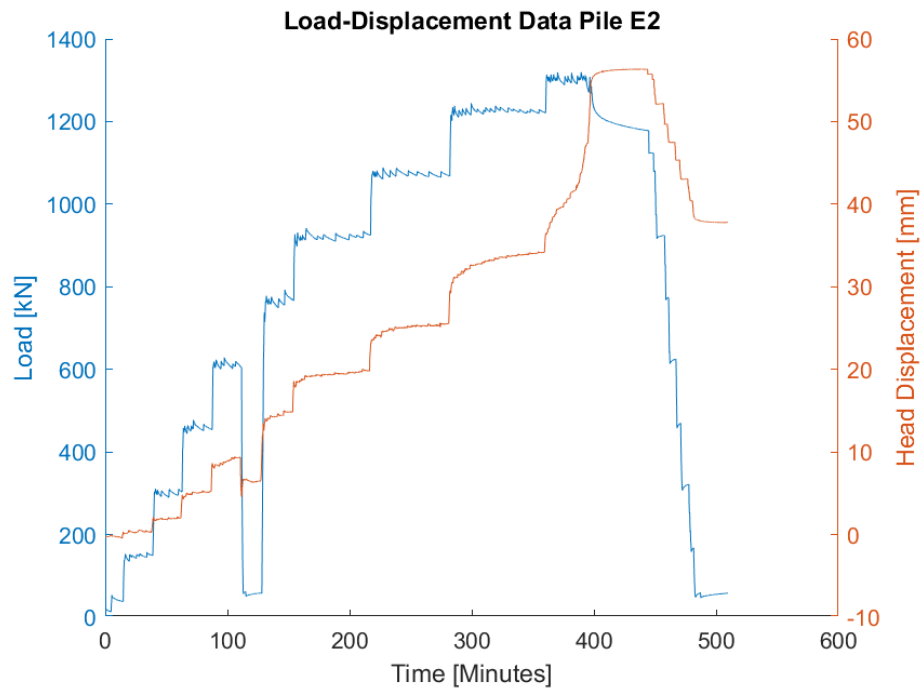


Figure D.14: Load vs pile head settlement for pile E2

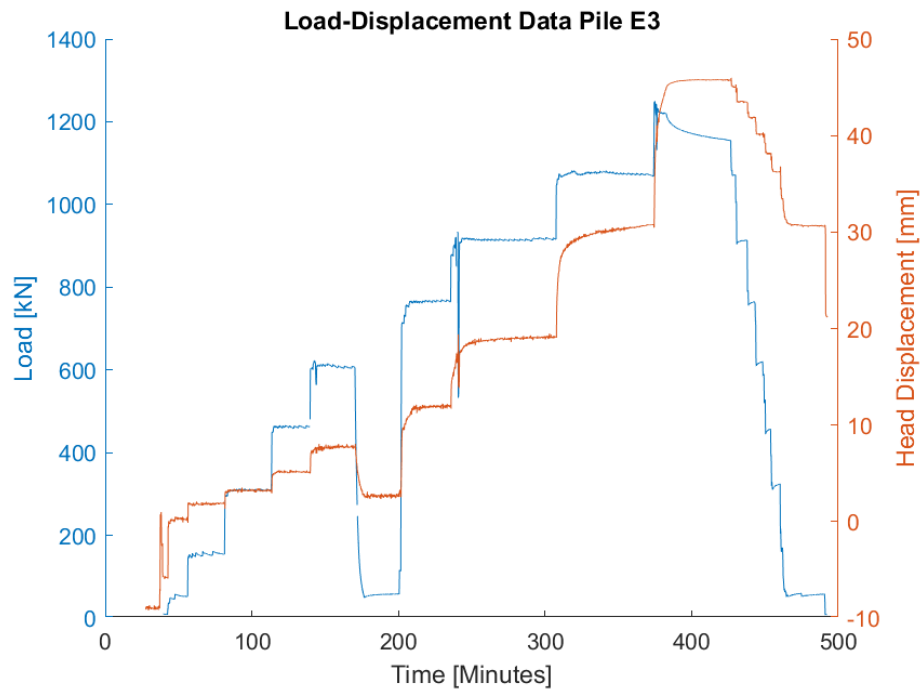


Figure D.15: Load vs pile head settlement for pile E3

# E

## **Appendix E: Laboratory Data on Grout Samples**

**BEPROEVING PRISMA'S RETOURSPOELING**

$$(x_n - w_n * 1000) / (1 + w_n) = x_n \quad w_n = (x_n - x_c) / (x_n - 1000)$$

Paaltje	[ ]	A				B				C				D				E									
Mengselnummer	[ ]	1				2				3				4				5									
Maakdatum	[ ]	24/02/2021				22/02/2021				23/02/2021				23/02/2021				23/02/2021									
Samenstelling	materiaal	CEMIII-42,5				CEMIII-42,5				CEMIII-42,5				CEMIII-42,5				GM42									
water / droge stof		1,31				2,2				3,9				2,19				2,81									
Cementgehalte (28 d)	[m - NAP]	Intron	RETOUR	waterverlies	samestelling	Intron	RETOUR	waterverlies	samestelling	Intron	RETOUR	waterverlies	samestelling	Intron	RETOUR	waterverlies	samestelling	Intron	RETOUR	waterverlies	samestelling						
6,0 m - NAP:																											
Volumegewicht prisma nat	[kg/m <sup>3</sup> ]	1882	1737	0,164		1874	1778	0,110		1832	1716	0,139		1843	1663	0,214		1876	1702	0,199		1876	1702	0,199			
Volumegewicht prisma droog	[kg/m <sup>3</sup> ]	1441	1132		65%	1427	1221		69%	1349	1094		64%	1379	985		59%	1406	1033		61%	1406	1033		61%		
Cementgehalte bepaald	[kg/m <sup>3</sup> ]	316	248		14%	251	215		12%	166	135		8%	272	194		12%	225	165		10%	225	165		10%		
Zandgehalte berekend	[kg/m <sup>3</sup> ]	1125	884		51%	1176	1006		57%	1183	959		56%	1107	791		48%	1106	813		48%	1106	813		48%		
Steenmeelgehalte berekend	[kg/m <sup>3</sup> ]																	75				75					
Watergehalte bepaald	[kg/m <sup>3</sup> ]	441	605		35%	447	557		31%	483	622		36%	464	678		41%	470	669		39%	470	669		39%		
wcf		1,40	2,44			1,78	2,59			2,91	4,63			1,71	3,49			2,09	4,04			2,09	4,04				
9,0 m - NAP:																											
Volumegewicht prisma nat	[kg/m <sup>3</sup> ]	1884	1753	0,148		1808	1777	0,038		1858	1740	0,138		1791	1650	0,178		1824	1736	0,107		1824	1736	0,107			
Volumegewicht prisma droog	[kg/m <sup>3</sup> ]	1451	1172		67%	1353	1284		72%	1405	1149		67%	1304	985		59%	1334	1139		67%	1334	1139		67%		
Cementgehalte bepaald	[kg/m <sup>3</sup> ]	396	320		18%	265	252		14%	164	134		8%	219	165		10%	232	198		12%	232	198		12%		
Zandgehalte berekend	[kg/m <sup>3</sup> ]	1055	852		49%	1088	1032		58%	1241	1015		59%	1085	819		49%	1025	875		51%	1025	875		51%		
Steenmeelgehalte berekend	[kg/m <sup>3</sup> ]																	77				77					
Watergehalte bepaald	[kg/m <sup>3</sup> ]	433	581		33%	455	493		28%	453	591		34%	487	665		40%	490	597		35%	490	597		35%		
wcf		1,09	1,82			1,72	1,96			2,76	4,39			2,22	4,02			2,11	3,01			2,11	3,01				
WCF gemiddeld		1,25	2,13			1,75	2,28			2,83	4,51			1,97	3,76			2,10	3,53			2,10	3,53				
<b>Verharde prisma's</b>		vol. gew.	f <sub>bt</sub>	f <sub>uc,1</sub>	f <sub>uc,2</sub>	f <sub>uc,gem</sub>	vol. gew.	f <sub>bt</sub>	f <sub>uc,1</sub>	f <sub>uc,2</sub>	f <sub>uc,gem</sub>	vol. gew.	f <sub>bt</sub>	f <sub>uc,1</sub>	f <sub>uc,2</sub>	f <sub>uc,gem</sub>	vol. gew.	f <sub>bt</sub>	f <sub>uc,1</sub>	f <sub>uc,2</sub>	f <sub>uc,gem</sub>	vol. gew.	f <sub>bt</sub>	f <sub>uc,1</sub>	f <sub>uc,2</sub>	f <sub>uc,gem</sub>	
		[kg/m <sup>3</sup> ]	[MPa]	[MPa]	[MPa]	[MPa]	[kg/m <sup>3</sup> ]	[MPa]	[MPa]	[MPa]	[MPa]	[kg/m <sup>3</sup> ]	[MPa]	[MPa]	[MPa]	[MPa]	[kg/m <sup>3</sup> ]	[MPa]	[MPa]	[MPa]	[MPa]	[kg/m <sup>3</sup> ]	[MPa]	[MPa]	[MPa]	[MPa]	
6,0 m - NAP	28 dgn	1	1836	2,3	9,7	9,4	1879	1,0	3,9	4,1	4	1805	0,3	1,7	0,6	1,15	1776	1,1	3,9	4,2	4,05	1805	0,5	2,1	2,1	2,1	
		2	1831	2,0	8,2	8,9	1834	0,6	2,5	2,5	2,5	1872	0,3	1,2	1,2	1,2	1792	0,8	3,2	3,4	3,3	1803	0,5	2,1	1,8	1,95	
		3	1872	2,0	9,7	9,0	1946	2,1	8,6	7,8	8,20	1855	0,4	1,9	1,9	1,90	1827	1,8	6,9	7,1	7,00	1845	0,8	2,5	2,4	2,45	
		gem	1846	2,10		9,15	1886	1,23			4,90	1844	0,33			1,42	1798	1,23			4,78	1818	0,60			2,17	
6,0 m - NAP	56 dgn	1	1800	2,6	12,7	13,4	1864	1,4	5,9	5,7	5,8	1809	0,5	2,2	2,3	2,25	1932	1,6	6,1	6,1	6,1	1741	0,8	3,0	3,0	3	
		2	1751	2,0	12,1	10,9	1936	0,8	3,3	3,3	3,3	1844	0,3	1,5	1,4	1,45	1811	1,3	4,6	4,4	4,5	1833	0,8	2,9	2,6	2,75	
		3	1917	2,0	10,7	14,3	1939	2,5	11,2	9,8	10,50	1828	0,6	2,6	2,6	2,60	1901	2,5	9,7	9,8	9,75	1876	1,2	3,7	3,5	3,60	
		gem	1823	2,20		12,35	1913	1,57			6,53	1827	0,47			2,10	1881	1,80			6,78	1817	0,93			3,12	
Toename			4,8%			35,0%		27,0%			33,3%		40,0%			48,2%		45,9%			41,8%		55,6%			43,8%	
6,0 m - NAP	200 dgn	1	1800	4,8	19,1	20,2	1864	1,1	4,4	4,3	4,35	1809	0,8	2,5	2,5	2,5	1932	3,4	15,8	15,2	15,5	1741	1,1	3,5	3,6	3,55	
		2					1936	3,7	16,0	28,0	22	1844	0,9	3,1	3,0	3,05											
		3					1939																				
		gem	1800	4,80		19,65	1913	2,40			13,18	1827	0,85			2,78	1932	3,40			15,50	1741	1,10			3,55	
Toename			128,6%			114,8%		94,6%			168,9%		155,0%			95,9%		175,7%			224,0%		83,3%			63,8%	
9,0 m - NAP	28 dgn	1	1839	1,8	9,1	9,0	1832	1,2	4,7	4,4	4,55	1835	0,6	2,5	2,5	2,5	1827	0,7	2,5	2,6	2,55	1829	0,6	2,3	2,2	2,25	
		2	1836	2,4	10,8	11,9	1881	0,5	2,0	1,9	1,95	1855	0,5	1,8	1,7	1,75	1801	0,9	3,9	3,8	3,85	1826	0,6	2,3	2,0	2,15	
		3	1841	2,3	10,7	10,7	1921	2,5	9,6	9,3	9,45	1847	0,5	1,9	1,9	1,90	1887	2,1	7,6	8,2	7,90	1783	0,8	2,6	2,6	2,60	
		gem	1839	2,17		10,37	1878	1,40			5,32	1846	0,53			2,05	1838	1,23			4,77	1813	0,67			2,33	
9,0 m - NAP	56 dgn	1	1775	2,5	12,0	12,6	1853	1,7	6,7	6,4	6,55	1812	0,7	3,5	3,4	3,45	1784	0,8	3,5	3,5	3,5	1789	0,8	2,7	2,8	2,75	
		2	1785	2,7	16,4	14,8	1894	0,6	2,6	2,8	2,7	1924	0,6	2,2	2,2	2,2	1820	1,2	5,4	5,6	5,5	1771	0,8	2,8	2,8	2,8	
		3	1908	3,0	14,4	15,2	14,80	1916	2,6	12,2	12,6	12,40	1832	0,5	2,5	2,5	2,50	1928	2,5	10,4	11,3	10,85	1830	1,1	3,5	3,5	3,50
		gem	1823	2,73		14,23	1888	1,63			7,22	1856	0,60			2,72	1844	1,50			6,62	1797	0,90			3,02	
Toename			26,2%			37,3%		16,7%			35,7%		12,5%			32,5%		21,6%			38,8%		35,0%			29,3%	
9,0 m - NAP	200 dgn	1	1800	4,3	20,7	19,0	1864	1,0	3,1	2,7	2,9	1809	1,3	4,1	4,0	4,05	1932	4,2	15,9	17,0	16,45	1741		3,5	3,5	3,5	
		2					1936	3,9	12,1	4,0	8,05	1844		3,4	3,6	3,5											
		3					1939																				
		gem	1800	4,30		19,85	1913	2,45			5,48	1827	1,30			3,78	1932	4,20			16,45	1741				3,50	
Toename			98,5%			91,5%		75,0%			3,0%		143,8%			84,1%		240,5%			245,1%					50,0%	

<b>Verharde prisma's</b>		f <sub>bt</sub>	f <sub>uc,gem</sub>	f <sub>uc,gem</sub> / f <sub>bt</sub>	f <sub>bt</sub>	f <sub>uc,gem</sub>	f <sub>uc,gem</sub> / f <sub>bt</sub>	f <sub>bt</sub>	f <sub>uc,gem</sub>	f <sub>uc,gem</sub> / f <sub>bt</sub>	f <sub>bt</sub>	f <sub>uc,gem</sub>	f <sub>uc,gem</sub> / f <sub>bt</sub>	f <sub>bt</sub>	f <sub>uc,gem</sub>	f <sub>uc,gem</sub> / f <sub>bt</sub>	
		[MPa]	[MPa]	[%]													
6,0 m - NAP	28 dgn	1	-2,3	9,6	-24%	-1,0	4,0	-25%	-0,3	4,1	-26%	-1,1	4,1	-27%	-0,5	2,1	-24%
		2	-2,0	8,6	-23%	-0,6	2,5	-24%	-0,3	1,2	-25%	-0,8	3,3	-24%	-0,5	2,0	-26%
		3	-2,0	9,4	-21%	-2,1	8,2	-26%	-0,4	1,9	-21%	-1,8	7,0	-26%	-0,8	2,5	-33%
		gem	-2,1	9,15	-23%	-1,2	4,90	-25%	-0,3	1,42	-24%	-1,2	4,78	-26%	-0,6	2,17	-28%
6,0 m - NAP	56 dgn	1	-2,6	13,1	-20%	-1,4	5,8	-24%	-0,5	2,3	-22%	-1,6	6,1	-26%	-0,8	3,0	-27%
		2	-2,0	11,5	-17%	-0,8	3,3	-24%	-0,3	1,5	-21%	-1,3	4,5	-29%	-0,8	2,8	-29%
		3	-2,0	12,5	-16%	-2,5	10,5	-24%	-0,6	2,6	-23%	-2,5	9,8	-26%	-1,2	3,6	-33%
		gem	-2,2	12,35	-18%	-1,6	6,53	-24%	-0,5	2,10	-22%	-1,8	6,78	-27%	-0,9	3,12	-30%
Toename			4,8%	35,0%		27,0%	33,3%		40,0%	48,2%		45,9%	41,8%		55,6%	43,8%	
6,0 m - NAP	200 dgn	1	-4,8	19,7	-24%	-1,1	4,4	-25%	-0,8	2,5	-32%	-3,4	15,5	-22%	-1,1	3,6	-31%
		2				-3,7	22,0	-17%	-0,9	3,1	-30%						
		3															

**BEPROEVING PRISMA'S RETOURSPOELING**

Sondering	[ ]	-	9	17	18		12	13	15		4	6	7		1	8	14		2	5	11
Paalde	[ ]	A1	A1 2e keer	A2	A3		B1	B2	B3		C1	C2	C3		D1	D2	D3		E1	E2	E3
Mengselnummer	[ ]	1	2	1	1		1	2	3		1	2	3		1	2	3		1	2	3
Maakdatum	[ ]	24/02/21	24/02/21	24/02/21	23/02/21		22/02/21	23/02/21	22/02/21		22/02/21	23/02/21	22/02/21		23/02/21	23/02/21	24/02/21		24/02/21	24/02/21	23/02/21
Samenstelling	materiaal	CEMIII-42.5	CEMIII-42.5	CEMIII-42.5	CEMIII-42.5		GM42	GM42	GM42												
Monsternames	water / droge stof	1,25	1,25	1,25	1,25		2,50	2,50	2,50		3,75	3,75	3,75		2,50	2,50	2,50		2,00	2,00	2,00
Menger						gemiddeld															
Volumegewicht mengsel	[kg/m³]	1385	1414,4	1400	1404		1260	1169	1196		1169	1156	1152		1261	1247	1292		1232	1244	1206
water/droge stof WBF	[ ]	1411	1,26	1,31	1,30	1,29	2,20	3,57	3,03	2,94	3,57	3,90	4,01	3,83	2,19	2,34	1,92	2,57	2,45	2,31	2,81
Retourspoeling																					
de monsters van mengsels 2,4, 5 en m.n. 3 vertoende duidelijk uitzakking van vast materiaal. Dit heeft invloed op de kwaliteit van de metingen en verklaart verschillen met de prisma's																					
Monster 6,0 m - NAP:																					
Volumegewicht retour	[kg/m³]	1800	1741	1737	1769	1749	1778	1790	1810	1793	1690	1716	1721	1709	1663	1639	1627	1660	1704	1693	1702
Bleeding na 1 uur -6,0 m NAP	[% w/v]	4	2	7	5		9	11	9		10	13	13		15	13	13		4	8	8
Gewicht monster nat	gram	-	-	189	-		132	-	-		-	99	-		-	-	-		-	-	102
Gewicht monster na drogen	gram	-	-	126	-		91	-	-		-	47	-		-	-	-		-	-	65
Gewicht water	gram	-	-	63	-		41	-	-		-	52	-		-	-	-		-	-	37
Watergehalte	[% m/m]	-	-	33%	-		31%	-	-		-	53%	-		-	-	-		-	-	36%
Monster 9,0 m - NAP:																					
Volumegewicht retour	[kg/m³]	geen retour	1771	1753	1770	1765	1777	1811	1852	1813	1744	1740	1744	1743	1650	1666	1765	1706	1753	1757	1736
Bleeding na 1 uur -9,0 m NAP	[% w/v]	geen retour	1	4	6		3	6	1		7	11	7		16	11	18		4	4	3
Gewicht monster nat	gram	-	-	182	-		116	-	-		-	140	-		-	-	-		-	-	133
Gewicht monster na drogen	gram	-	-	120	-		79	-	-		-	110	-		-	-	-		-	-	89
Gewicht water	gram	-	-	62	-		37	-	-		-	30	-		-	-	-		-	-	44
Vochtgehalte retour -9,0 m NAP (tov droge stof)	[%]	-	-	34%	-		32%	-	-		-	21%	-		-	-	-		-	-	33%
Cementgehalte verharde prisma's																					
6,0 m - NAP:																					
Volumegewicht nat	[kg/m³]			1882	129	Δ water	1874					1832			1843						1876
Cementgehalte indicatief	[% m/m]			14%			12%					8%			12%						10%
Zandgehalte berekend	[% m/m]			51%			57%					56%			48%						48%
Steenmeelgehalte berekend	[% m/m]																				0%
Watergehalte bepaald	[% m/m]			35%			31%					36%			41%						39%
wcf	[% m/m]			2,44			2,59					4,63			3,49						4,04
9,0 m - NAP:																					
Volumegewicht nat	[kg/m³]			1884			1808					1858			1791						1824
Cementgehalte indicatief	[% m/m]			18%			14%					8%			10%						12%
Zandgehalte berekend	[% m/m]			49%			58%					59%			49%						51%
Steenmeelgehalte berekend	[% m/m]																				0%
Watergehalte bepaald	[% m/m]			33%			28%					34%			40%						35%
wcf	[% m/m]			1,82			1,96					4,39			4,02						3,01
wCF gemiddeld	[% m - NAP]			2,13			2,28					4,51			3,76						3,53
Verharde prisma's																					
6,0 m - NAP:																					
Volumegewicht	[kg/m³]	28 dgn	1836	1831	1872	1846	1879	1834	1946	1896	1805	1872	1855	1844	1776	1792	1827	1798	1805	1803	1845
Volumegewicht nat NAP -9,0m	[kg/m³]	56 dgn	1800	1751	1917	1823	1864	1936	1939	1913	1809	1844	1828	1827	1932	1811	1901	1881	1741	1833	1876
Gemiddelde	[kg/m³]		1818	1791	1895	1835	1872	1885	1943	1900	1807	1858	1842	1836	1854	1802	1864	1840	1773	1818	1861
9,0 m - NAP:																					
Druksterkte	[MPa]	28 dgn	9,6	8,6	9,4	9,2	4,0	2,5	8,2	4,9	1,2	1,2	1,9	1,4	4,1	3,3	7,0	4,8	2,1	2,0	2,5
Druksterkte NAP -6,0m	[MPa]	56 dgn	13,1	11,5	12,5	12,4	5,8	3,3	10,5	6,5	2,3	1,5	2,6	2,1	6,1	3,0	9,8	6,3	3,0	2,8	3,6
Druksterkte toename	[%]		37%	35%	34%	35%	45%	32%	28%	33%	96%	21%	37%	48%	51%	-11%	39%	31%	43%	41%	47%
Druksterkte NAP -9,0m	[MPa]	28 dgn	9,1	11,4	10,7	10,4	4,6	2,0	9,5	5,3	2,5	1,8	1,9	2,1	2,6	3,9	7,9	4,8	2,3	2,2	2,6
Druksterkte NAP -9,0m	[MPa]	56 dgn	12,3	15,6	14,8	14,2	6,6	1,3	12,4	6,8	3,5	2,2	2,5	2,7	3,5	5,5	10,9	6,6	2,8	2,8	3,5
Druksterkte toename	[%]		36%	37%	38%	37%	44%	-31%	31%	27%	38%	26%	32%	33%	37%	43%	37%	39%	22%	30%	35%
Treksterkte																					
Buigtreksterkte NAP -6,0m	[MPa]	28 dgn	2,3	2,0	2,0	2,1	1,0	0,6	2,1	1,2	0,3	0,3	0,4	0,3	1,1	0,8	1,8	1,2	0,5	0,5	0,8
Buigtreksterkte NAP -6,0m	[MPa]	56 dgn	2,6	2,0	2,0	2,2	1,4	0,8	2,5	1,6	0,5	0,3	0,6	0,5	1,6	1,3	2,5	1,8	0,8	0,8	1,2
Buigtreksterkte toename	[%]		13%	0%	0%	5%	40%	33%	19%	27%	67%	0%	50%	40%	45%	63%	39%	46%	60%	60%	50%
Buigtreksterkte NAP -9,0m	[MPa]	28 dgn	1,8	2,4	2,3	2,2	1,2	0,5	2,5	1,4	0,6	0,5	0,5	0,5	0,7	0,9	2,1	1,2	0,6	0,6	0,8
Buigtreksterkte NAP -9,0m	[MPa]	56 dgn	2,5	2,7	3,0	2,7	1,7	0,6	2,6	1,6	0,7	0,6	0,5	0,6	0,8	1,2	2,5	1,5	0,8	0,8	1,1
Buigtreksterkte toename	[%]		39%	13%	30%	26%	42%	20%	4%	17%	17%	20%	0%	13%	14%	33%	19%	22%	33%	33%	38%
Cementgehalte																					
cementgehalte NAP -6,0m	[kg/m³]			315,6			251,0					271,7			271,7						225,0
cementgehalte NAP -9,0m	[kg/m³]			396,1			265,2					219,1			219,1						232,1
Gemiddelde	[kg/m³]			355,9			258,1					245,4			245,4						228,5

Ter info	Materiaal	massa ρ	w.d.f.	dosering	Water	Groot
	[type]	[kg/m³]	[ ]	[kg/m³]	[kg/m³]	[kg/m³]
Mengsel 1	CEMIII-42.5	2950	1,25	629	787	1416
Mengsel 2	CEMIII-42.5	2950	2,5	382	881	1233
Mengsel 3	CEMIII-42.5	2950	3,75	245	917	1162
Mengsel 4	GM42 *	2858	2,0	426	851	1277
	zand	2650				
	water	1000				

2837.5

\* soortelijk gewicht GM42 kan relatief sterk variëren door variatie s.g. kalksteenmeel